博士論文

トンネル分光法による高温超伝導体の電子状態に関する研究

Study on Electronic States of High-T_C Superconductor by Tunneling spectroscopy

The institute of Scientific and Industrial Research
Osaka University

川山　巌
Iwao Kawayama

博士論文

トンネル分光法による高温超伝導体の電子状態に関する研究

Study on Electronic States of High-T_c Superconductor by Tunneling spectroscopy

The institute of Scientific and Industrial Research
Osaka University

川山　巌
Iwao Kawayama

Contents

Chapter 1

General Introduction

The discovery of high-T_c superconductor (HTSC), $La_{2-x}Ba_xCuO_4$ (LBCO) by Bednorz and Muller in 1986 [1], was a surprising event not only because of the large increase in T_c, but also because it revealed that the oxides formed a new class of superconducting material with great potential. Shortly thereafter, several kinds of cuprate superconductors [2-4] with higher T_c were discovered and it appeared that these materials have various interesting properties, such as doping dependence of physical properties [5] different from conventional superconductors. Those properties of HTSC are thought to be originated from a strong coulomb repulsion between conducting electrons because of narrow 3d band, and this system is called " strongly correlated electron system". Properties of strong correlation systems, especially 3d transition metal oxides, have been widely studied since the discovery of HTSC and a number of interesting phenomena, *e.g.* colossal magnetoresistance [6], have been successively discovered. Thus, it is most important subject for the material science to elucidate properties of the strongly correlated electron systems, and the investigation of superconducting properties of HTSC must play a significant role for this subject.

From the reason described above, a lot of efforts have been made towards elucidation of superconductivity of HTSC. Especially, the symmetry of a pair wave function remains the subject of intense research activity. In the superconducting state, electron pairs, so called Cooper pairs, are formed with an appropriate attractive interaction between electrons, and Cooper pairs which have spin zero and have many attributes of bosons are in the Bose-Einstein condensation state. A symmetry of wave functions of Cooper pairs provides significant information on the origin of the attractive interaction between electrons. In the case of conventional superconductors, the superconducting mechanism was explained by Badeen, Cooper and Schrieffer (BCS theory) in 1957 [7], and an attractive interaction emerges through electron-lattice interaction. Many experimental results confirmed this theory and that the pair wave function of conventional superconductors has s-wave symmetry. In the case of HTSC, however, it is thought that the electron-lattice interaction assumed by BCS theory can not cause such a high transition temperature, and some kinds of magnetic interactions have been proposed as attractive interactions [8-10]. Since such theories based on magnetic

interactions usually have led to d-wave pairing, extreme number of researches have been performed to elucidate the pair symmetry of HTSC by using various methods, such as NMR [11], angle-resolved photoemission spectroscopy [12,13] and Josephson junctions [14,15].

Tunneling spectroscopy is one of powerful methods to investigate a pair symmetry of superconductors. This method is undertaken by setting a counter electrode onto a sample surface via insulating barrier as shown in Fig. 1-1, and electron transfer between the sample and the electrode through the potential barrier by a quantum mechanical tunneling effect is observed. By using this phenomenon, direct information of the electronic states can be obtained with high energy resolution. This method primarily can deliver the density of state (DOS) near the Fermi level [16]. The difference between s-wave and d-wave directly appears in the structure of DOS in the superconducting energy gap as shown in Fig. 1-2. Superconducting gap Δ which is a minimum excitation energy between a superconducting ground state and exited states have same symmetry as a pair wave function. In the case of s-wave symmetry, the value of superconducting gap Δ is finite over all directions in a momentum space, as a result, there is no DOS within the superconducting gap (Fig. 2 (a)). In the case of d-wave symmetry, the gap has nodes of $\Delta = 0$ along the certain directions, which means that the DOS is finite even in the gap (Fig. 1-2 (b)). The pairing symmetry, therefore, can be determined by a measurement of DOS with the tunneling spectroscopy. In the studies of conventional superconductors, tunneling measurements have played an important role in verification of the BCS theory. Tunneling spectroscopy, however, has been recognized as less reliable method than other experimental methods in the case of HTSC, because various kind of spectra were obtained and it is difficult to identify the spectra reflecting true DOS.

I consider that the most serious problem in the tunneling study is imperfections of tunneling barrier such as pin holes and interdiffusion. In the previous tunneling studies of HTSC, scanning tunneling spectroscopy (STS) [17-21], break junction [22,23], point contact [24] and planar junction [25-26] have been used. Break junction and point contact have disadvantages because the nature of interface and tunneling barrier are not characterized in such junctions. If these imperfections exist in the barrier, the intrinsic spectra cannot be

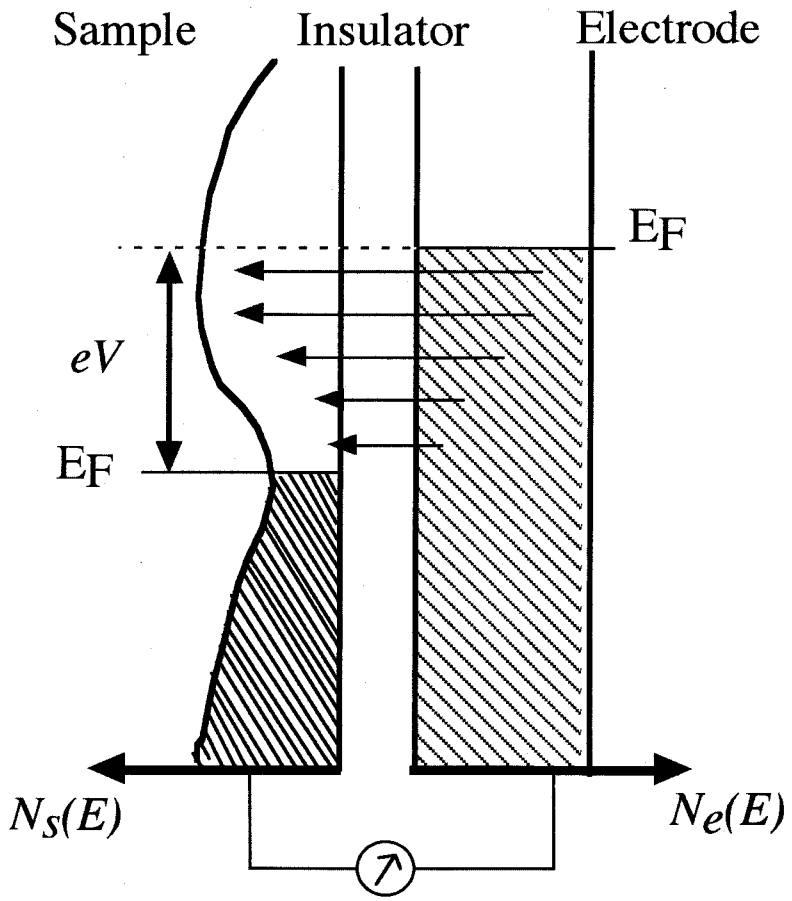

Figure 1-1 Schematic illustration of tunneling spectroscopy. *Ns(E)* and *Ne(E)* denote density of states of sample and electrode, respectively, and are plotted horizontally vs. energy vertically. Shading denotes states occupied by electrons. The difference of Fermi energy between a sample and an electrode corresponds to bias voltage *eV*. As a result, electrons transfer into empty states from occupied states.

obtained because HTSC has short coherence length and the surface electronic state is easily disturbed by the slight degradation at the interface. Planar junctions have been popular methods in the studies of conventional superconductors because such a junction is stable enough for quantitative studies of temperature dependence of the spectra and understanding on the k-dependence of the tunneling is established. However it is much difficult to prepare flat insulating layer with HTSC compared with conventional metal superconductors from the reasons described below. In the case of conventional superconductors such as Al, Sn and Pb, oxide layer of themselves at the interface work as good tunneling barriers, but, this technique could not be applied to HTSC which themselves are oxide. Therefore, it is necessary to prepare hetero-structures with oxide thin films for the fabrication of tunnel junctions. However, oxide thin films such as HTSC generally have higher growth temperature than simple metals. Therefore, it is difficult to control surface structure and to prevent interdiffusion between layers. The purpose of this thesis is to elucidate the pair symmetry of HTSC with tunneling spectroscopy by preparing well-defined barrier layers. I have used pulsed laser deposition (PLD) technique to prepare flat insulating layers. PLD technique is suitable for the formation of oxide thin films because the pressure and the oxidation gas can be controlled freely.

At first, to prepare flat insulating barrier layers, the growth mechanism of the oxide thin films on atomically flat substrates was studied as described in chapter 2. Based on the results obtained from this study, I fabricated planar junctions with a well-defined tunneling barrier, and obtained tunneling spectra with clear gap structures. These spectra were analyzed and the pair symmetry was examined in chapter 3. In scanning tunnel microscopy (STM), the sharp tip is used as a electrode and tunneling current between the sample and the tip is measured through the vacuum barrier. In this method, imperfection of barrier layer can be neglected and reliable spectra will be obtained because tunneling region is extremely small and the vacuum barrier with highly insulating nature is used. In the ordinary STM and scanning tunnel spectroscopy (STS) studies on HTSC, the junction is constructed by superconducting sample-vacuum barrier-normal metal tip, namely superconductor-insulator-normal metal (SIN) junction. In chapter 4, I apply this method to superconductor- insulator-

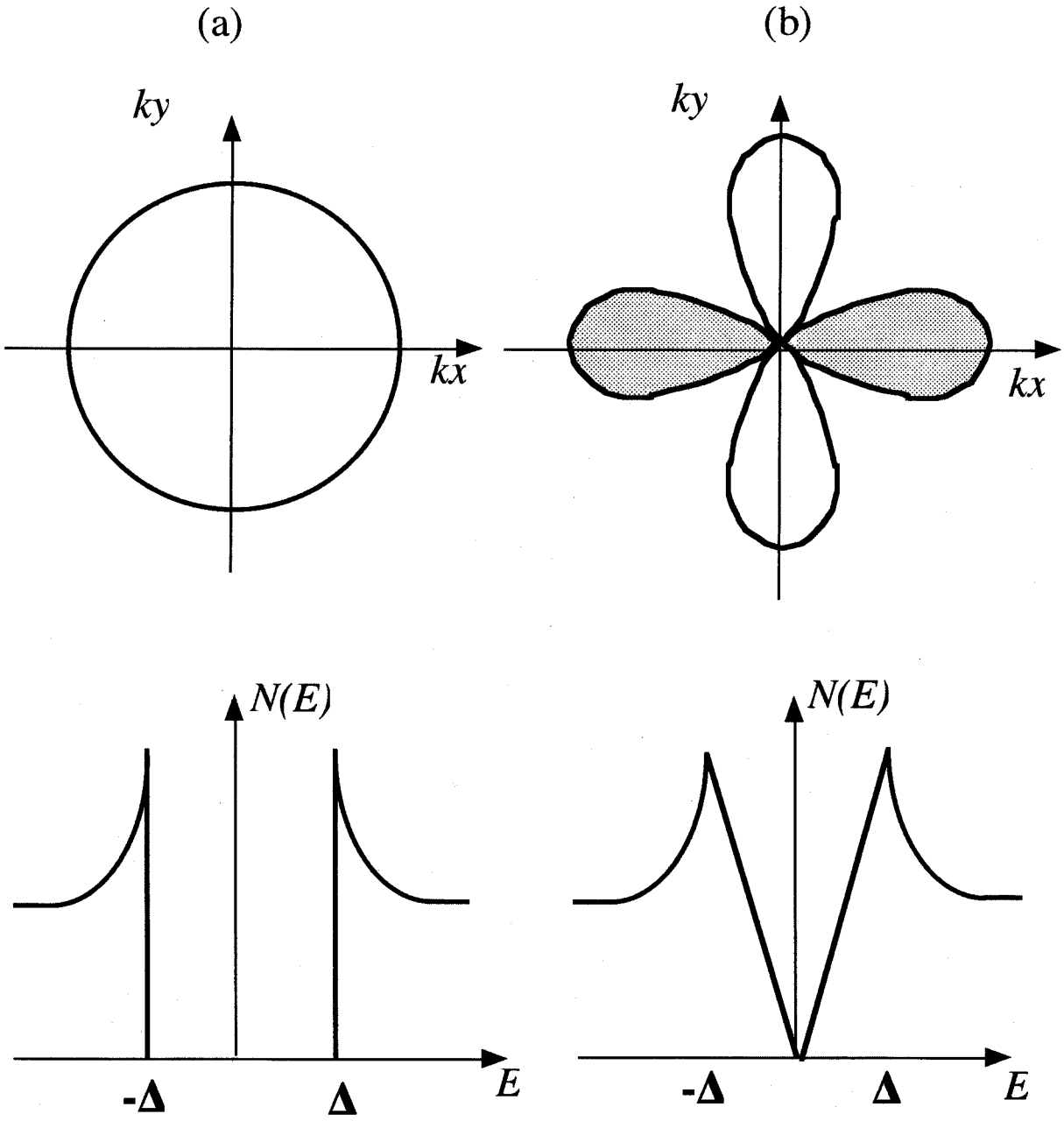

Figure 1-2 Schematic illustration of energy gap Δ in *k*-space and density of states of (a) s-wave and (b) d-wave.

superconductor (SIS) junction as a unique method using a superconducting whisker tip in STM and measured SIS tunneling spectra. In chapter 5, I show the results of properties on Josephson tunnel junction with HTSC. I measured Josephson current between $Bi_2Sr_2CaCu_2O_8$ and Nb. Josephson current flows between two superconductors separated by a thin insulating layer and behaviors of Josephson current are much sensitive to the phase of pair wave functions [16]. Therefore, the phase shift of d-wave symmetry under 90° degree rotation causes different Josephson effects from that of s-wave. I investigated properties of s-wave component in HTSC by detailed analysis of Josephson effects in $Bi_2Sr_2CaCu_2O_8$/Au/Nb Junctions. Finally, these investigations on the pair symmetry of HTSC by tunneling measurements are summarized in chapter 6.

References

1. J. G. Bednorz and K. A. Muller, Z. Phys. B 64, 189 (1986)
2. M. K. Wo et al., Phys. Rev. Lett. 58, 908 (1987)
3. H. Maeda et al. Jpn. J. Appl. Phys. 27, L209 (1988)
4. Z. Z. Sheng and A. M. Hermann, Nature 232, 55 (1988)
5. Y. Tokura: in "*Physics of High-Temperature Superconducotors*", S. Maekawa and M. Sato (eds.) (Springer-Verlag, 1992)
6. Y. Tokura, A. Urushibara, Y. Moritomo, T. Arima, A. Asamitsu, G. Kido, and N. Fukuyama, J. Phys. Soc. Jpn. 63 (1994) 3931
7. J. Bardeen, L. N. Cooper, J. R. Schrieffer, Phys. Rev. 108, 1175 (1957)
8. P. W. Anderson, Science 235, 1196 (1987)
9. N. E. Bickers, D. J. Scalapino, S. R. White, Phys. Rev. Lett 62, 961 (1989)
10. P. Monthoux, A. V. Balatsky, D. Pines, Phys. Rev. Lett. 67, 3448 (1991)
11. Y. Kitaoka, K. Ishida., and K. Asayama, J. Phys. Soc. Jpn. 63, 2052 (1994)
12. T. Yokoya and T. Takahashi, Phys. Rev. B 53, 14055 (1996)
13. Z. X. Chen, Phys. Rev. Lett. 70, 1553 (1993)
14. D. A. Wollman, D. J. Van Harlingen, W. C. Lee, D. M. Ginsberg, and A. J. Leggett, Phys. Rev. Lett. 71, 2134 (1993)
15. C. C. Tuei, J. R. Kirtley, M. Rupp, J. Z. Sun, A. Gupta, M. B. Ketchen, C. A. Wang, Z. F. Ren, J. H. Wang, and M. Bhushan, Sience 271, 329 (1996)
16. For example, M. Tinkham , *Introduction to Superconductivity* (McGraw-Hill, New York, 1996)
17. C. Manabe, M. Oda, and M. Ido, Physica C 235-240, 797 (1991)
18. Ch. Renner and Ø. Fisher, Phys. Rev. B 51, 9208 (1995)
19. H. Murakami and R. Aoki, J. Phys. Soc. Jpn. 64, 1287 (1995)
20. K. Ichmura and K. Nomura, J. Phys. Soc. Jpn. 62, 3661 (1993)
21. H. J. Tao, A. Chang, Farun. Lu, and E. L. Wolf, Phys. Rev. B 45, 10622
22. J. I. Gorina, G. A. Kaljujnaia, V. I. Ktitrov, V. P. Martovisky, V. V. Rodin, V.

A. Stepanov, A. A. Tsvetkov, and S. I. Vendneev, Solid state comun. 85, 695 (1993)

23. L. Buschmann, M. Boekhot, and G. Guntherodt, Physica C 203 68 (1992)
24. J. Chen et al., Phys. Rev. B 49, 3683 (1994)
25. T. Matsumoto, Supab. Choopun, and T. Kawai, Phys. Rev. B 52, 591 (1995)
26. A. M. Cucolo, R. Di. Leo, A. Nigro, P. Romao, and F. Bobba, Phys. Rev. Lett. 76, 1920 (1996)

Chapter 2

Growth of $SrCuO_2$ Thin Films on Oxygen-Annealed $SrTiO_3$ (100) Substrates

Abstract

Annealing effect on the surface of $SrTiO_3$ (100) substrates and initial growth of $SrCuO_2$ thin films on the $SrTiO_3$ were studied by reflection high energy electron diffraction (RHEED) and atomic force microscopy (AFM). The surface of $SrTiO_3$ (100) substrates annealed at 1000 °C in O_2 atmosphere has atomically flat surfaces with high crystallinity and steps of one unit-cell height (3.9 Å). The deposition of $SrCuO_2$ on the annealed substrates makes islands near the steps with 4-7 Å height resulting in the surface roughening in spite of the flat substrate surface. By depositing Sr as a buffer layer on the annealed substrates, the flatness of $SrCuO_2$ thin films was improved.

2. 1 Introduction

$SrTiO_3$ (100) has been widely used as a substrate for oxide thin films, such as high-T_c superconductors (HTSC), because its structure and lattice constants are similar to those of the films [1, 2]. The growth of thin films is usually affected by the crystallinity and flatness of substrates, and higher crystallinity and flatter surface are desirable for the preparation of better-quality films especially for tunneling junction of HTSC. Commercially available $SrTiO_3$ (100) substrates, however, usually have rough surface and low crystallinity, which makes them unsuitable for deposition of oxide materials using atomic layer epitaxy. Recently, some groups have obtained an atomically flat surface by treatment of commercial $SrTiO_3$ (100) substrates. One effective treatment is etching using pH-controlled HF-NH_4F solution [3] and another is oxygen annealing. [4, 5] Investigation of thin film growth on these atomically flat substrates is important for improving the quality of films growth by the layer-by-layer growth technique. In this work, we have annealed $SrTiO_3$ (100) substrates at various temperatures under oxygen atmosphere because preparation by O_2 annealing is easier than HF-NH_4F etching, and studied their crystallinity and flatness. Furthermore, layers of $SrCuO_2$, which is the fundamental structure of oxide superconductors, [6, 7] were deposited on the substrates, and the initial growth was observed. Based on the obtained results, we discuss the important factors for the preparation of flatter films. I believe that the results of this study provide fundamental information to preparation of tunneling junction with HTSC.

2. 2 Experimental

Commercially available $SrTiO_3$ (100) substrates, which were mechanically polished in an alkaline solution containing colloidal silica particles, were annealed at 600-1000 °C for 1-10 hours under 1 atm oxygen with purity of 99.995 % (referred to as annealed substrates). Following these treatments, the substrates were transferred into an ultrahigh vacuum (UHV) chamber with a base pressure of 1×10^{-8} mbar, and heated at 500 °C under 1×10^{-5} mbar NO_2 atmosphere. These are typical conditions for the preparation of $SrCuO_2$ thin films [7].

$SrCuO_2$ was deposited on these substrates by laser ablation using an ArF excimer laser (193

nm). The laser beam was focused on a sintered disk target of $SrCuO_x$. The target was prepared by calcining a mixture of $SrCO_3$ and CuO in a 1:1 ratio. The surfaces of substrates and the $SrCuO_2$ thin films were observed in situ by reflection high-energy electron diffraction (RHEED). RHEED measurements were performed with an [010] incident beam direction and acceleration voltage of 15 kV. Atomic force microscopy (AFM) measurements of the substrates and the films were performed in air at room temperature. All the images were taken in constant force mode by applying a force of about 0.1-1.5 nN.

2. 3 Results and Discussion

2. 3. 1 The surface of $SrTiO_3$ substrates

Figure 2-1 shows the annealing temperature dependence of RHEED patterns of the $SrTiO_3$ (100) substrates. Annealing at temperatures below 600 °C gives essentially the same RHEED pattern as that of an as-delivered substrate (Fig. 1(a)). In the RHEED pattern of 800 °C-annealed substrates (Fig. 2-1(b)), streaks of the 0th Laue zone become shorter, and weak streaks which are regarded as a (2×2) structure or a twin structure of (2×1) appear. Since the (1/2, 1/2) diffraction spot is observed using an [011] incident electron beam, these streaks are assigned to a (2×2) structure. The RHEED streaks of 1000 °C-annealed substrates are shorter than those of 800 °C-annealed substrates and form a spotty pattern in the 0th Laue zone, which shows that the crystallinity or flatness of the substrate is improved by the annealing. The RHEED patterns showed no dependence on annealing time in the range of 1-10 hours. In order to discuss the crystallinity and flatness quantitatively, the full width at half-maximum (FWHM) values of the (02) rod in the RHEED patterns of substrates annealed at 700-1000 °C are plotted in Fig. 2-2. The FWHM decreases with increase in the annealing temperature. Since the FWHM depends on both flatness and crystallinity of the surfaces, the change of the FWHM indicates that partial rearrangement in the substrate surface begins at 700 °C, and progresses as the annealing temperature is increased. The difference between the maximum and the minimum of the FWHM for substrates annealed at 1000 is quite small compared with those for substrates annealed below 900 °C, which shows that the crystallinity and flatness of

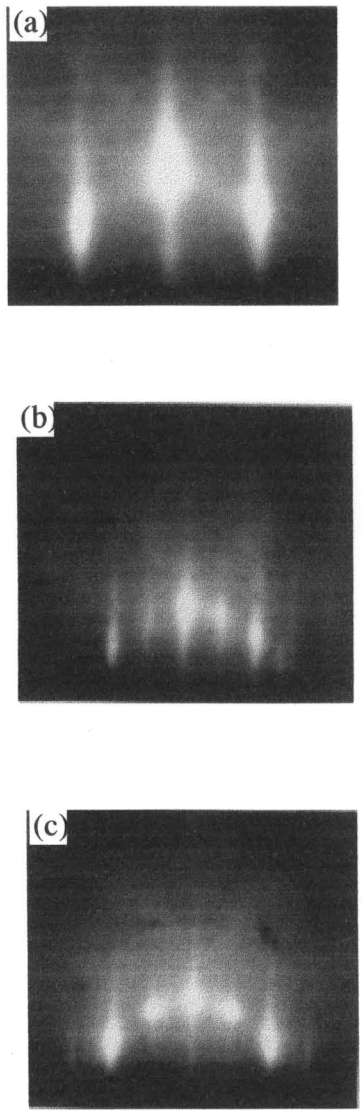

Figure 2-1 RHEED patterns of (a) as-delivered SrTiO3 (100) substrate, (b) 800℃-annealed substrate and (c) 1000℃-annealed substrate. With increasing the annealing temperature, RHEED streaks become shorter, indicating the improvement of the crystallinity or the flatness of the substrates.

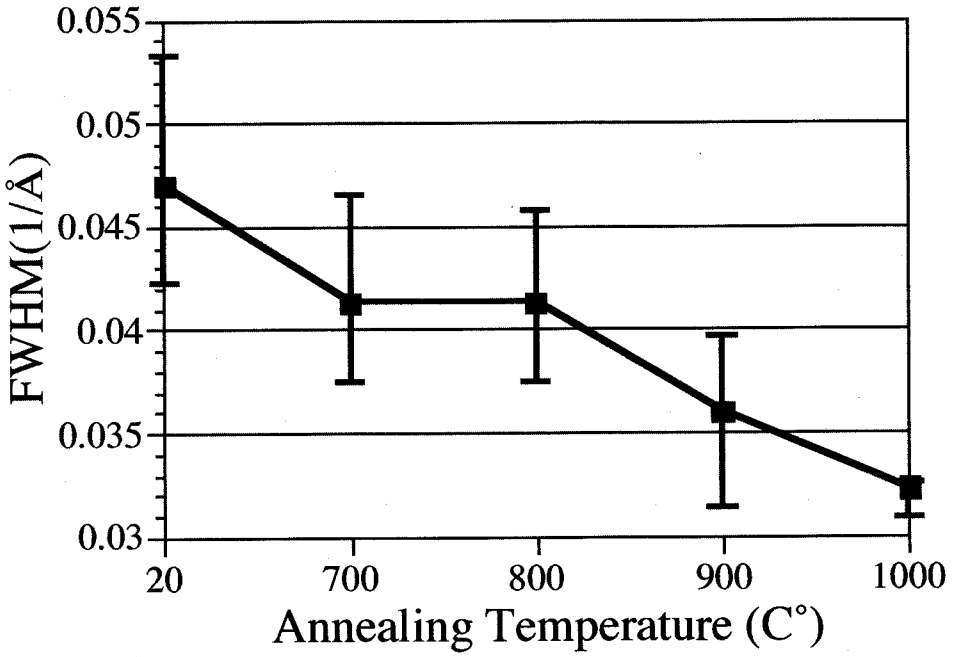

Figure 2-2 FWHM of (02) rod in RHEED patterns at various annealing temperature. The top and bottom of error bars respectively mean maximum and minimum of FWHM at each annealing temperature.

1000 °C-annealed substrates do not depend on those before annealing and that the surface rearrangement is almost complete at this temperature. To observe the surface rearrangement process in real space, AFM measurements were performed. While an as-delivered substrate has uneven features with corrugation 2-4 Å high as shown in Fig. 2-3 (a), an 800 °C-annealed substrate (Fig. 2-3 (b)) exhibits partially formed linear steps on the surface. Figure 2-3 (c) shows that the surface of 1000 °C-annealed substrates consists of atomically flat terraces and parallel steps 3.9 Å high corresponding to the unit cell height of $SrTiO_3$. Judging from the results of RHEED and AFM, some of the surface ions, which may be in weakly bonded amorphous regions, in the as-delivered substrate begin to diffuse and rearrange at above 700 Å. The rearrangement takes place over the whole surface at about 1000 Å, and substrates with a flat and well-crystallized surface can be obtained.

2. 3. 2 The growth of $SrCuO_2$ on $SrTiO_3$ substrates

Figure 4 shows the RHEED patterns of $SrCuO_2$ thin films which were deposited on as-delivered and 1000°C-annealed substrates. The thickness of the films is about 100Å. Co-deposited $SrCuO_2$ films on as-delivered substrates maintained the streaky RHEED pattern (Fig. 2-4 (a)), which shows that the surface of $SrCuO_2$ thin films is flat to some extent. On the other hand, the RHEED pattern of $SrCuO_2$ thin films deposited on 1000 °C-annealed substrates is composed of transmission-type spots as seen in Fig. 2-4 (b), which indicates that a quite rugged surface formed even though the substrates were atomically flat. To investigate the initial growth of $SrCuO_2$ thin films, half amount of a unit cell layer of $SrCuO_2$ was deposited on the substrates, and the surface morphology was observed by AFM. The thickness of the film was estimated from RHEED intensity oscillations. Figure 2-5 (a) shows the AFM image of the $SrCuO_2$ deposited on an as-delivered substrate. The surface exhibits 3-5-Å-high corrugation. Although the surface after deposition is slightly rougher than the substrate, the surface morphology does not change essentially during the deposition. In contrast, Fig. 2-5 (b) shows that islands with a height of 4-7Å are grown after the deposition of $SrCuO_2$ on 1000 °C-annealed substrates. These islands align at a regular interval which is nearly equal to that of the steps of the

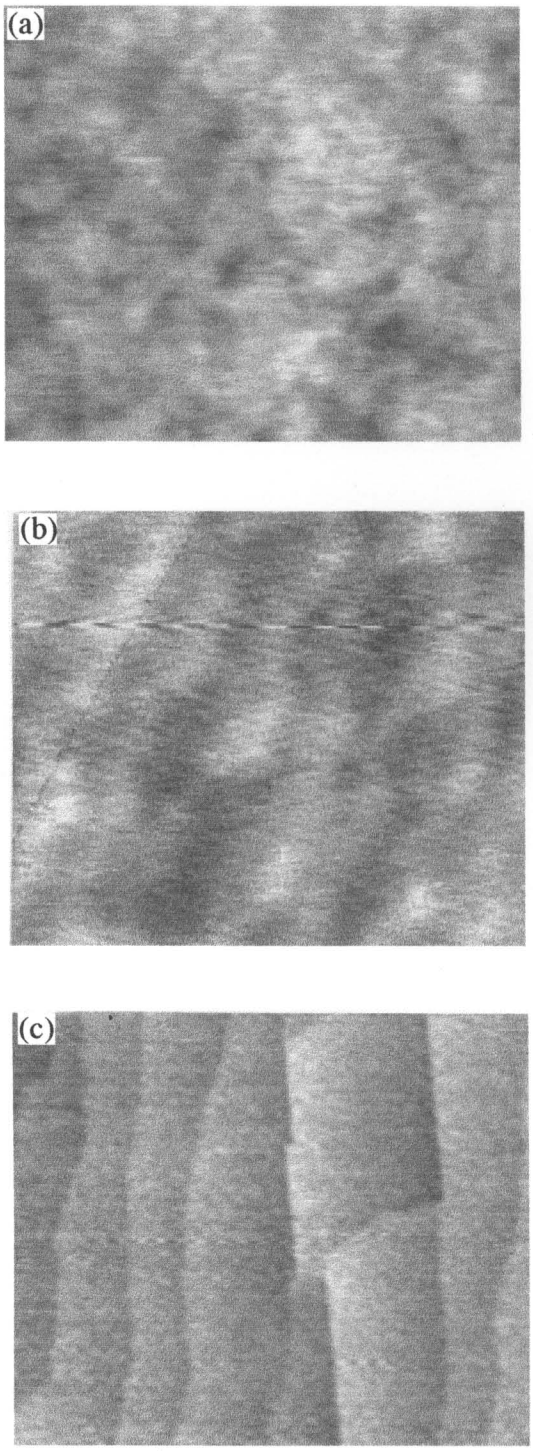

Figure 2-3 AFM images of (a) as-delivered substrate, (b) 800℃-annealed substrate and (c) 1000℃-annealed substrate. The 1000℃-annealed surface consists of atomically flat terraces and unit cell height steps.

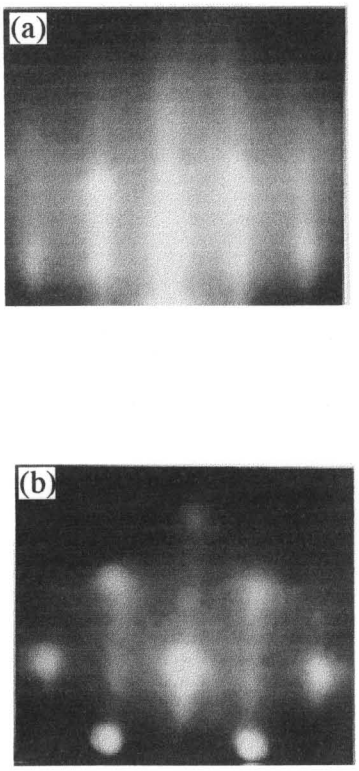

Figure 2-4 RHEED patterns of SrCuO2 deposited on (a)as-delivered substrate and(b) 1000 ℃-annealed substrate. The film on the 1000℃-annealed substrate has spotty RHEED pattern, namely very rough surface.

substrate. These results show that the deposited ions and atoms adsorb at the steps selectively to form large $SrCuO_2$ islands. We consider that the reasons why $SrCuO_2$ forms islands at the steps are as follows. The first reason is surface stability of the $SrCuO_2$ layer on the substrate. $SrCuO_2$ has a layer structure in which Sr layers and CuO_2 layers are stacked along the c-axis [6,7]. Since the topmost layer of 1000 °C-annealed substrates is TiO [2, 8] the surface of $SrCuO_2$ becomes copper oxide. From the results of RHEED measurement, it is known that a copper oxide surface is a less stable two-dimensional structure than a SrO_x surface and sometimes forms a three-dimensional phase under a oxidizing atmosphere [9]. The second reason is as follows. Because annealed substrates have atomically flat terraces, the deposited particles may have a sufficient diffusion length to reach steps. Therefore most of the deposited particles can accumulate around the steps which are stable sites compared with terraces. Moreover, the lattice mismatch in the c direction (c = 3.4 Å for $SrCuO_2$, c = 3.9 Å for $SrTiO_3$) prevents two-dimensional growth in the step-flow growth mode. Consequently $SrCuO_2$ particles form islands at the steps as shown by Fig. 2-5 (b). It is thought that $SrCuO_2$ on as-delivered substrates forms islands in the same way, but particles do not concentrate owing to the corrugation, i.e steps with high density, of the substrates. Therefore $SrCuO_2$ on as-delivered substrates does not form large islands.

In order to prepare flatter $SrCuO_2$ thin films on annealed substrates, we deposited Sr as a buffer layer. It has already been shown by Kawai et al. that a Sr buffer layer strongly affects the growth of $SrCuO_2$ thin films [10]. We deposited one atomic layer of Sr on 1000 °C-annealed substrates, which changes the topmost layer of substrates from TiO_2 to SrO_x. Subsequently half amount of unit cell layer of $SrCuO_2$ was deposited and AFM measurement was performed (Fig. 2-5 (c)). Due to the SrO_x buffer layer, it is thought that the topmost layer of $SrCuO_2$ changed from CuO_2 to Sr. Figure 2-5 (c) shows that the surface exhibits corrugation 3-5 Å high and large islands cannot be observed. The effect of the SrO_x buffer layer is confirmed. This result shows the importance of the stability of the surface layer. Consequently, it is concluded that not only substrate flatness but also control of the topmost layer of films is important in preparing flat thin films.

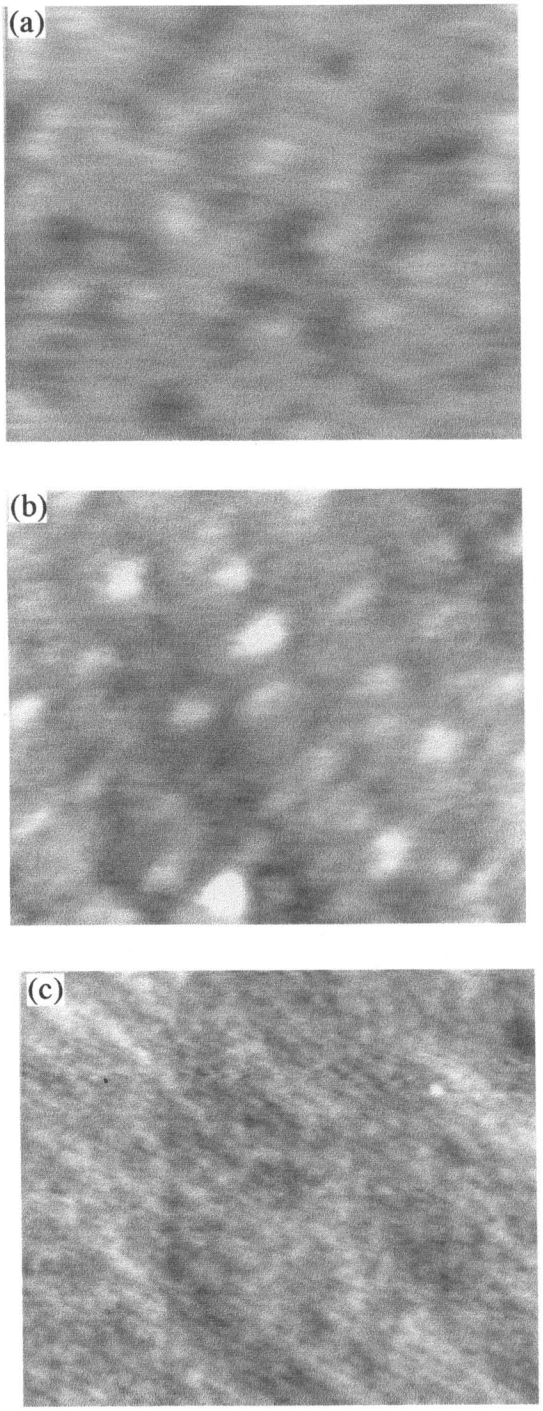

Figure 2-5 AFM images of SrCuO2 deposited on (a) as-delivered substrate, (b)1000℃ -annealed substrate and (c)1000℃-annealed substrate with a SrOx buffer layer. On the surface of the film on the 1000℃-annealed substrate, large islands aligned with line shapes. The distance between the islands line are about 100 nm which is equal to that between the steps of the basis substrate. The surface roughness was improved by SrO buffer layer.

2. 4 Conclusions

The effect of oxygen-annealing on $SrTiO_3$ (100) substrates was investigated by RHEED and AFM. Surface rearrangement of $SrTiO_3$ occurred at annealing temperature above 700 °C and crystallinity and flatness improved with the increase of annealing temperature. Surface structure was independent of annealing time in the range of 1-10 hours. When $SrCuO_2$ was deposited on 1000 °C-annealed substrates with atomically flat terraces, island growth occurred at the steps. By changing the topmost layer of $SrCuO_2$ from copper oxide to strontium oxide by depositing a SrO_x buffer layer on the substrate, smoother films without islands were obtained. This indicates that the topmost layer of the films is important for the preparation of flat films of $SrCuO_2$ on the atomically flat $SrTiO_3$ substrate.

References

1) M. Kanai, T. Kawai and S. Kawai: Appl. Phys. Lett. 58 (1991) 771.

2) S. Matunari, M. Kanai and T. Kawai: Jpn. J. Appl. Phys. 34 (1995) L20.

3) M. Kawasaki, K. Takahashi, T. Maeda, R. Tsuchiya, M. Shinohara, O. Ishiyama, T. Yonezawa, M. Yoshimoto and H. Koinuma: Science. 226 (1994) 1540.

4) M. Naito and H. Sato: Physica C 229 (1994) 1.

5) R. Sum, H. P. Lang and H.-J. Güntherodt: Physica C 242 (1995) 174.

6) M. Takano, M. Azuma, Z. Hiroi, Y. Bando and Y. Takeda: Physica C 176 (1991) 445.

7) X. M. Li, T. Kawai and S. Kawai: Jpn. J. Appl. Phys. 31 (1992) L934

8) M. Yoshimoto, T. Maeda, K. Shimozono, H. Koinuma, M. Shinohara, O. Ishiyama and F. Ohtani: Appl. Phys. Lett. 65 (1994) 3197.

9) M. Kawai, S. Watanabe and T. Hanada: J. Cryst. Growth 112 (1991) 745.

10) M. Kawai, Z.-Y. Liu, T. Hanada, M. Katayama, M. Aono and C. F. McConville:Appl. Surf. Sci. 82/83 (1994) 487.

Chapter 3

Tunneling Spectra of $Bi_2Sr_2CaCu_2O_8$ Single Crystal with Well-defined Artificial Barrier

Abstract

I tried to fabricate planar type tunnel junctions with a high T_c superconductor to obtain intrinsic tunneling spectra along the c direction of the high T_c superconductor. The growth of $CaTiO_3$ thin films on the cleaved surface of $Bi_2Sr_2CaCu_2O_8$ single crystals was investigated by reflection high energy electron diffraction (RHEED) and atomic force microscopy (AFM) in detail, and I obtained $Bi_2Sr_2CaCu_2O_8/CaTiO_3/Ag$ trilayer junctions with atomically flat interfaces. It was shown that the observed tunneling spectra agree with line node d-wave model which includes Andreev reflection.

3. 1 Introduction

Many tunneling studies of high T_c superconductors (HTSC) have been performed with the various methods, such as a break junctions [1,2], planar junctions [3-6] and scanning tunneling spectroscopy (STS) [7-12]. Experimental tunneling data of HTSC, however, have been widely scattered, and few reliable information about a symmetry of the pair wavefunction have been obtained, because of imperfection of a barrier layer. Therefore, scanning tunneling spectroscopy (STS) have been preferred to other tunneling methods such as a planar junction and a break junction because well-defined vacuum barrier can easily obtained. In STS studies, however, it is difficult to measure temperature dependence of the spectra. In contrast, planar junction is stable enough for quantitative studies of temperature dependence of the spectra, moreover the *k*-dependence of the tunneling is established in such junction. In planar junctions, however, few reliable spectra have been obtained yet because it is difficult to exclude imperfections of a barrier layer as described above. To measure intrinsic tunneling spectra on HTSC, it is important to fabricate planar junction with a well-defined barrier layer which should be thin enough for tunneling and has atomically flat interface without pin-holes and interdiffusion. I consider that recent epitaxial growth technique of oxide thin films as shown chapter 2 enables us to prepare such ideal junctions. In this study, I prepare $CaTiO_3$ thin films as the barrier layer on the cleaved surface of $Bi_2Sr_2CaCu_2O_8$ (BSCCO) single crystals. $CaTiO_3$ is suitable for a barrier layer because $CaTiO_3$ has very close structure and a lattice constant to those of $Bi_2Sr_2CaCu_2O_8$ and sufficient resistivity for tunneling barrier. In fact, atomic force microscopy (AFM) images showed that the surface of $CaTiO_3$ thin films was atomically flat. Tunneling spectra of such junctions showed d-wave like gap structure. I analyzed the spectra with fitting curves based on an s-wave and a d-wave symmetry including Andreev reflection effect.

3. 2 Experimental

$Bi_2Sr_2CaCu_2O_8$ single crystal was prepared by a traveling solvent floating zone method [19]. The crystal has a rod shape of 5 mm in diameter and 70 mm in length . The rod is cut into 8 mm in length by a wire saw and cleaved in air along the ab plane. The surface Figure

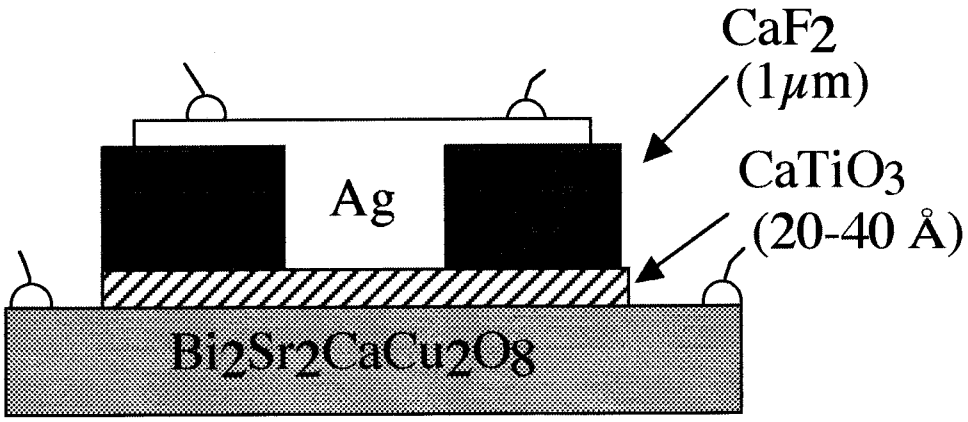

Firure 3-1 Schematic configuration of $Bi_2Sr_2CaCu_2O_8/CaTiO_3/Ag$ junction.

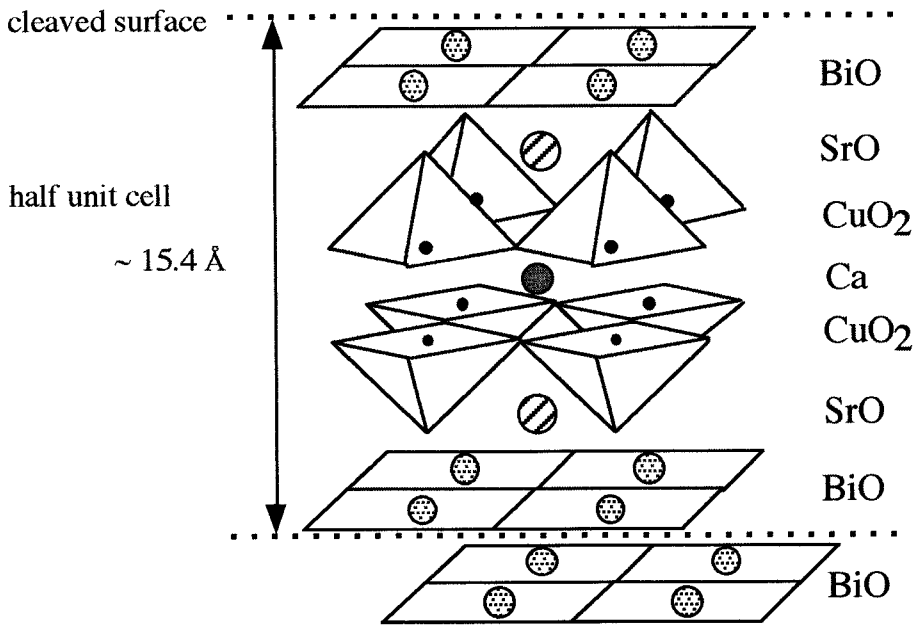

Figure 3-2 Schematic illustration of the structure of $Bi_2Sr_2CaCu_2O_8$.

structures of cleaved plane of the crystal were observed by reflection high energy electron diffraction (RHEED) and atomic force microscopy (AFM). $CaTiO_3$ thin films were deposited on the cleaved surface by laser molecular beam epitaxy (laser MBE) method. The beam of ArF excimer laser (193 nm) is focused on $CaTiO_3$ target. The target is held on a rotating disk controlled by a pulsed motor, so that the laser beam always hits a fresh surface. Surfaces were observed in situ by RHEED during the growth. The deposition rate was measured by the number of oscillation of specular spot intensity in RHEED pattern. The typical growth conditions are 1×10^{-6} mbar of NO_2 and 600 °C as a growth temperature. The thicknesses of deposited $CaTiO_3$ thin films were 20-60 Å. After the deposition, the samples were annealed at 400 °C for 5 hours under 1 atm oxygen with purity of 99.995 % in order to decrease the oxygen defects induced into the $CaTiO_3$ thin films. After the annealing, CaF_2 and Ag were deposited by conventional evaporation, and Au wires were attached to electrodes by Ag paste. A schematic configuration of the junction is shown in Fig. 3-1. The tunneling electrode has areas of 0.0025-0.25 mm^2. Resistance- temperature (R-T) and current-voltage (I-V) characteristics of the junctions were measured by conventional four probe technique.

3. 3 Results and Discussions

3. 3. 1 Growth of $CaTiO_3$ on the cleaved surfaces of $Bi_2Sr_2CaCu_2O_8$

Fig. 3-2 shows the structure of a BSCCO. A BSCCO have double BiO layers which are combined with van der Waals bond and easily cleaved. Fig. 3-3 (a) and (b) show RHEED patterns of the cleaved surface of BSCCO single crystal with the incident beam parallel to the [100] and [010] direction, respectively. The superstructure due to the incommensurate modulation in the Bi2212 crystal was clearly observed as shown in Fig. 3-3 (a). The superstructure was not observed using incident beam parallel to [010] direction as shown in Fig. 3-3 (b). These RHEED measurements shows that the cleaved surface consists of a single grain without twin structure. Furthermore AFM images show the surfaces consist of atomically flat terraces and straight steps along the a axis (Fig. 3-4 (a)). The most of steps have 15 Å height which is a half unit cell in the c axis. From these measurement, we confirmed that the cleaved surfaces of $Bi_2Sr_2CaCu_2O_8$ single crystals were the suitable for fabrication of tunneling junctions with

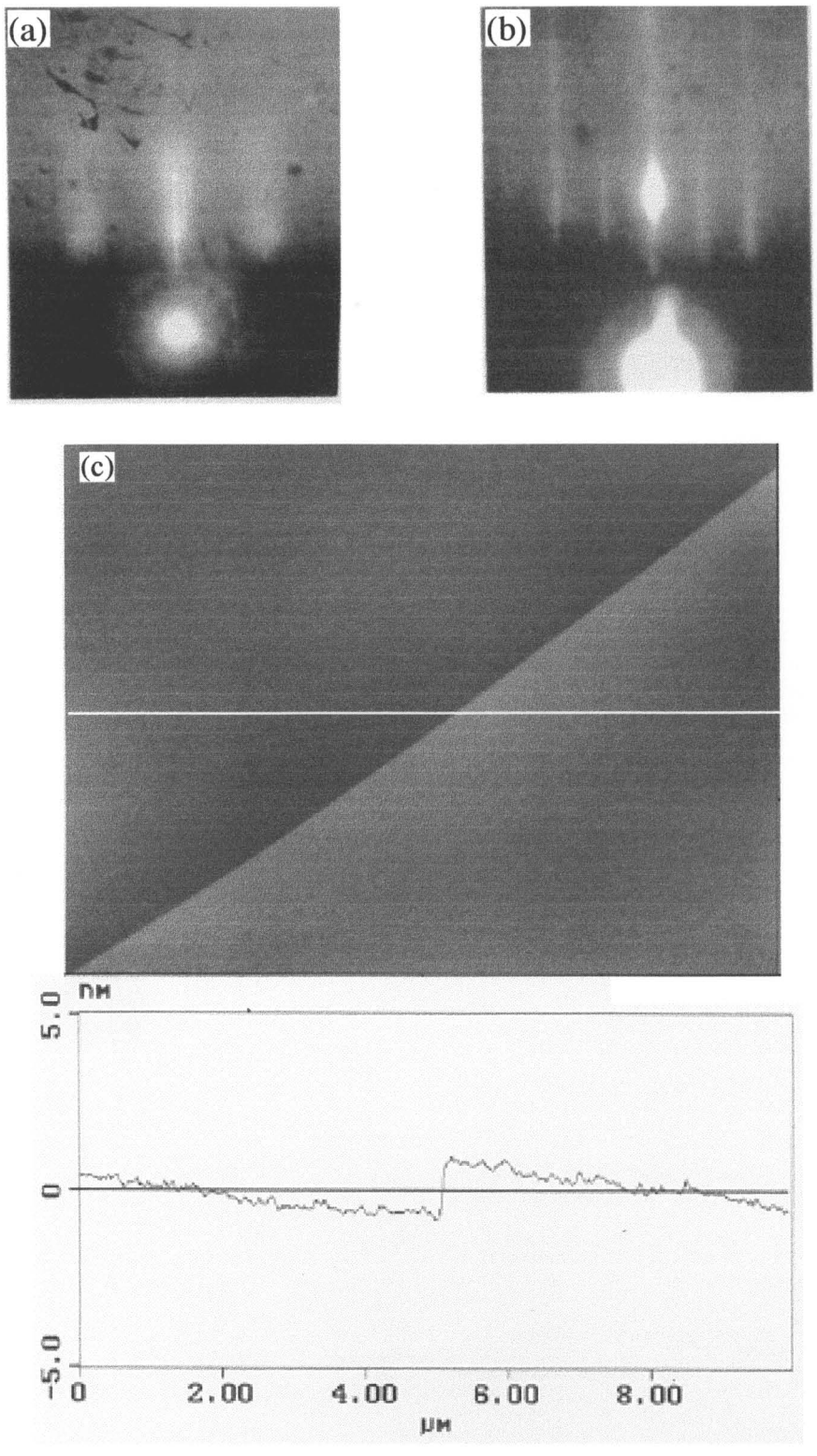

Figure 3-3 RHEED patterns with the incident beam parallel to the (a) [100] and (b) [010] direction and (c) AFM images and the cross sectionof the cleaved surface of $Bi_2Sr_2CaCu_2O_8$ single crystal .

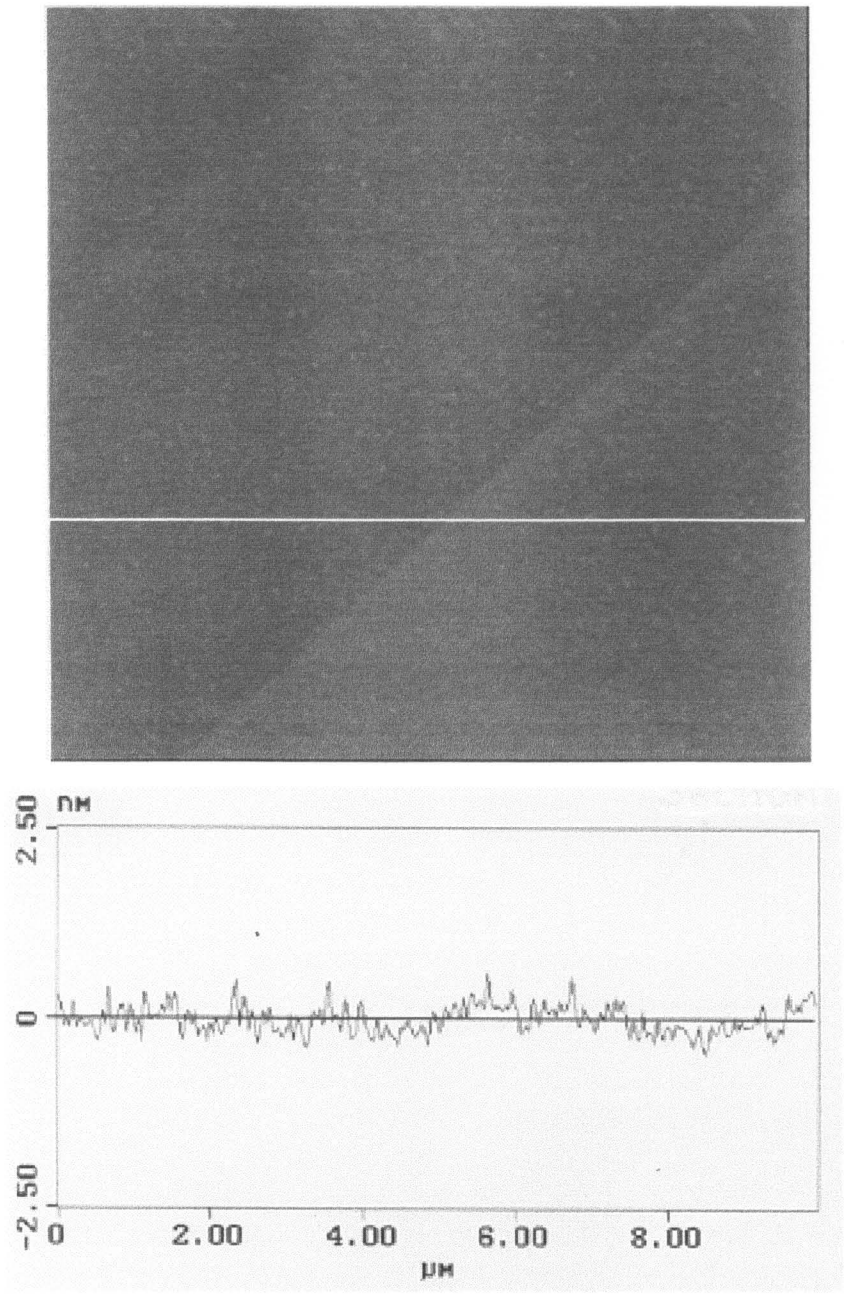

Figure 3-4 AFM images and the cross section of the surface of $CaTiO_3$ thin film deposited on the cleaved surface of $Bi_2Sr_2CaCu_2O_8$ single crystal. The corrugation on the terrace is about 2-3 Å

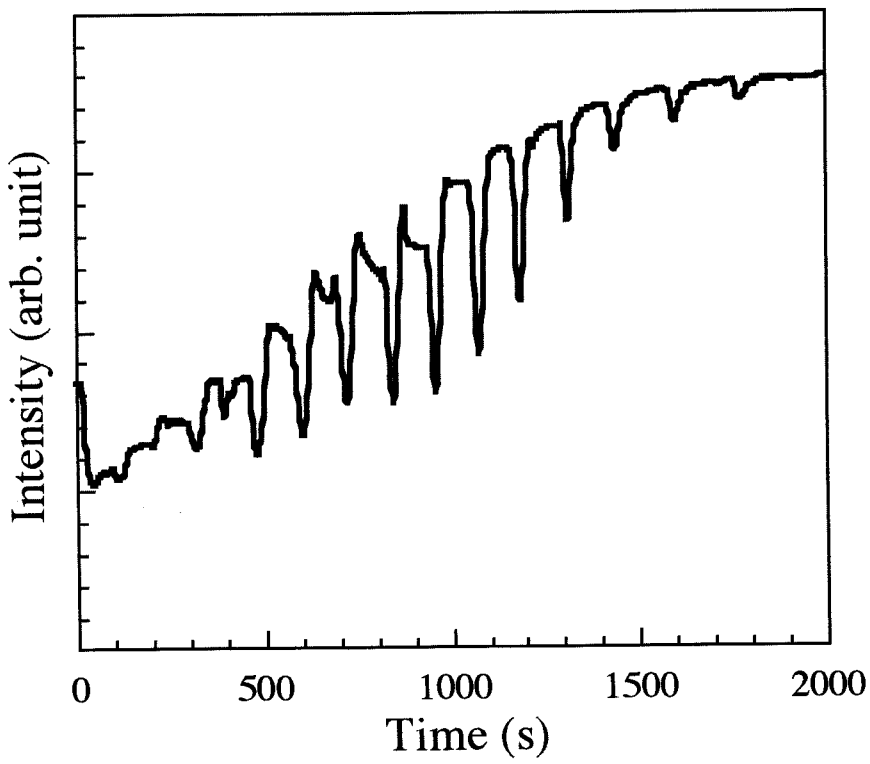

Figure 3-5 RHEED intensity oscillation during the deposition of $CaTiO_3$ thin film on the cleaved surface of $Bi_2Sr_2CaCu_2O_8$ single crystal. One intensity oscillation corresponds to one molecular layer growth of $CaTiO_3$.

well-defined tunneling barrier. Fig. 3-4 (b) is the AFM image of the surface of a $CaTiO_3$ thin film on Bi2212. It shows that the surface consists of flat terraces with the corrugation of about 2-3 Å and straight steps as well as the cleaved surfaces. The step height is close to 3.8 Å which is unit cell height of $CaTiO_3$. The oscillation of specular spot in RHEED pattern was clearly observed during the deposition as shown fig. 3-5. One period of the oscillation correspond to the growth of one molecular layer [20]. Thus, the thickness of $CaTiO_3$ thin films can be exactly evaluated. Judging from the experiments described above, the junctions we prepared now have better quality with respect to the flatness of the barrier layer than the planar type SIN junctions fabricated before [3-5]. Tunneling measurements were performed on these junctions.

3. 3. 2 Data and analysis

In conventional tunneling model, normalized differential conductance in SIN junction, G_{ns}/G_{nn}, is given by

$$G_{ns} / G_{nn} = N_n(0)^{-1} \int_{-\infty}^{\infty} N_s(E) \left[-\frac{\partial f(E+eV)}{\partial (eV)} \right] dE \quad (1)$$

where $N_s(E)$ and $N_n(E)$ is a density of state (DOS) of the superconductor and normal metal, respectively, and $f(E)$ is Fermi function [21]. The tunneling spectrum of $Bi_2Sr_2CaCu_2O_8/CaTiO_3$/Ag junction at 15 K is showed in Fig. 3-6. Clear conductance peaks are observed at about 27 meV. The structure in the gap has larger intensity than the prediction from the BCS theory. The ratio between the differential conductance at zero and that at 100 mV is about 0.27. This value is considerably larger than the value predicted by conventional tunneling model described by eq. (1). Figure. 3-7 shows the resistance of this junction near zero bias. In the temperature above T_c, the zero bias resistance of junction (Rj) is independent of temperature. It shows that Rj is governed by a tunneling process. Rj temporarily decreased just below the T_c and increases in the lower temperature region. This Re curve indicates that excess current begins to flows just below T_c, and this phenomena can be qualitatively understood by taking Andreev reflection into account [22, 23]. As shown in Fig. 3-8, in

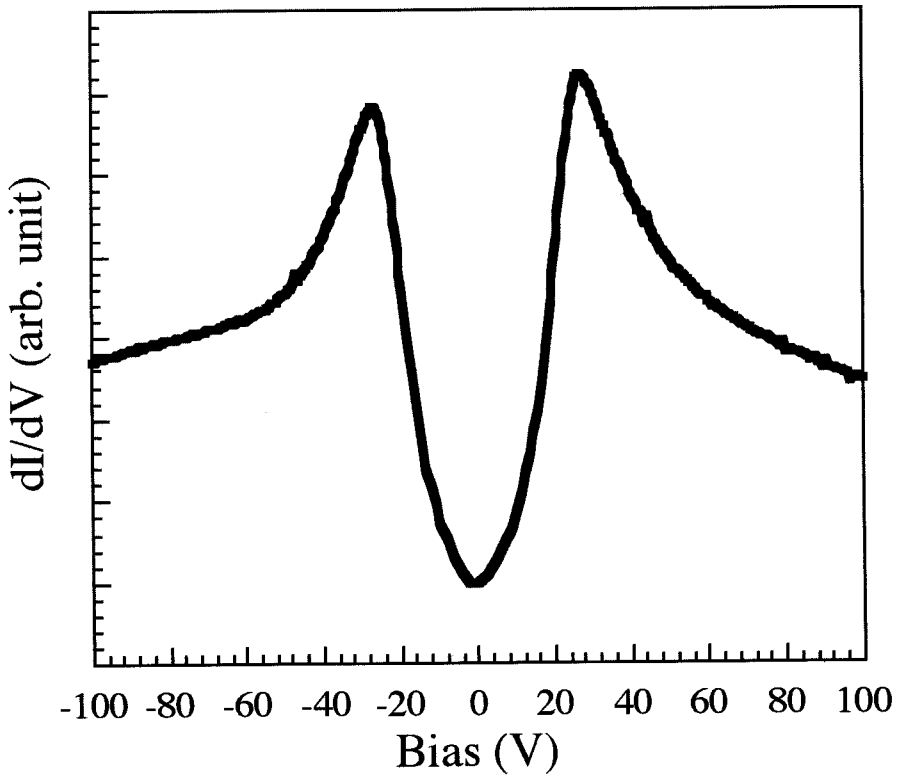

Figure 3-6 dI/dV-V curve measured at 15K. The area of the junction is 0.5×0.5 mm2. The thickness of $CaTiO_3$ is about 20 Å.

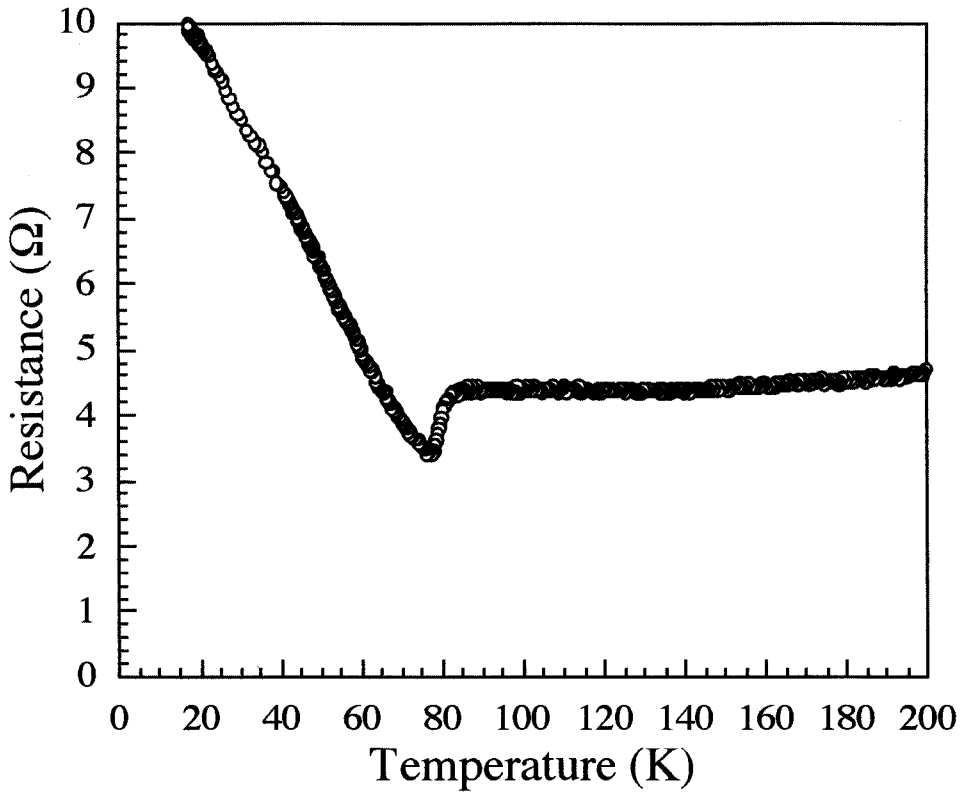

Figure 3-7 Temperature dependence of the resistance for $Bi_2Sr_2CaCu_2O_8/CaTiO_3/Ag$ junction.

superconductor-normal metal (SN) junction, if the electron in the normal metal at energy E < Δ reach the interface, they cannot enter as quasi-particles because there are no quasi-particles states in the gap. Instead, they pass through as Cooper pairs, and are reflected back into the normal metal as holes by the request of charge conservation law. As a result, total 2e charge transfer across the interface into the superconducting Cooper pair condensation state, which process increase conductance twice as that in the normal state if all incident electrons pass through a SN interface by this process. This transfer process was firstly introduced by Andreev [22, 23]. Because $CaTiO_3$ layer is extremely thin and has low resistance in our system, Andreev reflection should be considered. The analysis of tunneling spectra based on an s-wave including Andreev reflection was performed by Matsumoto et al., there are, however, few studies which analyze tunneling spectra based on d-wave including Andreev reflection with planar type junction. Thus, I calculated the conductance by the extension of Blonder-Tinkham-Klapwidjk (BTK) formula to d-wave. In BTK formula, normalized junction conductance including Andreev reflection is given by

$$G_{ns} / G_{nn} = N(0)^{-1}(1+z^2)\int_{-\infty}^{\infty}\left[-\frac{\partial f(E+eV)}{\partial(eV)}\right][1+A(E,\Delta,z)-B(E,\Delta,z)]dE \quad (2)$$

where Δ is the value of superconducting gap, z is barrier potential parameter of SN interface, A(E, Δ, z) and B(E, Δ, z) are the probability of Andreev reflection and normal reflection [16]. A(E, Δ, z) and B(E, Δ, z) based on s-wave have the following forms:

$$A(E,\Delta,z) = \frac{\Delta^2}{E^2+(\Delta^2-E^2)(1+2z^2)^2} \quad (3)$$

$$B(E,\Delta,z) = 1-A(E,\Delta,z) \qquad \text{for } E<\Delta \qquad (4)$$

and

$$A(E,\Delta,z) = \frac{u_0^2 v_0^2}{\gamma^2} \quad (5)$$

$$B(E,\Delta,z) = \frac{(u_0^2-v_0^2)^2 z^2(1+z^2)}{\gamma^2} \qquad \text{for } E>\Delta \qquad (6)$$

with

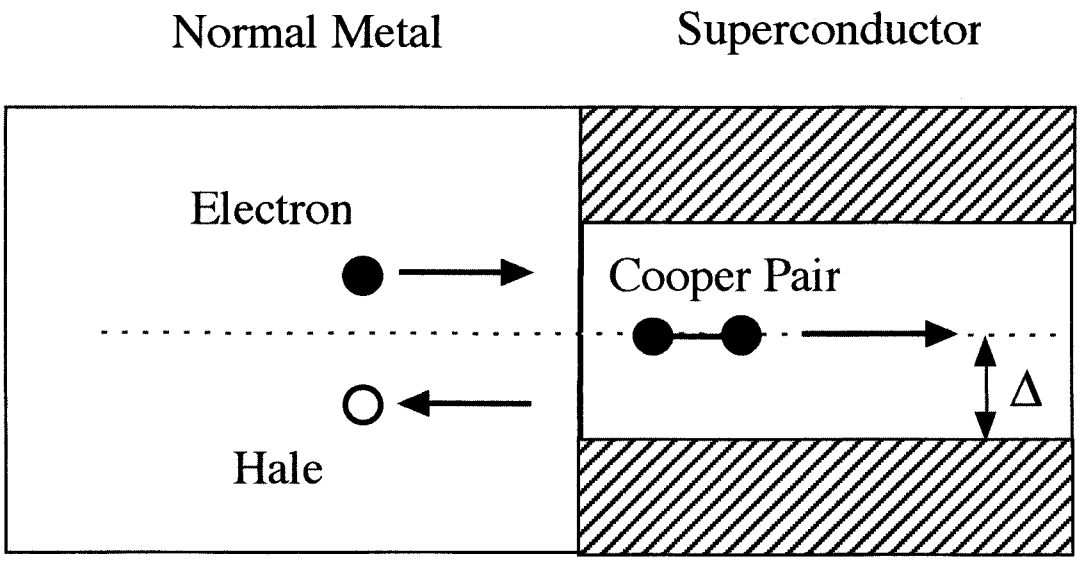

Figure 3-8 Schematic illustration of the process of Andreev reflection. This process increase conductance of junctions.

$$\gamma^2 = \left[u_0^2 + Z\left(u_0^2 - v_0^2\right)\right]^2 \qquad (7)$$

and

$$u_0^2 = 1 - v_0^2 = \frac{1+\sqrt{\left(E^2-\Delta^2\right)/E^2}}{2} \qquad (8)$$

Now I extend eq. (2) to apply to anisotropic Δ in k-space as below.

$$G_{ns}/G_{nn} = N(0)^{-1}(1+z^2)\int_{-\infty}^{\infty}\left[-\frac{\partial f(E+eV)}{\partial(eV)}\right]\left[1+\alpha(E,\Delta_0,z)-\beta(E,\Delta_0,z)\right]dE \qquad (9)$$

with

$$\alpha(E,\Delta_0,z) = \int_E^{\Delta_0} D(\Delta)a(E,\Delta_0,z)d\Delta + \int_0^E D(\Delta)b(E,\Delta_0,z)d\Delta$$

$$\beta(E,\Delta_0,z) = \int_E^{\Delta_0} D(\Delta)c(E,\Delta_0,z)d\Delta + \int_0^E D(\Delta)d(E,\Delta_0,z)d\Delta$$

where a(E, Δ_0, z) and c(E, Δ_0, z) are A(E, Δ, z) and B(E, Δ, z) for E < Δ, and b(E, Δ_0,z) and d(E, Δ_0, z) are A(E, Δ, z) and B(E, Δ, z) for E > Δ respectively. D(Δ) is the gap density function that of line node d-wave is given by

$$D(\Delta) = \begin{cases} \dfrac{2}{\pi\sqrt{\Delta_0^2-\Delta^2}} & \text{for } |\Delta| < \Delta_0 \\ 0 & \text{for } |\Delta| > \Delta_0 \end{cases} \qquad (10)$$

More detailed explanation of $D(\Delta)$ is described in chapter 4. With eq. (2) and (9), the conductance curves were calculated based on both s-wave and d-wave as symmetry of the pair potential. Figure 3-9 shows calculated tunneling conductance compared with the measured conductance spectrum. The barrier potential parameter, z, was determined to fit the peak height at $\pm\Delta$ of the calculated curve with that of the observed spectra. A calculated curve based on s-wave symmetry does not fit the experimental conductance curve even if Andreev reflection is in consideration with any barrier potential parameter z . The experimental curve has larger intensity in the gap than the calculated curve based on an s-wave. The calculated curve based on the d-wave with z = 2.0 agrees with the observed gap structure. Figure 3-10

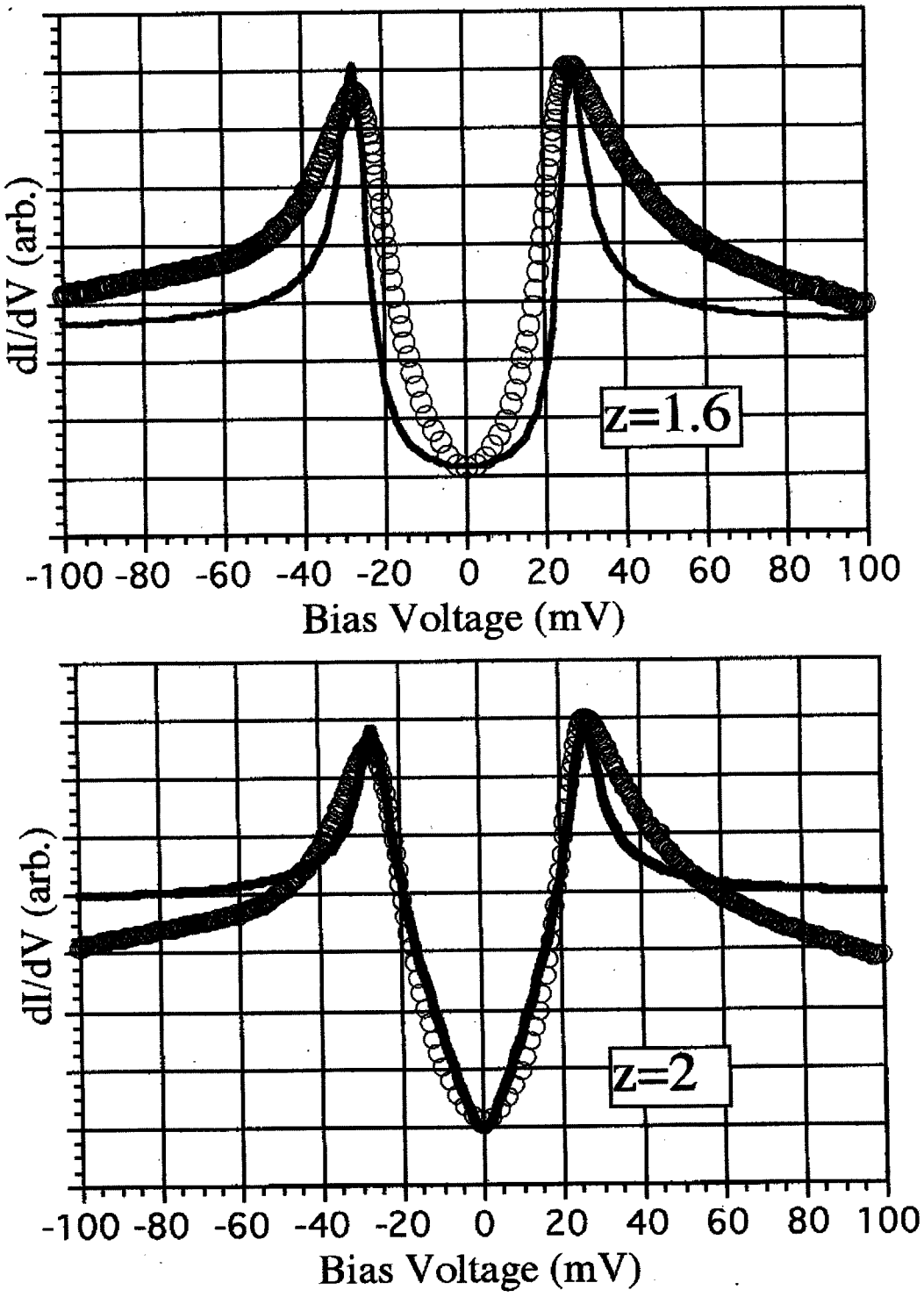

Figure 3-9 The same dI/dV-V curve in Fig. 3-6 (open circles). Thick lines are (a) s-wave fitting curve (Δ = 27 meV, z = 1.6, T = 15K) and (b) d-wave fitting curve (Δ = 27 meV, z = 2.0, T = 15K).

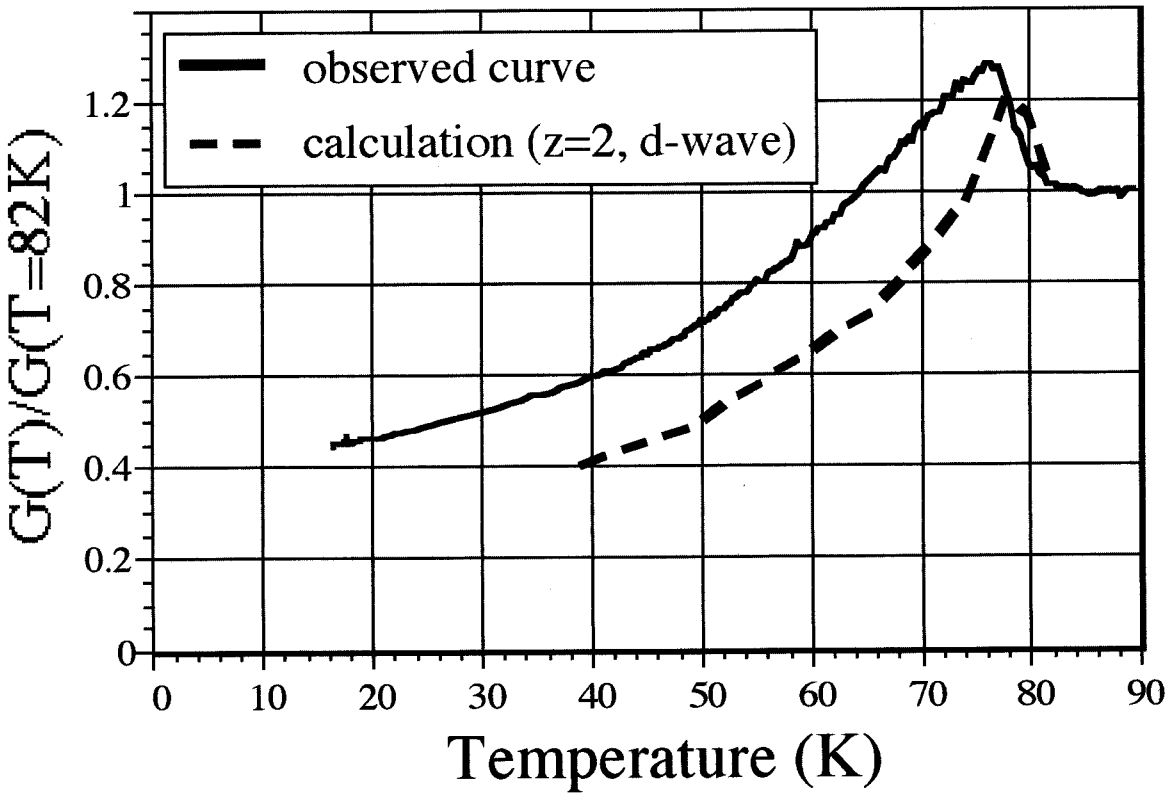

Figure 3-10 Comparison between measured conductance of the junction (solid line) and calculated one (dashed line) considered Andreev reflection with same parameters as these used in Fig. 3-9.

shows the temperature dependence of the conductance curve of this junction and calculated temperature dependence of conductance curve with ex. (9) and $z = 2.0$ which is same as that of the fitting curve in fig. 3-9. The increase of the conductance at T_c and the behavior below T_c are qualitatively reproduced, which shows that the value of the barrier potential parameter z used in my analysis of the tunneling conductance curve is appropriate. Namely, tunneling spectrum of the planar type tunneling junction with well-defined $CaTiO_3$ barrier layer fabricated in this study indicates line node d-wave symmetry as the pair potential. There are, however, some discrepancies between the observed spectra and the fitting curve. In particular, the conductance peaks at $\pm\Delta$ are broader than the calculations, and the observed differential conductance in the low bias region in the gap does not exactly fit linear spectra predicted for a d-wave symmetry. Hereafter it is necessary to fabricate the barrier layer which has high resistance enough for neglecting Andreev reflection, and verify contributions of some other factors which were not considered now, e.g. a lifetime of quasi particle, anisotropy of DOS in normal state, etc., to tunneling spectra.

3. 4 Conclusion

I prepared $CaTiO_3$ thin films on the cleaved surfaces of $Bi_2Sr_2CaCu_2O_8$ single crystals and investigated surfaces of $Bi_2Sr_2CaCu_2O_8$ single crystals and $CaTiO_3$ thin films in detail by RHEED and AFM. These investigations showed that these junctions had well-characterized $CaTiO_3$ tunneling barrier. On these junction, tunneling spectra with superconducting gap structures and clear conductance peaks at gap edge were obtained. Observed differential conductance had larger intensity in the gap than the prediction by a conventional tunneling model and we analyzed the spectra by the fitting including Andreev reflection. The result showed that line node d-wave was more suitable than s-wave as the symmetry of pair wave function.

References

1. J. I. Gorina, G. A. Kaljujnaia, V. I. Ktitrov, V. P. Martovisky, V. V. Rodin, V. A. Stepanov, A. A. Tsvetkov, and S. I. Vendneev, Solid state comun. 85, 695 (1993)
2. L. Buschmann, M. Boekhot, and G. Guntherodt, Physica C 203 68 (1992)
3. K. Takahashi. K. Shimaoka, K. Yamamoto, T. Usuki, Y. Yoshisato, and S. Nakano. Jpn. J. Appl. Phys. 31, 231 (1992)
4. H. J. Tao, A. Chang, Farun. Lu, and E. L. Wolf, Phys. Rev. B 45, 10622 (1992)
5. T. Matsumoto, Supab. Choopun, and T. Kawai, Phys. Rev. B 52, 591 (1995)
6. A. M. Cucolo, R. Di. Leo, A. Nigro, P. Romao, and F. Bobba, Phys. Rev. Lett. 76, 1920 (1996)
7. C. Manabe, M. Oda, and M. Ido, Physica C 235-240, 797 (1991)
8. Ch. Renner and Ø. Fisher, Phys. Rev. B 51, 9208 (1995)
9. H. Murakami and R. Aoki, J. Phys. Soc. Jpn. 64, 1287 (1995)
10. K. Ichmura and K. Nomura, J. Phys. Soc. Jpn. 62, 3661 (1993)
11. A. Chang, Z. Y. Rong, Y. M. Ivanchenko et al., Phys. Rev B 46, 5692 (1992)
12. J. Liu, Y. Li, and C. M. Lieber, Phys. Rev. B 49, 6234 (1994)
13. Y. Kitaoka, K. Ishida., and K. Asayama, J. Phys. Soc. Jpn. 63, 2052 (1994)
14. D. A. Wollman, D. J. Van Harlingen, W. C. Lee, D. M. Ginsberg, and A. J. Leggett, Phys. Rev. Lett. 71, 2134 (1993)
15. C. C. Tuei, J. R. Kirtley, M. Rupp, J. Z. Sun, A. Gupta, M. B. Ketchen, C. A. Wang, Z. F. Ren, J. H. Wang, and M. Bhushan, Sience 271, 329 (1996)
16. T. Yokoya and T. Takahashi, Phys. Rev. B 53, 14055 (1996)
17. Z. X. Chen, Phys. Rev. Lett. 70, 1553 (1993)
18. K. Kitazawa, Science 271, 313 (1996)
19. I. Shigaki, K. Kitahama, K. Shibutani et al., Jpn. J. Appl Phys. 29, L2013 (1990)
20. J. H Neave, B. A. Joyce, P. J. Dobson et al., Appl. Phys. A 31, 1 (1983)
21. M. Tinkham, Introduction to Superconductivity (McGrow-Hill, New York, 1975)
22. A. F. Andreev, Sov. Phys. JETP 19, 1228 (1964)

23. G. E. Blonder, M. Tinkham, T. M. Klapwijk, Phys. Rev. B 25, 4515 (1982)

24. Y. Tanaka, S. Kashiwaya, Phys. Rev. Lett. 74, 3451 (1995)

25. Y. Tanaka, S. Kashiwaya, Phys. Rev. B 53, 9371 (1996)

Chapter 4

Tunneling Studies by Low Temperature STM/STS with Superconducting Whisker Tip

Abstract

To realize SIS junction, I designed new type superconductor / insulator / superconductor junction with well-defined vacuum barrier, namely scanning tunneling spectroscopy (STS) on the cleaved surface of $Bi_2Sr_2CaCu_2O_8$ single crystal with superconducting whisker tip. The SIS gap structure was observed in the tunneling spectrum by this method. This tunneling spectrum was analyzed by the calculations based on an s-wave and a d-wave pairing symmetry. As a result, the observed spectrum could be explained by d-wave symmetry.

4. 1 Introduction

Many tunneling measurements have been performed from both applicative and basic interest. In basic studies, superconductor-insulator- normal metal (SIN) [1-8], or superconductor-normal metal-normal metal (SN'N) junctions were usually used [9]. Superconductor-insulator-superconductor (SIS) junctions were scarcely used except for some studies because it is very difficult to prepare well-defined barrier layer [10]. SIS junction requires much higher quality of the barrier layer than SIN junction, because a few pin holes are responsible for superconductive leak current enough to suppress the information of electronic state. The fabrication of SIS junction is, however, important for not only applications but also basic researches. Since the signal around the superconducting energy gap is enhanced in SIS spectra compared with SIN spectra, the difference between s-wave and d-wave appears more clearly [11]. To realize SIS junction, I designed new type SIS junction with vacuum barrier , which is scanning tunneling spectroscopy (STS) on the cleaved surface of $Bi_2Sr_2CaCu_2O_8$ (BSCCO) single crystal with BSCCO whisker as a STM tip. Since this technique utilizes the well-defined vacuum barrier without pinholes or interdiffusion, it is expected to obtain reproducible and reliable spectra. Though some experimental studies using SIS junctions have already performed, the surface structure which was the interface of the junction could not be observed, so that the condition of junction interface which is the very important factor for the tunneling measurement was not confirmed in these reports [11]. In my study, it was confirmed that the BSCCO whisker tip had enough potential to observe surface structure, which means that the junctions can be fabricated at the selected points in the surface. SIS gap structure was observed by this method, and investigation concerning the pairing symmetry was performed. As a result, observed tunneling spectra can be explained by assuming d-wave as the pair symmetry.

4. 2 Experimental

Fig. 4-1 shows the schematic configuration of the low temperature STM system [12]. Both a sample and a tip were cooled at about 70 K with liquid N_2 with a vacuum pumping. Bi2212 whisker was supplied from Dr. I. Matsubara of Industrial Research Institute of Osaka Prefecture [14]. The schematic illustration of the crystal direction of BSCCO whisker is

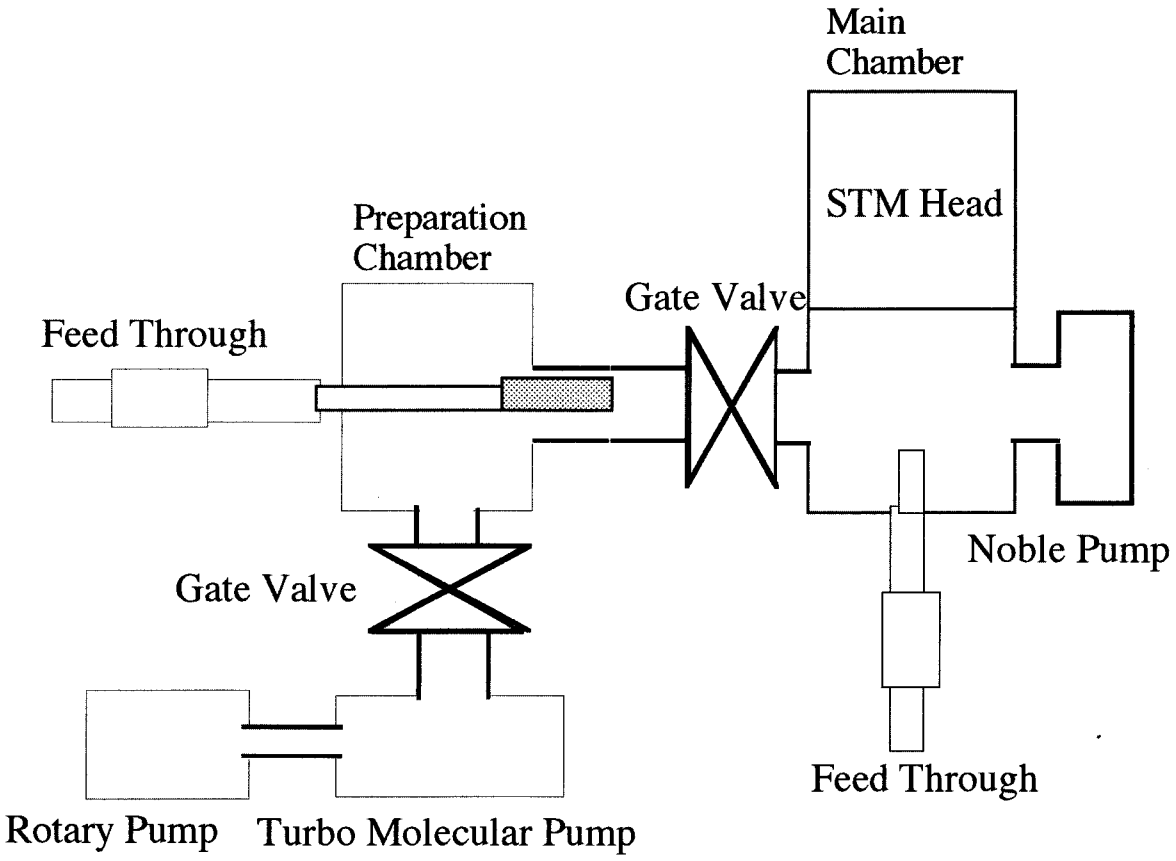

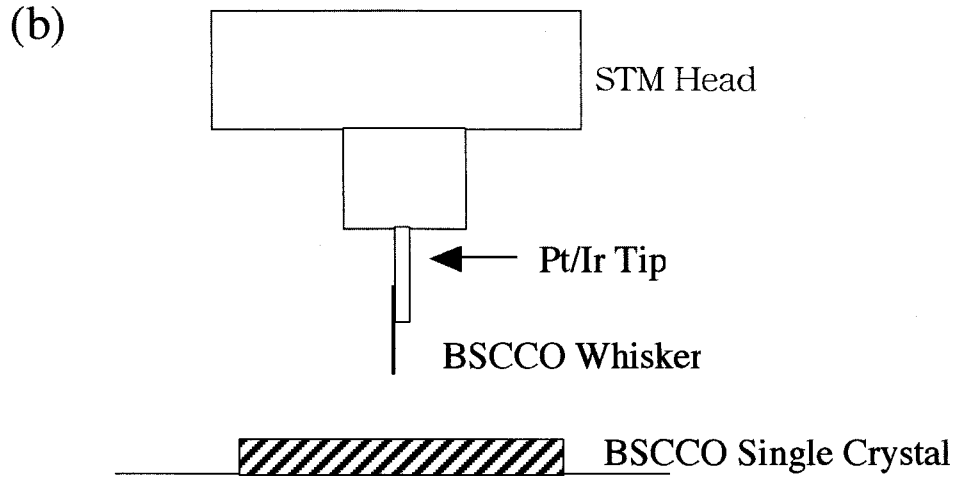

Figure 7-1 (a) Illustration of the low temperature STM apparatus. The pressure of the preparation chamber and the main chamber are about $1x10^{-7}$ mbar and $1x10^{-10}$ mbar, respectively. (b) Schematic configuration of BSCCO whisker tip and the sample in the main chamber of the low temperature STM.

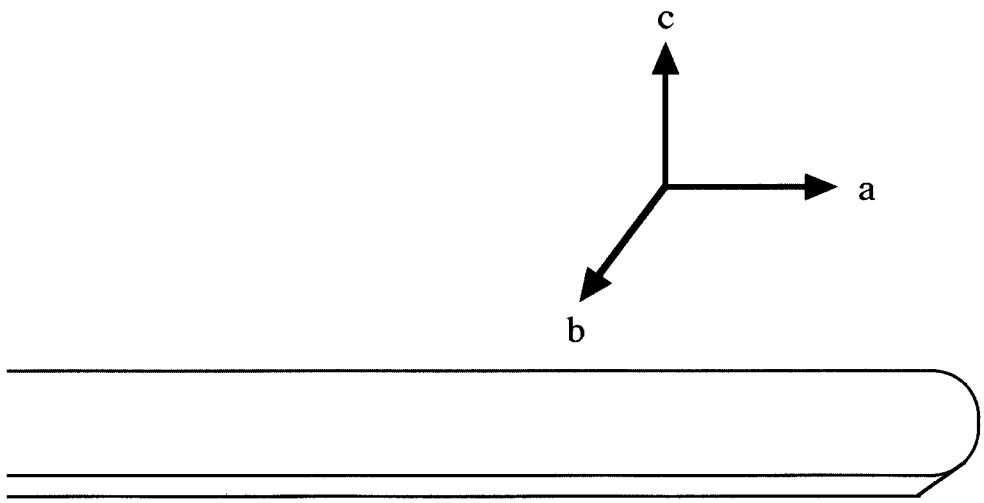

Figure 4-2 Schematic illustration of the crystal direction of BSCCO whisker. The top of the crystal is in the a-axis direction.

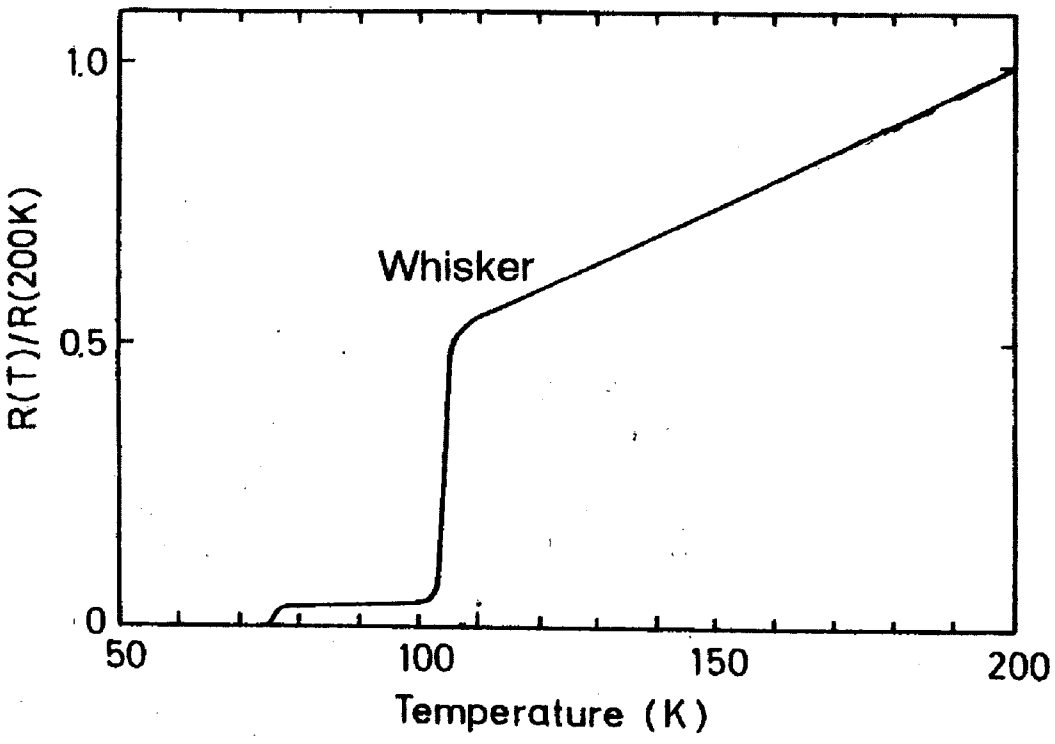

Figure 4-3 Normalized resistance-temperature curve of the whisker. This curve shows that the whisker is a mixture of $Bi_2Sr_2CaCu_2O_8$ phase with T_c of 75 K and $Bi_2Sr_2Ca_2Cu_3O_{10}$ phase with T_c of 105 K.

shown in Fig. 4-2. The top of the whisker needle is along a-direction. Fig. 4-3 is a resistance-temperature curve of the whisker. It shows that the whisker is the mixture of $Bi_2Sr_2CaCu_2O_8$ (Bi2212) phase with T_c of 75 K and $Bi_2Sr_2Ca_2Cu_3O_{10}$ (Bi2223) phase with T_c of about 105 K [14]. This whisker was glued to Pt/Ir tip by silver paste. The photograph of this whisker tip is shown in Fig. 4-4. To remove the degraded part of the whisker, the top of the whisker tip was cut off in air and immediately transferred to the vacuum chamber. As a first step, STM/STS measurements were performed at room temperature on the Au (100) surface in order to investigate property of the whisker tip. After that, the cleaved surfaces of BSCCO single crystals were observed with the whisker tip at 70K. BSCCO single crystal was prepared by traveling solvent floating zone (TSFZ) method and the T_c was 86 K [13]. This single crystal was cleaved in the preparation chamber at the pressure of 1×10^{-7} mbar and transferred into the main chamber with the base pressure of 1×10^{-10} mbar and then, the system was cooled down to 70 K with liquid nitrogen. The surface images and tunneling spectra were measured with the whisker tip. The spectra were analyzed by fitting based on an s-wave and a d-wave.

4. 3 Results and Discussion

4. 3. 1 Tunneling measurement with the whisker tip

Fig. 4-5 shows the dI/dV spectrum obtained on cleaned Au (100) surface with the whisker tip at room temperature. Since the density of state (DOS) of Au is nearly constant around the Fermi level, this spectrum reflects the DOS of the whisker. Judging from the spectrum, DOS of the whisker has finite value at Fermi level. This result indicates that the DOS of the metallic behavior of CuO_2 plane which is electronic conducting layer of Bi2212 is reflected in the spectrum. Next, the cleaved surface of BSCCO single crystal was observed with the superconducting whisker tip at 70 K. Fig. 2-6 shows the STM image of the cleaved surface of Bi2212 single crystal observed with the whisker tip. The incommensurate superstructure in the cleaved surface with a periodicity of 25 Å along the b direction was clearly observed [7]. These results shows that the whisker have enough potential for the

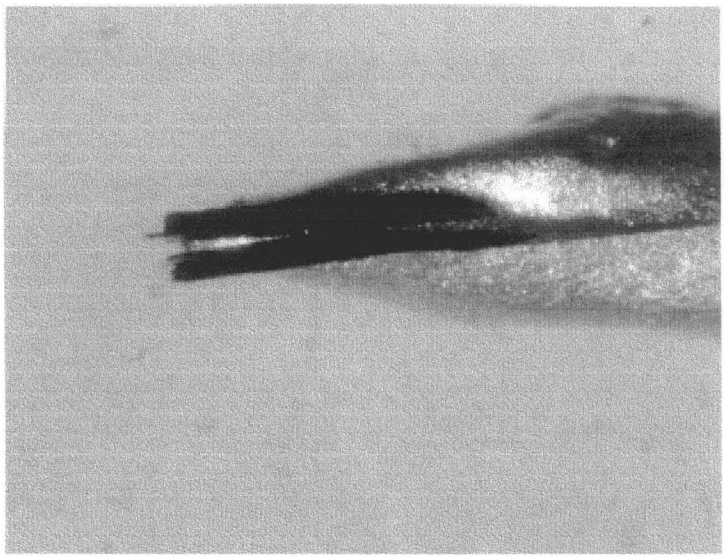

Figure 4-4 Photograph of BSCCO whisker tip. BSCCO whisker is glued to Pt/Ir tip by silver paste.

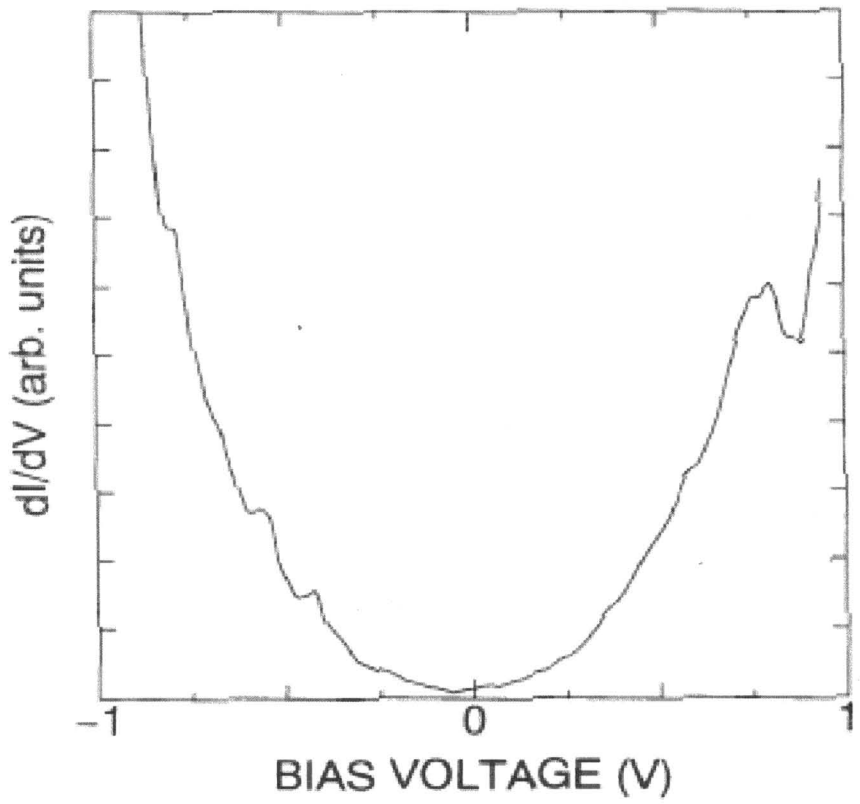

Figure 4-5 dI/dV-V spectrum obtained on the surface of Au with the whisker tip at room temperature. This spectra shows that the top of the whisker has a metallic character.

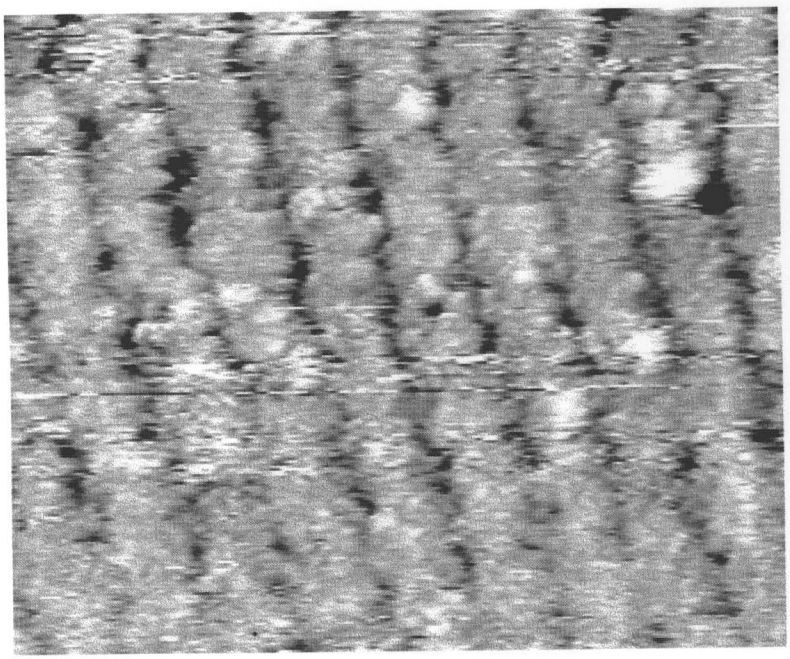

Figure 4-6 STM image of the cleaved surface of $Bi_2Sr_2CaCu_2O_8$ single crystal observed with a superconducting whisker tip at 70 K. Incommensurate superstructure with periodicity of 25 Å along b-axis direction was clearly observed.

measurement of reliable spectra as a STM tip. Tunneling spectra were measured in this condition and the gap structure was obtained as shown in Fig. 2-7. The dI/dV-V curve shows that the gap edge of the observed spectrum is at ±60 meV. The gap value obtained by SIS junction is the sum of the superconducting energy gaps (Δ) of two superconductors which are both sides of the barrier. The past STS measurements with normal metal tip on cleaved surface of B2212 report that the value for the gap in c direction (Δ_c) is 24-30 meV at 4.2K and temperature dependence of Δ can be explained by conventional BCS theory [7, 9]. From these reports, Δ_c of the cleaved surface of Bi2212 (T_c = 85 K) at 70 K is estimated to be Δ_c = 15-18 meV. On the other hand, the energy gap for the whisker tip should be Δ along the a-axis (Δ_a), because in the top of top of the whisker is in the a direction. The Δ_a of Bi2212 was measured by J. Kane et al using STS, and the value of about 40 meV was reported at 4.2 K. [9] Thus, Δ_a of Bi2212 whisker (T_c = 75 K) is estimated to be about 15 meV at 70 K according to the BCS-type temperature dependence. In these estimation, the value for SIS gap should be 30-33 meV, which is inconsistent with the measurement and about the half of the observed value for the observed gap. I think that the disagreement is responsible for the inter growth of Bi2223 phase in the whisker. Resistance-temperature curve in Fig. 3 shows the existence of Bi2223 phase (T_c = 105 K) in BSCCO whisker. Assuming that Δ is in proportion to T_c (this assumption can be roughly applied to various superconductor), Δ_a of Bi2223 is estimated at 50 meV at 0 K and 45 meV at 70 K. In this case, the value of SIS gap is about 60 meV which agree with the observed gap well. Thus I used the values of Δ_c = 15 meV for the single crystal and Δ_a = 45 meV for whisker tip in the following calculation. The observed STS spectra was analyzed by the fitting based on conventional semiconductor model under consideration of an s-wave and a d-wave pair symmetry.

4. 3. 2 Data analysis

The tunneling current was calculated by conventional semiconductor model. The current equation is given by

$$I = \frac{2\pi e}{\hbar}|T^2|\int_{-\infty}^{+\infty} N_1(E)N_2(E+eV)[f(E)-f(E+eV)]dE \qquad (1)$$

where T is tunneling matrix , $N_1(E)$ and $N2(E)$ is DOS of the sample and the tip, and $f(E)$ is

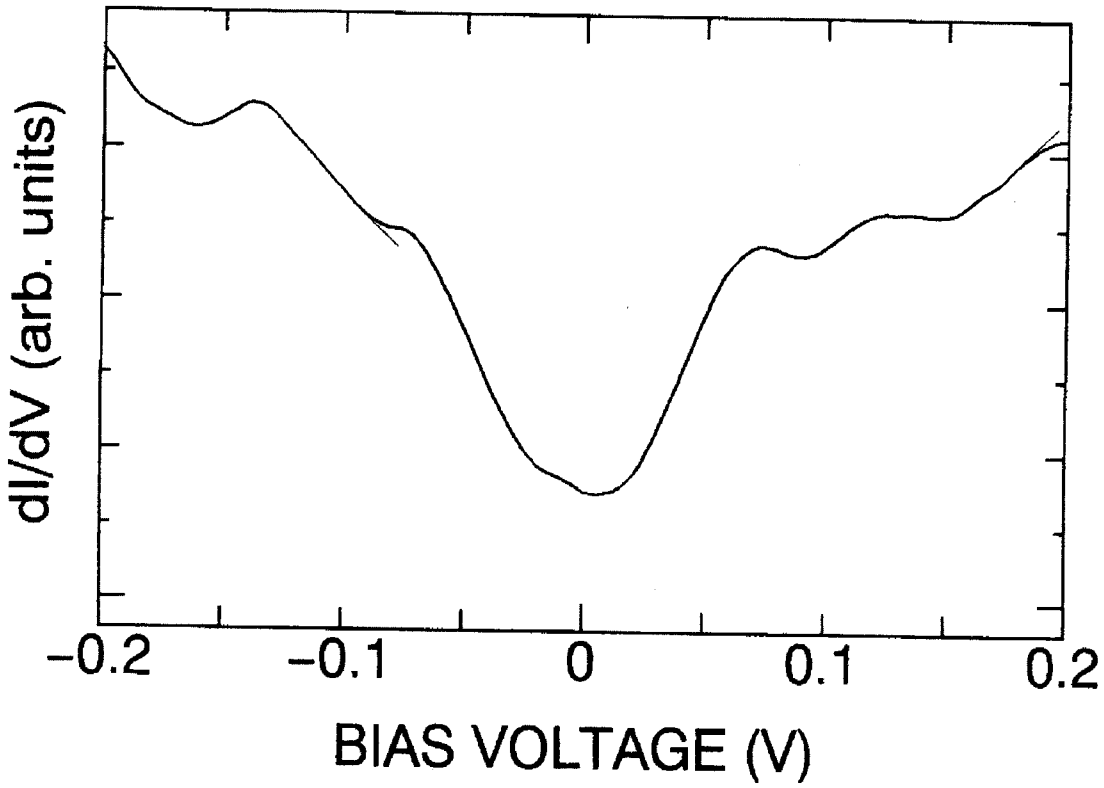

Figure 4-7 dI/dV spectrum obtained on the surface of BSCCO single crystal with the whisker tip at 70 K. The superconducting gap structure of the SIS junction was observed. The value of the gap was about 60 meV.

Fermi function [15]. The superconducting DOS, *N(E)*, of an s-wave is given by

$$N(E)/N_n = \mathrm{Re}\left[\frac{E}{\sqrt{E^2-\Delta^2}}\right] \qquad (2)$$

where Re means real part, Δ is the value of the superconducting gap and N_n is DOS of normal state which is almost constant [15]. For the calculation of the DOS of a d-wave model, I followed the way reported in reference 4. At first, gap density function D(Δ) is introduced. It is given by

$$A\int d\Omega\delta(\Delta'-\Delta(k)) \equiv D(\Delta') \qquad (3)$$

where Ω is solid angle. A is normalization factor which is chosen as satisfying the following condition of

$$\int D(\Delta')d\Delta' = 1 \qquad (4)$$

The superconducting DOS is generally described with D(Δ) as following form

$$N(E)/N_n = \int_0^E D(\Delta)\frac{E}{\sqrt{E^2-\Delta^2}}d\Delta \qquad (5)$$

In case of the line node d-wave, Δ is given by

$$\Delta(\theta) = \Delta_0 \cos 2\theta \qquad (6)$$

where ø is the azimuth and Δ_0 is maximum value of Δ. D(Δ) was calculated by eq. (3), and obtained as

$$D(\Delta) = \begin{cases} \dfrac{2}{\pi\sqrt{\Delta_0^2-\Delta^2}} & \text{for } |\Delta| < \Delta_0 \\ 0 & \text{for } |\Delta| > \Delta_0 \end{cases} \qquad (7)$$

As a result, from eq. (5) and (7) the DOS of a line node d-wave superconductor is given by

$$N(E)/N_n = \int_0^E \frac{2}{\pi\sqrt{\Delta_0^2-\Delta^2}}\frac{E}{\sqrt{E^2-\Delta^2}}d\Delta \qquad (8)$$

The eq. (2) or eq. (8) were substituted for eq. (1) in order to calculate tunneling currents and the fitting curves were obtained by differentiating this calculated tunneling current. The results of fitting based on both an s-wave and a d-wave were shown in Fig. 4-8. The fitting indicates the calculation based on an s-wave cannot explain the spectrum and the calculation based on d-wave essentially fit the observed spectrum. Namely, the tunneling spectra obtained from the SIS junction with a vacuum barrier indicate that pairing symmetry is d-wave like.

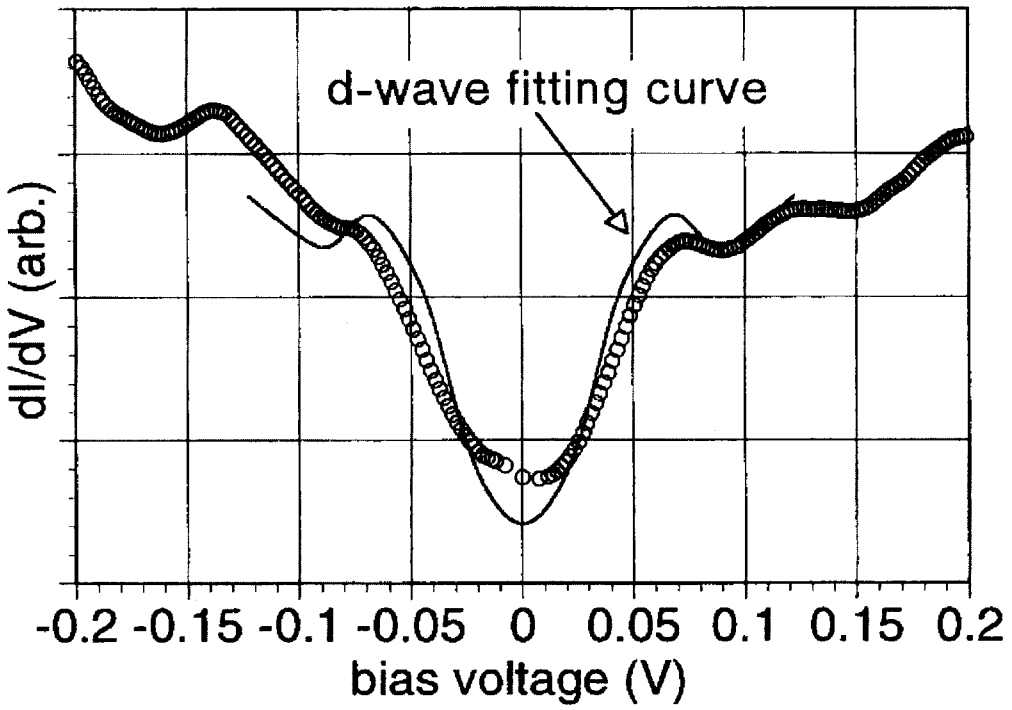

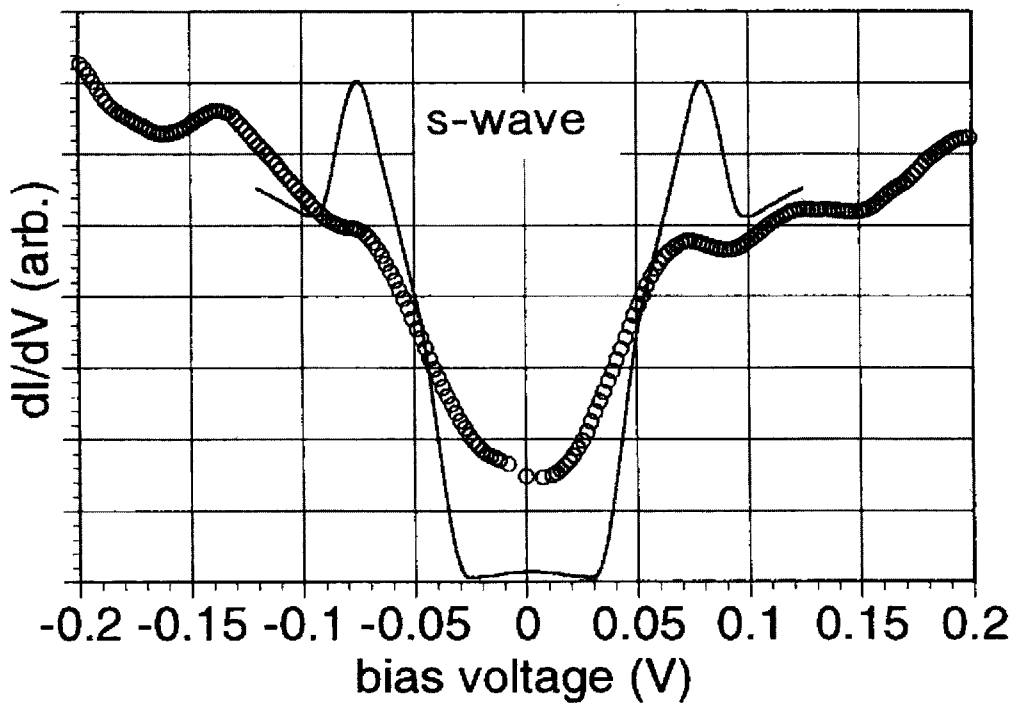

Figure 4-8 Fitting of the spectrum shown in Fig. 4-7 with the calculation of (a) d-wave and (b) s-wave model.

These results are consist with tunneling study with planar junctions described in chapter 3.

4. 4 Conclusion

In this study, I fabricated HTSC/insulator/HTSC junction with well defined vacuum barrier utilizing STS setup for the first time. Such a junction was realized by using BSCCO whisker as a STM tip. I succeeded the observation of the superstructure of cleaved surface of BSCCO single crystal with this superconducting whisker tip. The result shows that the whisker can sufficiently work as a STM tip. Since leak current can be neglected in this junction with vacuum barrier, reliable SIS tunneling spectra can be obtained. The observed tunneling spectra can be essentially explained by d-wave model, which agree with the recent reports of NMR, π-junction, angle resolved photo emission [16, 17] and the results in chapter 3.

References

1. J. I. Gorina, G. A. Kaljujnaia, V. I. Ktitrov, V. P. Martovisky, V. V. Rodin, V. A. Stepanov, A.A. Tsvetkov, and S. I. Vendneev, Solid state comun. 85, 695 (1993)
2. L. Buschmann, M. Boekhot, and G. Guntherodt, Physica C 203 68 (1992)
3. H. J. Tao, A. Chang, Farun. Lu, and E. L. Wolf, Phys. Rev. B 45, 10622 (1992)
4. K. Ichmura and K. Nomura, J. Phys. Soc. Jpn. 62, 3661 (1993)
5. A. M. Cucolo, R. Di. Leo, A. Nigro, P. Romao, and F. Bobba, Phys. Rev. Lett. 76, 1920 (1996)
6. C. Manabe, M. Oda, and M. Ido, Physica C 235-240, 797 (1991)
7. Ch. Renner and Ø. Fisher, Phys. Rev. B 51, 9208 (1995)
8. H. Murakami and R. Aoki, J. Phys. Soc. Jpn. 64, 1287 (1995)
9. T. Matsumoto, Supab. Choopun, and T. Kawai, Phys. Rev. B 52, 591 (1995)
10. A. M. Cucolo, R. Di. Leo, P. Romao, Phys. Rev. B 44, 2857 (1991)
11. Qun Chen and K.-W. Ng, Phys. Rev. B 45, 2569 (1992)
12. T. Nakagawa, H. Tanaka and T. Kawai, Surf. Sci. 370, L144 (1997)
13. I. Shigaki, K. Kitahama, K. Shibutani et al., Jpn. J. Appl Phys. 29, L2013 (1990)
14. I. Matsubara Doctor Thesis Osaka Univ. (1994)
15. M. Tinkham, Introduction to Superconductivity (McGrow-Hill, New York, 1975)
16. Y. Kitaoka, K. Ishida., and K. Asayama, J. Phys. Soc. Jpn. 63, 2052 (1994)
17. D. A. Wollman, D. J. Van Harlingen, W. C. Lee, D. M. Ginsberg, and A. J. Leggett, Phys. Rev. Lett. 71, 2134 (1993)

Chapter 5

Properties of c-axis Josephson Tunneling between $Bi_2Sr_2CaCu_2O_8$ and Nb

Abstract

I have fabricated well-defined c-axis $Bi_2Sr_2CaCu_2O_8$ (BSCCO) /Au/Nb junctions on cleaved surfaces of BSCCO single crystal and observed typical current-voltage characteristics of Josephson tunnel junctions. A magnetic field dependence of the supercurrent shows that a zero bias current is not a leakage from some pin-holes, but a Josephson current. These results strongly indicate a presence of an s-wave component at the surface of BSCCO. The results of the temperature dependence of the Josephson current indicate that the superconducting gap for the s-wave component in BSCCO is about 10^{-3} of the d-wave component, and that the T_c of the s-wave is about 10K.

5. 1 Introduction

A large number of studies have shown that the order parameter of HTSC predominantly has a $d_{x^2-y^2}$ symmetry [1, 2]. Studies in chapter 3 and 4 also showed tunneling conductance spectra were explained by the d-wave model. However, some experiments demonstrated the existence of Josephson coupling between $YBa_2Cu_3O_7$ and a conventional s-wave superconductor perpendicular to the CuO_2 planes with high-quality Josephson tunnel junctions [3, 4]. In such a junction a d-wave component is forbidden by the symmetry to contribute to the lowest order Josephson current, so that the observed current is due to a s-wave component of YBCO. These results can mainly be explained as a result of an orthorhonbic lattice distortion of YBCO as shown in Fig. 5-1 (a). This distortion allows a coupling between an s-wave and a d-wave and thereby forms a d+s state [5]. However, the results of such an experiment using heavily-twined YBCO also indicate the possibility of the presence of an additional s-wave component which is not originated in the distortion since the average of over all twin should yield a zero critical current if the presence of s-wave component is due to only the distortion. Furthermore, recently reported experiments and theory indicate the presence of various subdominant symmetries as an intrinsic nature of HTSC independent of structural distortions [6-8]. Therefore, it is much important to investigate whether there is an s-wave component in HTSC without the effect of structural distortions.

In this paper I shall report on the properties of c-axis Josephson junctions with BSCCO and Nb in order to elucidate this subject. Though BSCCO also has a structural distortion due to the incommensurate modulation of the BiO layer, this distortion can not induce an s-wave component because the direction of distortion is at an angle of 45° from the direction of CuO bonds, unlike in the case of YBCO as shown in Fig. 5-1. Moreover, the cleaved surface of BSCCO single crystal is atomically flat and ideal c-axis Josephson junctions with a specular interface can be fabricated. Therefore this material is considered to be most appropriate for our study. There are some reports concerning c-axis Josephson junction with BSCCO single crystals. The report by Durusoy *et al.* showed that a significant Josephson coupling could not be measured between BSCCO and Pb in the c direction [9]. In contrast to this result,

(a)

In the case of YBCO

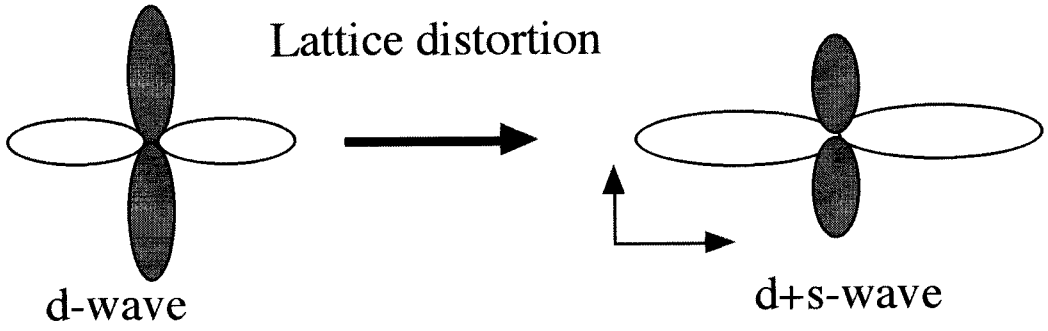

(b)

In the case of the BSCCO

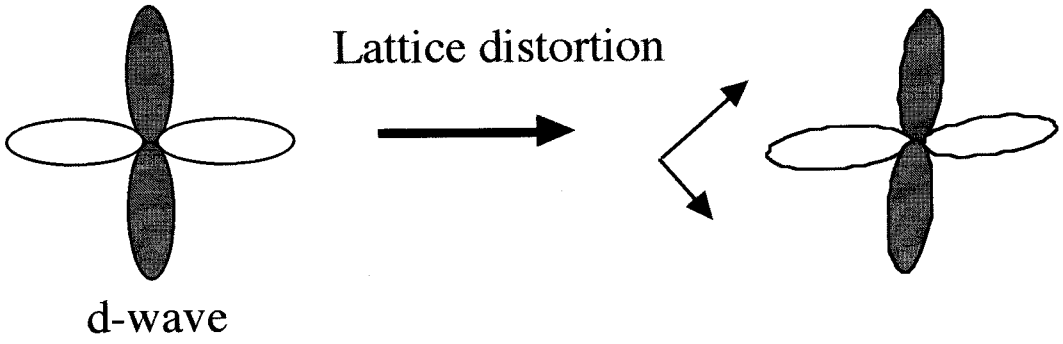

Figure 5-1 Schematic drawing of order-parameter distortion in (a) YBCO and (b) BSCCO. In the case of YBCO, the lattice distortion can produce an s-wave component as shown in Fig. 5-1 (a), because s-wave and d-wave belong to the same representation of the crystal symmetry group. However, in the case of BSCCO, s and d-wave belong to different representation group because the direction of distortion is 45° different from that of YBCO as shown in Fig. 5-1 (b).

Kleiner *et al.* reported a significant Josephson current in c-axis BSCCO/Pb junction [10, 11]. In both studies, the surface of BSCCO was exposed to air before the fabrication of junctions. In order to fabricate a well-defined c-axis junction, it is important not to expose the surface of BSCCO to air in order to avoid degradation at the interface of junctions because the coherent length of BSCCO is shorter and it is easy to be affected by surface degradations compared with YBCO. Moreover, it is most important for the purpose of our study to exclude current parallel to CuO_2 plane, because such a current can flow even if the symmetry of BSCCO is pure d-wave. Therefore, in this study, we have taken much attention to reducing the roughness and degradation at interfaces of junctions and fabricated well-defined c-axis Josephson tunnel junctions. Consequently I have observed an appreciable supercurrent along the c-axis in several junctions. Judging from current-voltage characteristics and the modulation of the current under the magnetic field, it is clear that the current is not a leakage from some pin-holes but a Josephson current. These results strongly indicate the presence of an s-wave component in HTSC without any structural distortion. Moreover, the value of the gap and the critical temperature of the s-wave component in BSCCO were estimated by the results of the temperature dependence of the Josephson current. The results showed that the gap and the T_c of the s-wave component are much smaller than those of the d-wave component.

5. 2 Josephson Effect between an s-wave and a d-wave

In 1962, Josephson made the prediction that a zero voltage supercurrent

$$I_c = I_0 \sin(\varphi_1 - \varphi_2) \qquad (1)$$

should flow between two superconductors separated by a thin insulating barrier. Here φ_1 and φ_2 are the phase of the wavefunction of Cooper pair in two superconductors and I_0 is maximum supercurrent which can be passed by the junction. Figure 5-2 shows schematic configuration of a Josephson junction and a typical current-voltage characteristics of Josephson junctions. It is important for the studies of a pair symmetry that Josephson current, that is a zero voltage supercurrent, depends on the phase difference φ_1 - φ_2 because the sign change of d-wave,

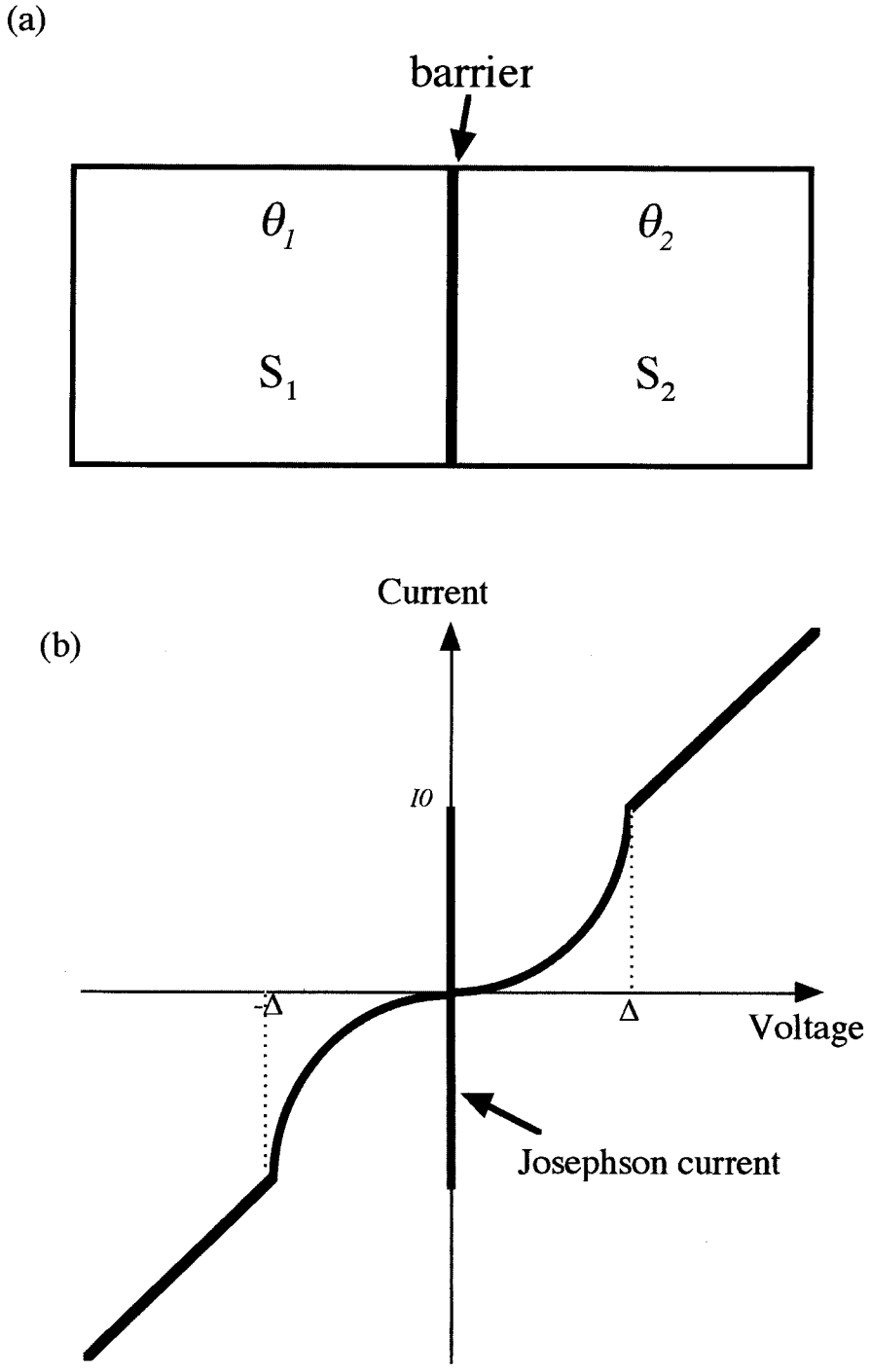

Figure 5-2 (a) Schematic configuration and (b) current - voltage characteristic of typical Josephson junction. S1 and S2 are two superconductors separated by a thin barrier layer, and $\theta 1$ and $\theta 2$ denote phases of superconducting wave functions of S1 and S2.

which corresponds to phase shift of π under 90° rotation, lead to different characteristics of Josephson currents from that of an s-wave superconductor in some case. For example, the Josephson current between an s-wave and a $d_{x^2-y^2}$-wave superconductor cannot flow perpendicular to x-y plane as described below. Roughly speaking, I_c between two superconductors S_1 and S_2 is proportional to $\Delta_1\Delta_2$. Assuming that S_1 and S_2 are s-wave and pure $d_{x^2-y^2}$-wave respectively, $\Delta_1(\theta)$ is constant and $\Delta_2(\theta)$ is given as $\Delta_0\cos 2\theta$ as a function of angle θ in x-y plane. Since

$$\int_0^{2\pi} \Delta_1(\theta)\Delta_2(\theta) = const \cdot \int_0^{2\pi} \Delta_0 \cos 2\theta \cdot d\theta = 0 \qquad (2)$$

then Josephson current I_c comes to zero within a first order approximation, that is to say, Josephson current between a s-wave superconductor and HTSC in c direction is responsible for s-wave component in HTSC. In this chapter, I quantitatively estimated amount of a s-wave component in HTSC by using this character of a Josephson junction.

5. 3 Experimental

The BSCCO single crystal used in this experiment was prepared with a traveling solvent floating zone method. This BSCCO crystal is a Ca rich sample with Sr to Ca ratio of 1.4: 1, because the largest single domains have been prepared with this ratio. Therefore, the BSCCO crystals used in this experiment are in slightly under-dope region with T_c of 80 K. The properties of BSCCO single crystals prepared in my laboratory were reported elsewhere [12]. Samples were cleaved in a vacuum chamber under a typical pressure of 1×10^{-7} mbar and Au was deposited to cover the surface of BSCCO using the laser sputtering method without exposing to air. The thickness of Au film was about 12 nm. Subsequently, the surface was coated with photoresist to define the area of junction which is 250×250 μm^2 using conventional photolithographic techniques, and a 700-800 nm thick insulating layer of SiO was deposited by the conventional evaporation method. We carefully selected a flat terrace as the position of a junction, because there were usually some large cleavage steps with the height of several hundreds nm in the cleaved surfaces. These large steps expose a-b-edge areas which may cause undesirable Josephson currents in perpendicular to c axis. Following a

liftoff of photoresist and a brief sputtering of the Au surface to remove contaminations, a Nb layer was deposited as a counterelectrode using Ar ion sputtering. The thickness of Au layer finally became about 100 Å in this process. Figure 5-3 shows a schematic illustration of the junctions used in this study. As shown in Fig. 3-4 (a) in chapter 3, a flat terrace of the cleaved surface of BSCCO consists of atomically flat areas and straight steps with a height of less than 15.4 Å corresponding to one molecular layer, and these steps are several tens of μm apart. From the AFM measurement, the edge area from these steps is estimated to be less than 10^{-5} of the area of a-b-plane, therefore Josephson current in the direction of a-b-plane can be neglected in our study.

Current-voltage characteristics of the junctions as a function of temperature were measured using a four-point probe technique. And the magnetic field variation of the Josephson current was measured at 4.2 K.

5. 4 Results and Discussion

5. 4. 1 Characteristics of $Bi_2Sr_2CaCu_2O_8$/Au/Nb Junction

Figure 5-4 shows a typical I-V spectrum of the $Bi_2Sr_2CaCu_2O_8$/Au/Nb junction at 3.7 K. We have observed small but significant Josephson currents and hysteric behaviors in several junctions. The variations of the Josephson current in all junctions were in the range of 1.8 - 8.0 μA and I_cR_n products were in the range of 1.8-4.5 μV. Figure 5-5 shows the differential conductance curve of this junction at 4.0 K in wider bias range. The gap structure can clearly be seen in 1.3 mV in this conductance curve. Judging from the temperature dependence of the value of the gap, this structure must be superconducting gap of Nb. This result shows that the conduction mechanism in our junctions is a tunneling which conserves the momentum of electrons. The barrier layer must have been formed between BSCCO and Au because the contact resistance of the interface between Au and Nb ought to be much lower than the junction resistances in our junctions. Since an Au deposition process was performed in an ultra high vacuum without heating, the barrier layer can not be formed from an oxidation

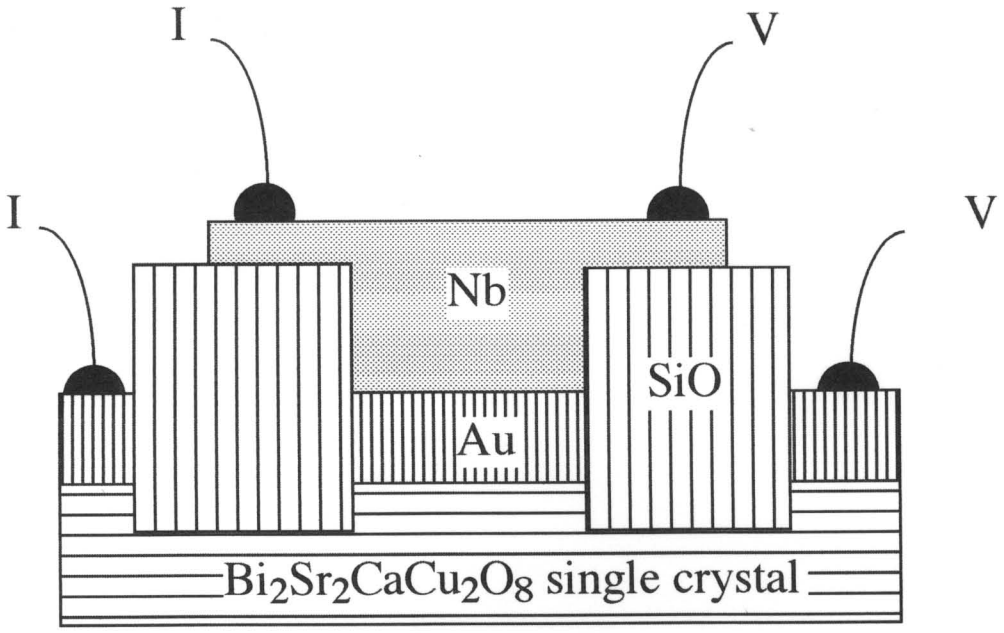

Figure 5-3 Schematic configuration of the c-axis $Bi_2Sr_2CaCu_2O_8$/Au/Nb junction.

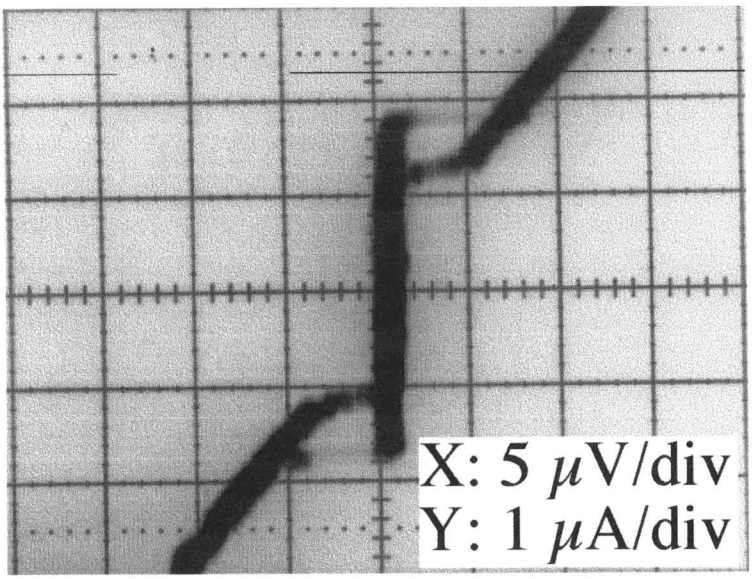

Figure 5-4 Typical I-V characteristics of the c-axis $Bi_2Sr_2CaCu_2O_8$/Au/Nb junction.

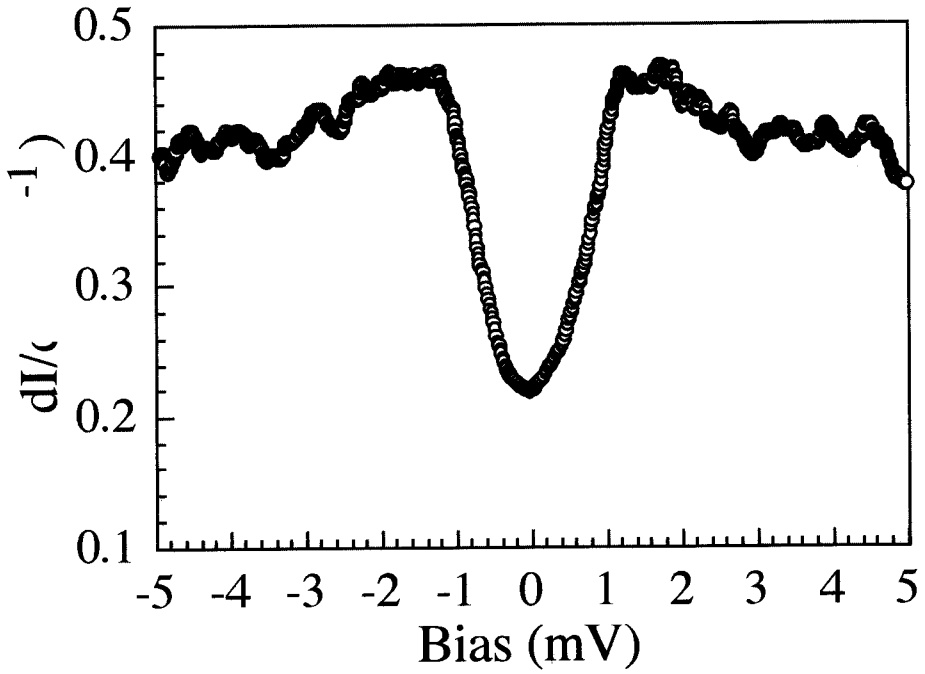

Figure 5-5 Differential conductance spectrum of the c-axis $Bi_2Sr_2CaCu_2O_8$/Au/Nb junction. The gap structure can clearly be seen in 1.3 mV in this conductance curve.

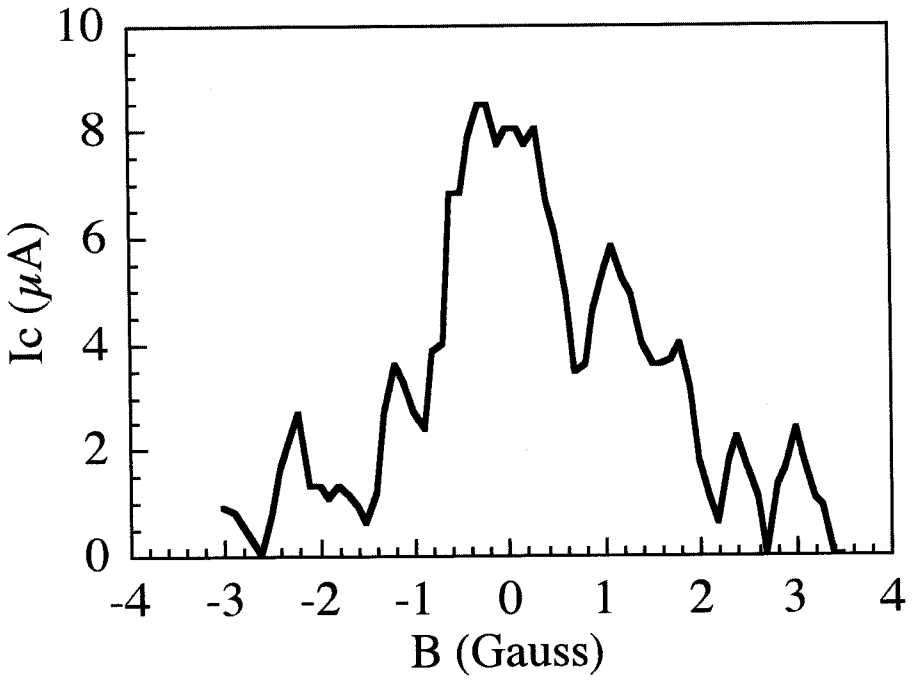

Figure 5-6 Magnetic-field dependence of *Ic* for the c-axis $Bi_2Sr_2CaCu_2O_8$/Au/Nb junction.

and a diffusion of Au. We consider that BiO and SrO layers between CuO_2 layer and Au can be a barrier layer similar to the intrinsic Josephson tunneling junction of BSCCO. Figure 5-6 shows the variation of the Josephson current (I_c) as a function of the applied magnetic field for the junction. The periodic modulation of I_c can be seen. Though this feature is not complete Fraunhofer pattern, the result shows that the supercurrent is not the result of a leakage from some pin-holes. These results strongly indicate the presence of the s-wave component in BSCCO.

5. 4. 2 Data Analysis

Subsequently, I analyzed the temperature dependence of I_c in order to investigate the properties of the s-wave component in BSCCO. We have estimated the value of the gap and T_c of the s-wave component in BSCCO by the fitting of this temperature dependence using the Tanaka-Kashiwaya's formula [13] as shown in fig. 5-7. In this theory, $I_c(T)$ of the c-axis BSCCO/ Nb tunnel junction at two dimensional limits is expressed as

$$I_c(T) = \frac{k_B T}{2R_n e} \sum_n \int_0^{2\pi} d\phi \frac{\Delta_{Nb}(T)\Delta_{BSCCO}(T)}{\sqrt{\omega_n^2 + \Delta_{Nb}^2(T)}\sqrt{\omega_n^2 + |\Delta_{BSCCO}(T)|^2}} \qquad (3)$$

where $\omega = 2\pi k_B T(n+1/2)$ denotes the Matsubara frequency, K_B denotes Boltzmann constant, R_n denotes a normal resistance, and $\Delta_{BSCCO}(T)$ and $\Delta_{Nb}(T)$ denote values of the gap of BSCCO and Nb, respectively. I assumed the s+d wave as the symmetry of BSCCO in our calculation because this formula was derived under the condition in which the time-reversal symmetry was conserved. Therefore the formula could not strictly be applied to d+is-wave which means that the time-reversal symmetry is broken. However, it does not mean that I deny d+is-wave as the symmetry because it seems that there are no significant differences between d+s and d+is in our calculation. Therefore the values of T_c and $\Delta_{s,\,BSCCO}$ obtained by our analysis are considered to be reliable even if d+is-wave is realized in BSCCO. In the case of d+s-wave, Δ_{BSCCO} is given as $\Delta_d\cos(2\phi) + \Delta_{s,\,BSCCO}$ where Δ_d and $\Delta_{s,\,BSCCO}$ are the values of the gap of the d-wave and the s-wave component in BSCCO, respectively. I assume that the temperature dependence of Δ_d, $\Delta_{s,\,BSCCO}$ and Δ_{Nb} follow BCS theory.

At first we assumed that Δ_d is 27 meV and T_c of the d-wave component ($T_{c,d}$) is 80 K,

respectively. These values were taken from our previous tunneling measurements with BSCCO/$CaTiO_3$/Au junctions with the same BSCCO single crystal [14]. T_c of Nb ($T_{c,Nb}$) and Δ_{Nb} were fixed at 9.2 K and 1.4 meV which are typical values obtained at Nb/Al_2O_3/Nb junctions fabricated with our sputtering chamber. In fig. 5-7, we selected 10.6 μeV as $\Delta_{s,BSCCO}$, because this value can reproduce the values of I_cR_N product in lower temperature region of below 4 K. We calculated $I_c(T)$ by using eq. (3) with 9.2 K, 10 K and 30 K as the T_c of s-wave component ($T_{c,s}$) in BSCCO. The results that the calculation with $T_{c,s}$ around 10 K is best suited to our experimental data. At least, $T_{c,s}$ is expected to be less than 30 K. These results mean that the s-wave component in BSCCO has interesting properties as described below. At first, the I_cR_n product shows that the s-wave component in BSCCO is extremely small and the ratio $\Delta_{s,BSCCO}/\Delta_d$ is considered to be about 10^{-3}. Secondly, $T_{c,s}$ is expected to be much less than $T_{c,d}$. This result is also considered to support the consideration that the observed s-wave component is not due to structural deformation, because the s-wave component should have been formed at the same temperature as the d-wave component, supposing the s-wave is induced by structural effect. Furthermore our results of $\Delta_{s,BSCCO}$ and $T_{c,s}$ yield the value of $2\Delta/k_BT_c \sim 10^{-2}$ which is an extremely small one. It is difficult for conventional pairing models to explain such a small value.

Some theoretical studies indicated that a proximity effects of d-wave in c direction can induce an s-wave component [15]. As another possibility, our data can not deny the possibilities of some proximity effects of Nb, because $T_{c,s}$ estimated in our calculations is close to $T_{c,Nb}$. Though I have no positive results to confirm the pairing mechanism of s-wave component, such a small value of s-wave component and $2\Delta/k_BT_c$ may be explained as small proximity attenuated by some proximity or surface effects. However, in a recent report of the properties of Pb/Ag/BSCCO Josephson junctions by Mößle *et al.*[11], they have concluded that the T_c of the s-wave component in BSCCO was about 10K and higher than that of Pb. Therefore, the T_c of s-wave in BSCCO may be universally about 10K without the proximity effects from another superconductor.

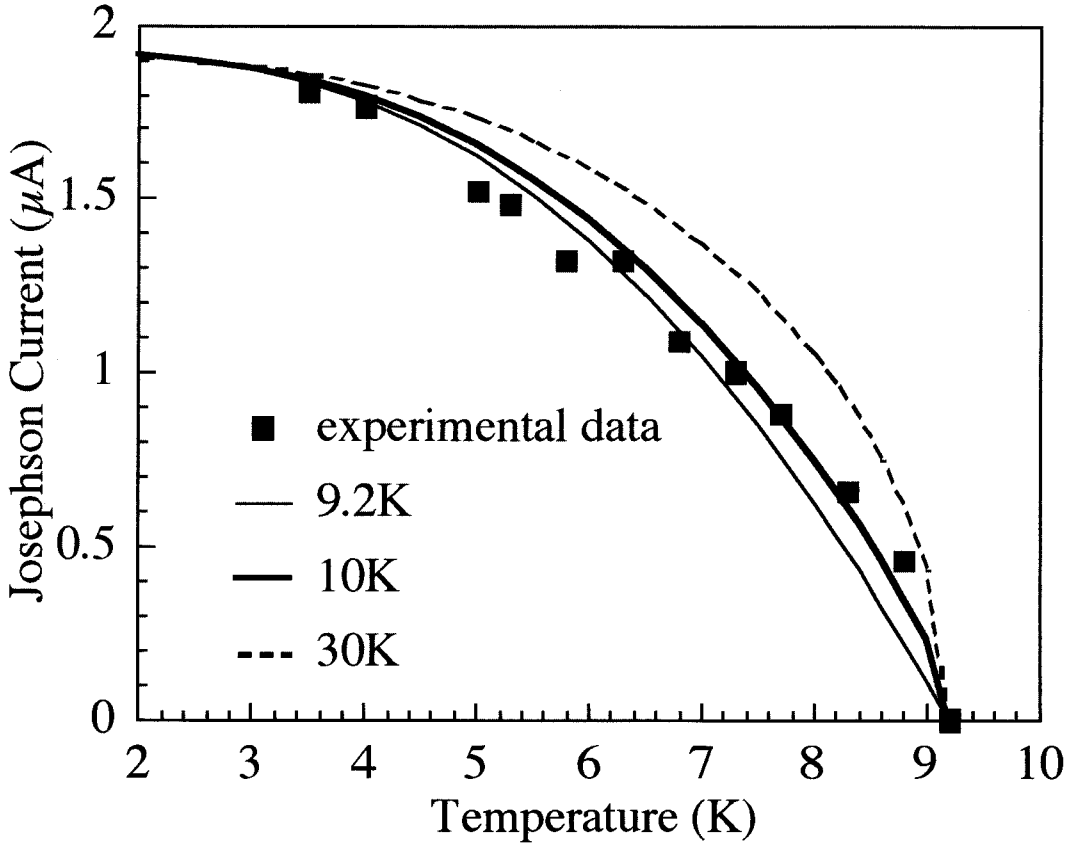

Figure 5-7 Temperature dependence of *Ic* for the c-axis Bi2Sr2CaCu2O8/Au/Nb junction (closed square) and the calculations by using eq.(3) with Δ_{Nb} =1.4 meV, $T_{c,Nb}$ = 9.2 K, Δ_d = 27 meV, $T_{c,d}$ = 80 K, $\Delta_{s,BSCCO}$ = 10.6 μV, and $T_{c,s}$ = 9.2 K (thin line), $T_{c,s}$ = 10 K (thick line) and $T_{c,s}$ = 30 K (dashed line).

5. 5 Conclusion

In this work, I have fabricated the BSCCO/Au/Nb junctions with particular attention to reducing a degradation of interfaces in the junctions. As a result, I have observed significant Josephson currents with these Josephson tunnel junctions for the first time. Such results indicate the presence of the s-wave component in BSCCO. The value of the gap and the T_c of the s-wave component in BSCCO were estimated by the analysis of the temperature dependence of I_c. The results show that the gap of the s-wave component is less than 10^{-3} of that of the d-wave component, and that the T_c of the s-wave component is much lower than that of the d-wave. These results mean that $2\Delta/k_BT_c$ is about 10^{-2} and such a small value could not be explained by any conventional pairing models. Therefore, I have considered that the s-wave is perhaps the result of some proximity effects of the d-wave component in BSCCO or Nb of counter electrode and that . I believe that it is important for understanding of the proximity effects of HTSC to elucidate the origin of the s-wave component.

References

1 D. A. Wallman, D. J. V. Harligen, J. Giapintzakis,D. M. Ginsberg, Phys. Rev. Lett. **74** (1995) 797.

2 J. R. Kirtley, C. C. Tsuei, J. Z. Sun, C. C. Chi, L. S. Yu-Jahnes, A. Gupta, M. Rupp,M. G. Ketchen, Nature **373** (1995) 225.

3 A. G. Sun, D. A. Gajewski, M. B. Maple,R. C. Dynes, Phys. Rev. Lett. **72** (1994) 2267.

4 K. A. Kouznetsov, A. G. Sun, B. Chen, A. S. Katz, S. R. Bahcall, J. Clarke, R. C. Dynes, D. A. Gajewski, S. H. Han, M. B. Maple, J. Giapintzakis, J.-T. Kim,D. M. Ginsberg, Phys. Rev. Lett. **79** (1997) 3050.

5 M. Sigrist, K. Kuboki, P. A. Lee, A. J. Millis,T. M. Rice, Phys. Rev. B **53** (1996) 2835.

6 K. Krishana, N. P. Ong, Q. Li, G. D. Gu,N. Koshizuka, Science **277** (1997) 83.

7 R. B. Laughlin, Phys. Rev. Lett. **80** (1998) 5188.

8 M. Ogata, J. Phys. Soc. Jpn **66** (1997) 3375.

9 H. Z. Durusoy, L. R. Tagirov, Solid State Commun. **97** (1996) 297.

10 R. Kleiner, M. Mößle, W. Walkenhorst, G. Hechtfischer, K. Schlenga,P. Müller, Physica C **282-287** (1997) 2435.

11 M. Möble, R. Kleiner, Phys. Rev. B **59** (1999) 4486.

12 I. Shigaki, K. Kitahama, K. Shibutani, S. Hayashi, R. Ogawa, Y. Kawabe,S. Kawai, Cryo. Eng. **27** (1992) 158.

13 Y. Tanaka, S. Kashiwaya, Phys. Rev. B **56** (1997) 892.

14 I. Kawayama, M. Kanai,T. Kawai, Physica C **298** (1997) 204.

15 S. R. Bahcall, Phys. Rev. Lett. **76** (1996) 3634.

Chapter 6

General Conclusion

The symmetry of the pair wavefunction of high-T_c superconductor (HTSC) have been studied by using tunneling spectroscopy with well-defined barrier layer in this work. As mentioned in General introduction, the pair symmetry provides significant information to investigation of superconducting mechanism, however, it was difficult to fabricate high quality tunneling junction of HTSC with a well-defined barrier layer. I made much efforts to prepare flat barrier layers and some significant information about the symmetry of HTSC was obtained through my work.

In chapter 2, I showed annealing effect on the surface of $SrTiO_3$ (100) substrates and initial growth of $SrCuO_2$ thin films on the $SrTiO_3$ with reflection high energy electron diffraction (RHEED) and atomic force microscopy (AFM). Information of initial growth of oxide thin films on flat substrates is important for preparation of flat barrier layer in tunneling junctions. Atomically flat $SrTiO_3$ (100) substrates with high crystallinity were obtained by annealing at 1000 °C in O_2 atmosphere. The growth of $SrCuO_2$ on the annealed substrates shows interesting behaviors that surface roughness increased in spite of using flat substrate surfaces. By depositing Sr as a buffer layer on the annealed substrates, the flatness of $SrCuO_2$ thin films was improved. These behaviors can be explained by considering properties of surface layer of thin films. Due to the SrO_x buffer layer, it is thought that the topmost layer of $SrCuO_2$ changed from CuO_x to SrO_x. This result indicates that a surface reconstruction of the CuO_x layer prevents thin films from a two-dimensional growth. Consequently, it is concluded that not only substrate flatness but also control of the topmost layer of films is important for preparing flat thin films.

We fabricated trilayer junctions with atomically flat interfaces to obtain intrinsic tunneling spectra along the c direction of the HTSC as shown in chapter 3. At first we prepared $CaTiO_3$ thin films on the cleaved surfaces of $Bi_2Sr_2CaCu_2O_8$ single crystals and investigated surfaces $CaTiO_3$ thin films in detail by RHEED and AFM. These measurements showed that these junctions had well-characterized $CaTiO_3$ tunneling barrier. On these junction, tunneling spectra with superconducting gap structures and clear conductance peaks at gap edge were obtained. It was shown that the observed spectra agree with line node d-wave model considered Andreev reflection.

As shown in chapter 4, I designed new type superconductor / insulator / superconductor (SIS) junction using scanning tunnelling microscopy with a superconducting whisker tip for the first time. I succeeded the observation of the superstructure of cleaved surface of $Bi_2Sr_2CaCu_2O_8$ single crystal with this superconducting tip. The observed tunneling spectra can be essentially explained by d-wave model as the result in chapter 3. This method can measure site selective SIS spectra, and the momentum dependence of tunneling spectra may be measured by changing the angle of a whisker tip, which is difficult for other tunneling methods. In this study, I could not obtained enough stability during the tunneling measurement to realize site selective SIS and angle dependence tunneling, but I believe that this new technique will produce significant information for tunneling and superconductivity, which can not obtain by other methods.

In chapter 3 and chapter 4, I showed that HTSC primarily had d-wave symmetry, but these results can not deny a presence of s-wave component in HTSC. I tried to confirm whether a s-wave component is in HTSC or not, and quantitatively estimate the amount of s-wave as shown in chapter 5. I have fabricated the BSCCO/Au/Nb Josephson junctions with particular attention to reducing a degradation of interfaces in the junctions. As a result, we have observed significant Josephson currents with these Josephson tunnel junctions. Such results indicate the presence of the s-wave component in BSCCO. The value of the gap and the T_c of the s-wave component in BSCCO were estimated by the analysis of the temperature dependence of I_c. The results show that the gap of the s-wave component is less than 10^{-3} of that of the d-wave component, and that the T_c of the s-wave component is much lower than that of the d-wave. I have considered that the s-wave may be the result of some proximity effects of the d-wave component in BSCCO or Nb of counter electrode. We believe that it is important to investigate proximity effects of s-wave superconductor/HTSC junction for not only basic research of superconductivity but also superconducting device. However, it is clear that such a small amount of the s-wave component can not play important role for superconducting mechanism of HTSC.

Though a large number of studies have shown that the order parameter of HTSC

predominantly has a $d_{x^2-y^2}$ symmetry, some studies still regard the contribution of s-wave component as a significant factor of the superconducting mechanism. I showed that the results of the tunneling measurements with a well-defined barrier were also consistent with d-wave model. Furthermore, I quantitatively measured the amount of a s-wave component in BSCCO for the first time and showed that s-wave component is less than 10^{-3} of the d-wave component. These results show that s-wave component is trivial and not important for superconducting mechanism of HTSC and that the tunneling spectroscopy is powerful method for investigation of electronic states in HTSC.

Apendix A

Modification of Cleaved Surfaces of $Bi_2Sr_2CaCu_2O_8$ Single Crystals Induced by ArF Excimer Laser Irradiation

Abstract

The variation of surface morphology and chemical composition of cleaved surfaces of (001) $Bi_2Sr_2CaCu_2O_8$ (BSCCO) crystals was investigated following irradiation in vacuum with an ArF excimer laser. Results were obtained for laser fluences in the range from 20 to 500 mJ/cm^2. Distinctive surface structures of BSCCO have been observed having a strong correlation with the laser fluence and number of pulses delivered to the site. The development of a relatively smooth surface (d~ 20 nm) has been observed for irradiation at 500 mJ/cm^2. The formation of a "hexatic" micro-structure on the surface of ablated crystals suggests that a two-dimensional phase transition has occurred. At lower laser fluences, rough surfaces (0.05 $\mu m < d < 3\ \mu m$) were developed with characteristic pyramids and/or cone-shape islands. The results indicate that surface modification is due to different mechanisms corresponding to the surface temperature being raised by direct laser irradiation and laser heated plasma.

A. 1 Introduction

Laser-induced modification of surfaces of various semiconductors [1, 2] and polymers [3-5], has been investigated in various laboratories because of the relevance of this process to the fabrication of advanced devices. Though some studies involving laser processing of oxide materials have been published to date [6-11], the structural variations of these materials induced by laser irradiation have not been investigated in detail. These studies mainly discussed etch rate as a function of laser fluence and/or pulse number for relatively high laser fluence.

Oxide materials, especially high-T_c superconductors, have considerable potential as next-generation electronic devices fabricated with laser techniques. The success of such an approach will depend on the ability to control the surface morphology of such materials. It is therefore important to study the surface modifications induced by laser irradiation for a wide range of laser fluences, as changes in the surface structure provide important information regarding the mechanism of interaction between the laser light and the surface.

In this report I investigate the structural changes occurring on the (001) $Bi_2Sr_2CaCu_2O_8$ (BSCCO) surface induced by irradiation with an ArF excimer laser. Atomically flat, cleaved surfaces of BSCCO were investigated in this report. This enable us to eliminate extrinsic effects concerning the influence of surface finish resulting from mechanical and/or chemically polishing, on the morphology developed upon laser irradiation. Several types of structures were observed with a strong correlation with the laser fluence and number of pulses delivered to a site.

A. 2 Experiment

The laser-processing chamber was evacuated using a turbomolecular pump. The base pressure in the chamber was 1×10^{-6} mbar. An ArF excimer laser with a wavelength of 193 nm and pulse duration of 15 nm was used in these experiments. The fluctuation of the laser fluence was about ±5%. The laser beam was passed through a 3×3 mm^2 aperture in order to choose a more uniform portion of the beam. The beam was introduced to the chamber through a synthetic silica window and focused on the surface of a sample at normal incidence. The

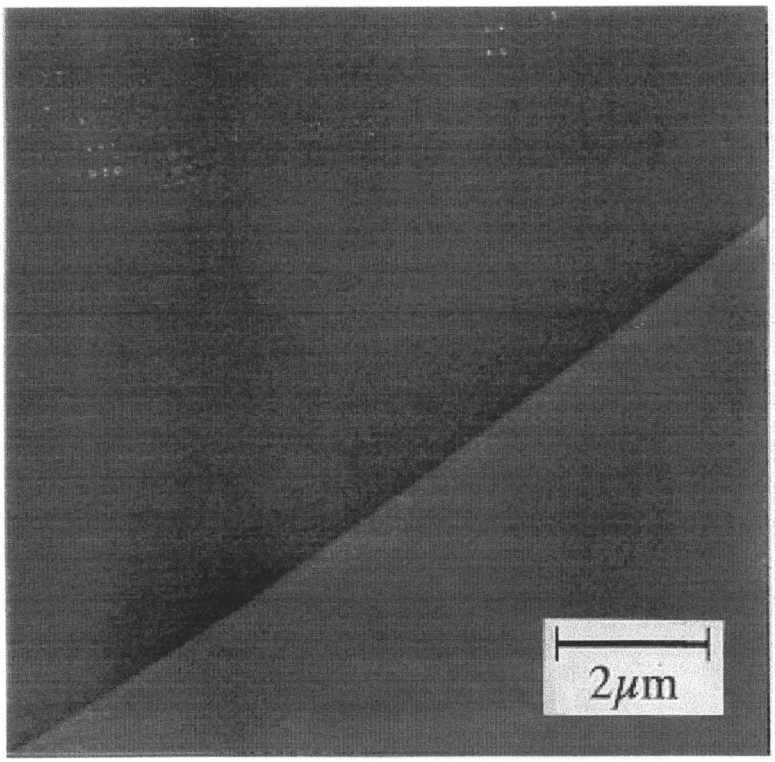

Figure A-1 AFM image of the cleaved surface of a (001) $Bi_2Sr_2CaCu_2O_8$ crystal. The straight line in the figure is a 15 Å step which corresponds to one molecular layer.

Density (g/cm^3)	6.7
Specific heat ($J\ g^{-1}\ K^{-1}$)	0.38
Thermal conductivity ($J\ s^{-1}\ cm^{-1}\ K^{-1}$)	10/T
Reflection coefficient	0.2
Absorption coefficient (cm^{-1})	$1x10^5$

Table A-I Thermal and optical properties of $Bi_2Sr_2CaCu_2O_8$ used in the calculations.

spot size was typically 0.2×0.2 mm^2.

The BSCCO single crystal used in this experiment was prepared using a travel solvent floating zone method. The crystal is easy to cleave and the cleaved surfaces are atomically flat since the material has a double BiO layer weakly bonded by van der Waals attraction. An atomic force microscopy (AFM) image of a typical cleaved surface of the BSCCO crystal used in this study is shown in Fig. 7-1. It illustrates near-atomic flatness of the BiO surface which has an average roughness of 0.3 nm. The samples, immediately after cleaving in air, were placed on the stage in the processing chamber. The temperature of the stage was near 300 K. After laser irradiation, the morphology of the sample surface was examined using AFM. The chemical composition of samples in the near-surface region was investigated using energy-dispersion X-ray analysis (EDX).

A. 3 Results and Discussion

The temperatures of the samples irradiated by excimer laser were calculated using a one dimensional heat flow equation [12, 13]:

$$c\rho\frac{\delta T}{\delta t} = I(z,t)\alpha + \frac{\delta}{\delta z}\left(\kappa(T)\frac{\delta T}{\delta z}\right) \qquad (1)$$

where c is the heat capacity, r is the mass density, a is the absorption coefficient for the laser light, k is the thermal conductivity, and I is the light intensity inside the target, which is a function of time t and depth z. This equation was used to estimate the laser fluence corresponding to the melting point of BSCCO, which is 870 °C. The calculations were carried out with the BSCCO parameters listed in Table I [14-19]. The laser fluence required to reach the melting point of this material was found to be about 35 mJ/cm^2.

For laser fluence of 500 mJ/cm^2 the surface of BSCCO is expected to melt and evaporate significantly. Indeed, the ablation plume was clearly observed at this fluence without the need of enhancement using an optical camera. After irradiation with 1 to 20 pulses, relatively smooth surfaces with the roughness amplitude of up to 20 nm were observed. Fig. 7-2 shows an AFM image of the surface obtained after irradiation with 10 laser pulses. A characteristic hexagonal microstructure with the diagonal of each hexagon being about 0.7-0.9 μm can be

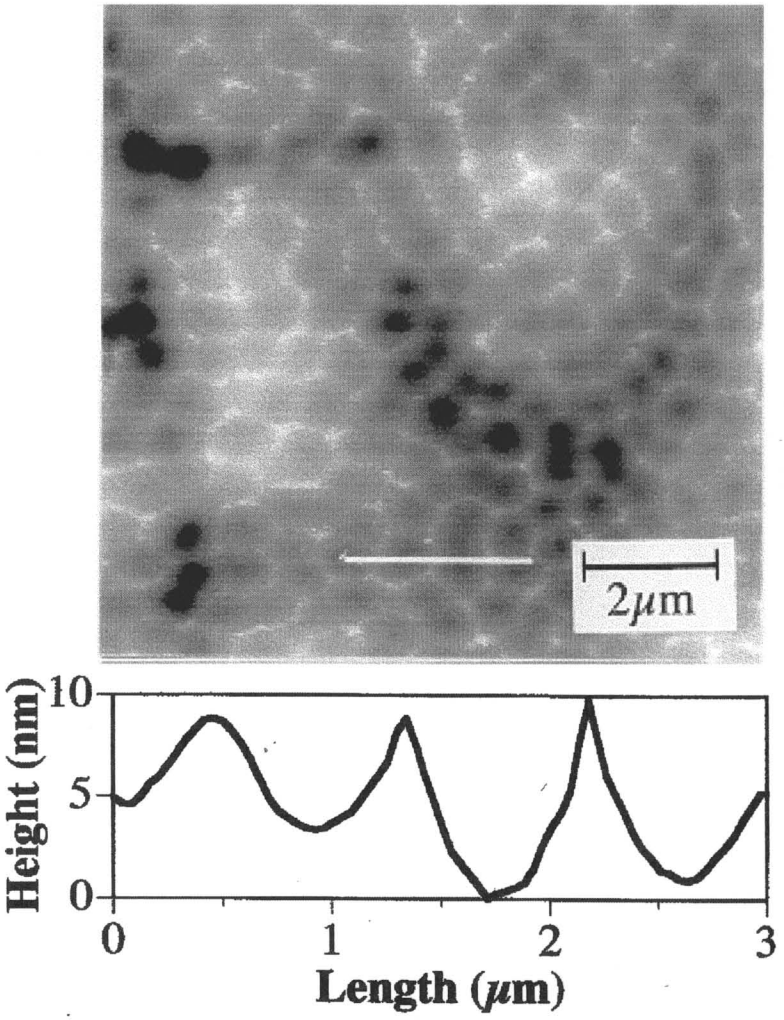

Figure A-2 AFM image of the (001) $Bi_2Sr_2CaCu_2O_8$ surface after laser irradiation at a fluence of 500 mJ/cm^2. The cross-section profile was taken along the white line in the image.

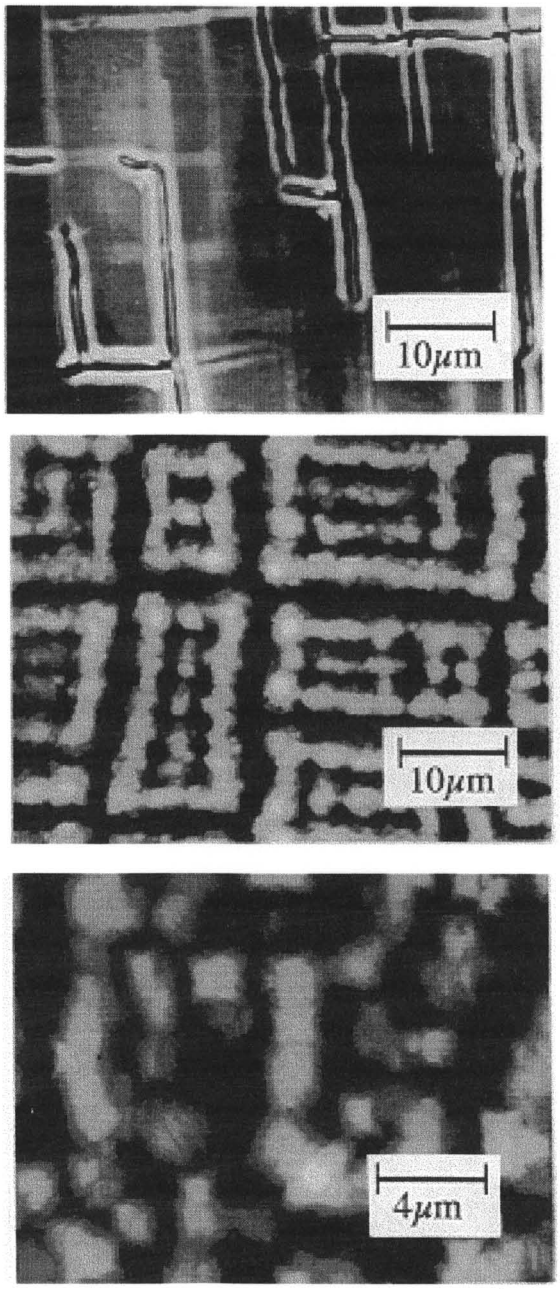

Figure A-3 AFM images of the (001) $Bi_2Sr_2CaCu_2O_8$ surface after irradiation with (a) 5 pulses at a fluence of 150 mJ/cm^2, (b) 50 pulses at a fluence of 150 mJ/cm^2, and (c) 1200 pulses at a fluence of 230 mJ/cm^2.

seen in this figure. The cross-section shows that the surface within each hexagon is smooth and the inter-hexagon boundaries are in this case about 10 nm high. The mechanism behind the formation of this hexagonal microstructure is not clear. The theory of two-dimensional phase transition predicts that a single crystal can melt into a so-called intermediate "hexatic" phase. There has been some experimental evidence concerning charged colloidal particles in a two-dimensional plasma system that supports the idea of hexagonal structure formation during melting [20]. The formation of plasma during laser ablation is a well-known process. The surface molten layer is thought to have little interaction with the solid surface, so the theory of two-dimensional phase transition may apply in our case.

The surface structure of BSCCO irradiated with pulses of fluence between 100-300 mJ/cm^2 depended strongly on the number of pulses delivered to a processed site. No plume formation could be observed at these laser fluences, indicating that the ablation process was less violent with no substantial heating of ablation products by the laser pulse. Fig. 7-3 (a) shows an AFM image of the surface, which was exposed to five pulses at the fluence of 150 mJ/cm2. This image shows 0.1-μm-deep cracks running along the a and b axes of the crystal. The crack formation is the evidence of a strong thermal stress induced in the irradiated material. In contrast to the results obtained with 500 mJ/cm^2, the original surface of BSCCO can easily be distinguished in this picture, without the evidence of any surface smoothing effects. Some protrusions can be seen at the edge of cracks. An AFM image of the surface after irradiation with 50 pulses at the same fluence is shown in Fig. 7-3 (b). The cracks grow deeper (2μm) and wider, the density of the cracks increases and the protrusions grow higher. An AFM image of the surface after irradiation with 1200 pulses of 230 mJ/cm^2 is shown in Fig. 7-3 (c). Pyramid-like 3-μm-high projections have clearly been developed under these conditions of irradiation. The regular shape (faceted) microstructure of these protrusions indicates that the crystallization of another phase took place on the surface of (001) $Bi_2Sr_2CaCu_2O_8$. The pyramids were found to have the ratio of the height to the half-width of the base of exactly 1:1. It is conceivable that the growth of such structures relates to non-congruent vaporization and/or re-deposition of some of the ablated material having different composition than that of the

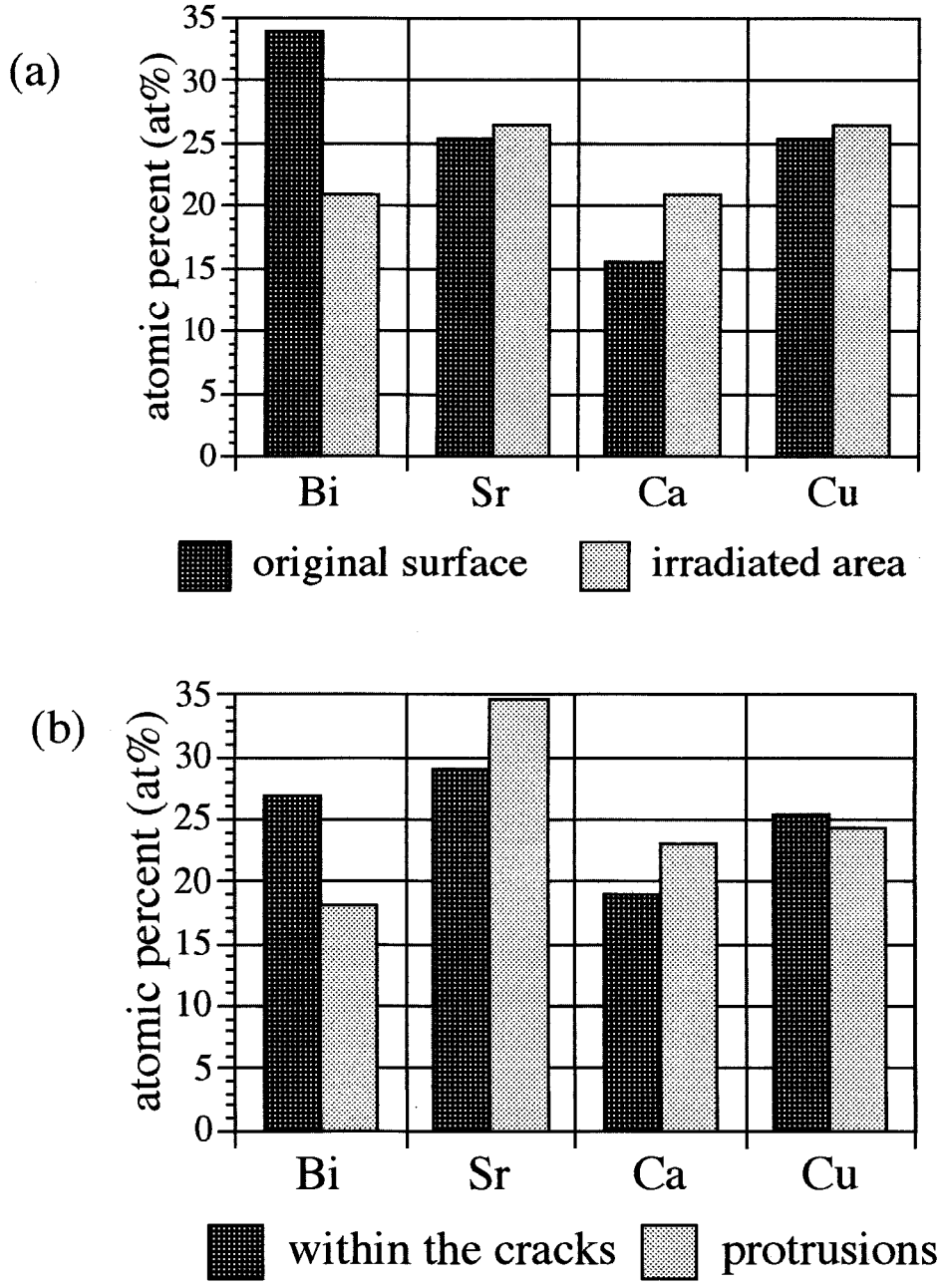

Figure A-4 EDX results comparing the chemical compositions of the original and the laser irradiated (001) $Bi_2Sr_2CaCu_2O_8$ surface (a), and the areas within the cracks and the protrusions (b). The irradiation was carried out at 150 mJ/cm^2.

original target. The change in the chemical composition of the laser-irradiated samples was observed with EDX. Fig. 7-4 (a) shows that overall concentration of Bi in the irradiated area decreased considerably compared with that in the original surface. In addition, it was found that within the irradiated area the concentration of Bi in the areas covered with protrusions was different from that in the areas containing cracks. The amount of Bi in the protrusions was less by about 9 at.% compared to that inside the cracks (Fig. 4 (b)). Less significant differences in chemical concentrations were observed for other elements. A likely structure for this new material formed on the surface of laser irradiated BSCCO would be (Ca, Sr)CuO_x doped with Bi. However, a more systematic study and precise micro-analysis are required to verify this hypothesis.

The formation of protrusions was also observed for samples irradiated with a laser fluence of 20 mJ/cm^2. According to Equation (1), the surface temperature of BSCCO induced with such a fluence is about 750 °C, which is below the melting point of this material. Thus, the protrusions in this case seem to be formed from vapors generated during vacuum sublimation of the target material. The AFM images shown in Fig. 5 illustrate the surface morphology of samples irradiated with 2 (Fig. 7-5 (a)) and 100 (Fig. 7-5 (b)) laser pulses at 20 mJ/cm2. Cone-shape protrusions can be easily distinguished in these images. The protrusions are uniformly distributed over the irradiated area and their diameter increased from 50-100 nm to about 500-800 nm for the surface irradiated 2 and 100 pulses, respectively. The height of the protrusions (islands) was found to be strongly dependent on the number of laser pulses. This is illustrated in Fig. 7-6. The height of an island increased rapidly within the first 20 pulses to about 350 nm, and it remained unchanged as the irradiation was continued. The increasing roughness of the target appears to be responsible for this saturation behavior. It leads to "dilution" of the laser pulse energy over larger surface areas and, consequently, to decay of the ablation rate. A similar effect of target roughening and material re-deposition that led to quenching of the vaporization process has been observed, e.g., during a Nd:YAG laser-induced sublimation of Cd [21].

Mechanisms of formation of cone-shape and pyramid-shape protrusions appear to be

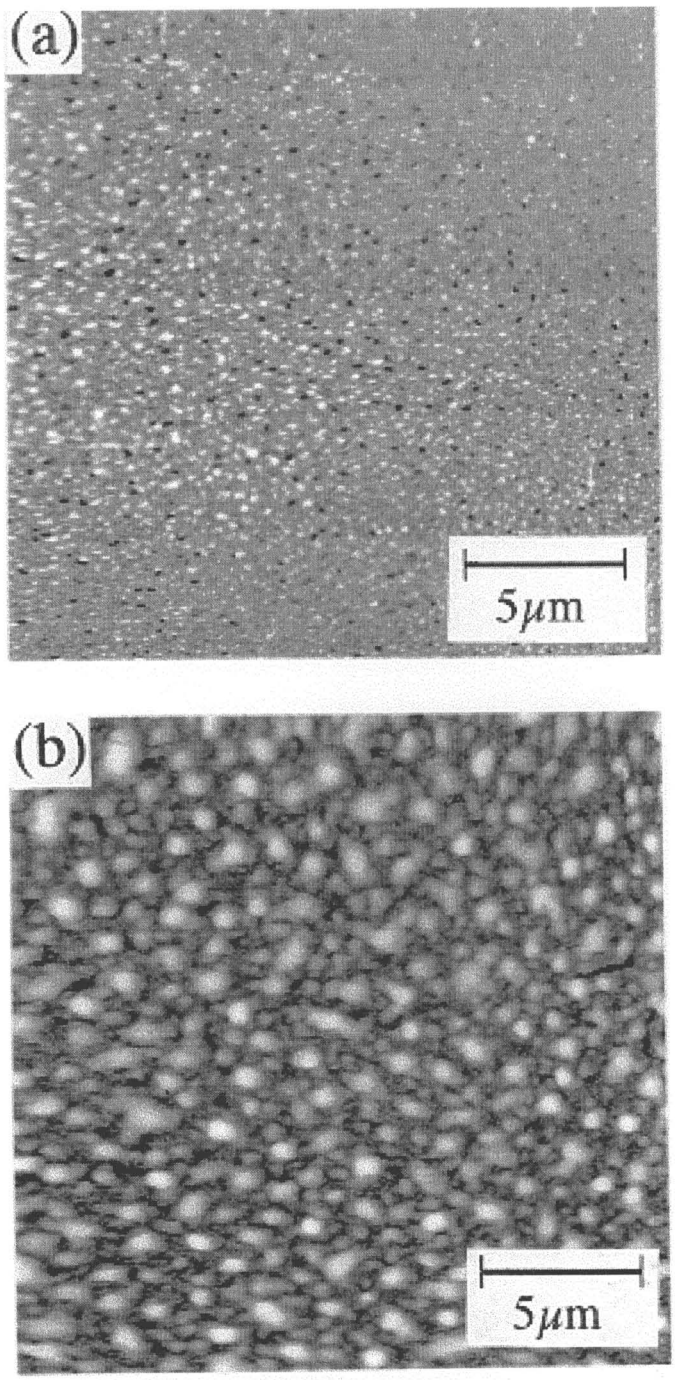

Figure 7-5 AFM images of the (001) $Bi_2Sr_2CaCu_2O_8$ surface after laser irradiation with 2 (a) and 100 (b) pulses at a fluence of 20 mJ/cm^2.

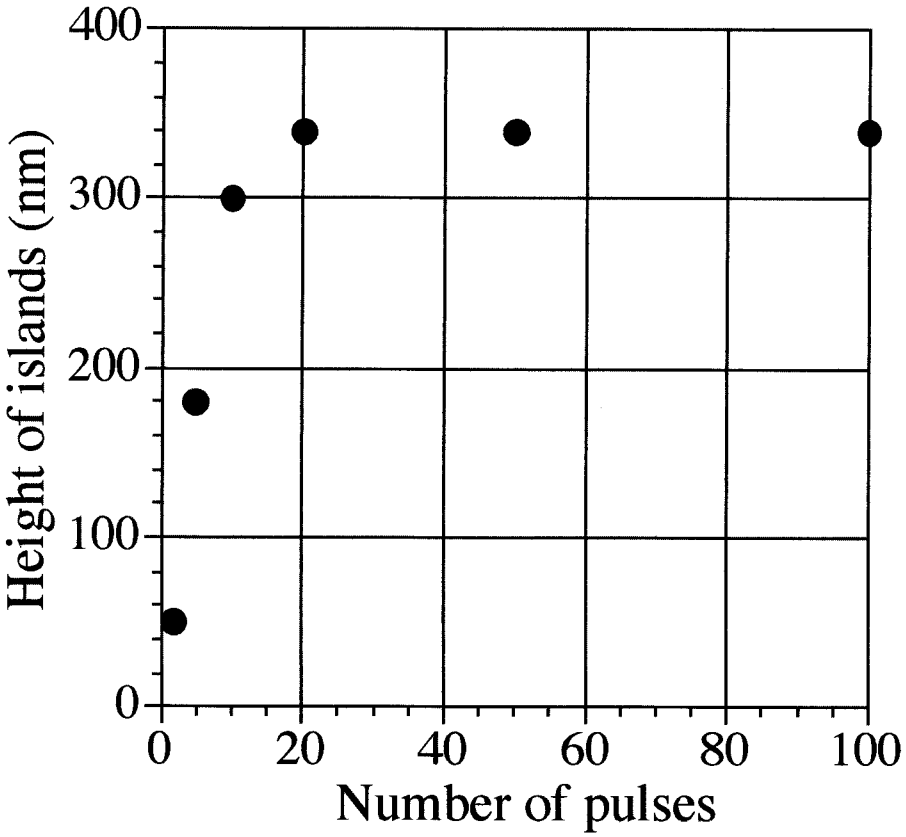

Figure 7-6 The height of the islands as a function of the number of laser pulses at a fluence of 20 mJ/cm^2.

different, mainly because these features have been formed at temperatures below and above the BSCCO melting point, respectively. The below-melting point irradiation results suggest that photo etching is the predominant mechanism responsible for the surface structuring. It has been reported [22] that desorption of Bi+ ions from the surface of crystalline BSCCO induced with 193 nm pulses follows a model for the non-thermal process. Photo-desorption is known to be very sensitive to surface defects. Thus, in contrast to a re-deposition hypothesis, the formation of cone-shape protrusions may be due to a reduced ablation efficiency from surface imperfections, such as metal-rich sites.

A. 4. Conclusions

The surface morphology of (001) $Bi_2Sr_2CaCu_2O_8$ bulk crystals irradiated in vacuum with an ArF excimer laser was investigated for laser fluences in the range of 20 mJ/cm^2 ≤ F ≤ 500 mJ/cm^2. Relatively smooth surfaces, with a roughness amplitude of about 20 nm, have been observed for irradiation at 500 mJ/cm2. A two-dimensional molten layer, which is formed following the cooling of laser heated plasma in the vicinity of the surface is most likely the cause of this smoothing effect. In some cases, the formation of hexagonal surface structures was observed. These structures seem to be formed by the solidification of a laser- heated thin liquid layer of BSCCO. The evidence of crystal fracture and crack formation has been observed for 100 mJ/cm^2 < F < 500 mJ/cm^2, especially at the initial stage of irradiation. The pyramid microstructures on the surface of BSCCO irradiated with large number of pulses suggest that crystallization of a new material, most likely (Ca, Sr)CuO_x and/or Bi-doped (Ca, Sr)CuO_x takes place in this case. The results indicate that laser-induced patterning/microstructuring of bulk (001) $Bi_2Sr_2CaCu_2O_8$, even with extremely low laser fluence, will most likely require the presence of a processing gas that would help to maintain surface stoichiometry and smooth surface morphology of the processed material.

References

1. J. J. Dubowski, B. E. Rosenquist, D. J. Lockwood, H. J. Labbé, A. P. Roth, C. Lacelle, M. Davies, R. Barber, B. Mason, G. I. Sproule, J. Appl. Phys. 78 (1995) 1488.
2. J. J. Dubowski, A. Compaan, M. Prasad, Appl. Surf. Sci. 86 (1995) 548.
3. P. Viville, S. Beauvois, G. Lambin, R. Lazzaroni, J. L. Brédas, K. Kolev, L. Laude, Appl. Surf. Sci. 96-98 (1996) 558.
4. H. Nishino, H. Okano, K. Inui, A. Yabe, Appl. Surf. Sci. 109-110 (1997) 259.
5. Y. Novis, J. J. Pireaux, A. Brezini, E. Petit, R. Caudano, P. Lutgen, G. Feyder, S. Lazare, J. Appl. Phys. 64 (1988) 365.
6. T. Oohira, S. Sakai, Y. Kasai, K. Shimizu, Thin Solid Films 281-282 (1996) 513.
7. J. G. Lunney, R. R. O'Neill, K. Schulmeister, Appl. Phys. Lett. 59 (1991) 647.
8. U. Varshney, R. J. Churchill, H. P. Groger, A. I. Kingon, J. Appl. Phys. 66 (1989) 1392.
9. S. Proyer, E. Stangl, P. Schwab, D. Bäuerle, P. Simon, C. Jordan, Appl. Phys. A 58 (1994) 471.
10. H. Ishibashi, S. Arisaka, K. Kinoshita, T. Kobayashi, Jpn. J. Appl. Phys. 33 (1994) 4971.
11. R. Aguiar, F. Sánchez, M. Varela, Appl. Surf. Sci. 96-98 (1996) 405.
12. R. F. Wood, G. E. Giles, Phys. Rev. B 23 (1981) 2923.
13. S. Otsubo, T. Minamikawa, Y. Yonezawa, A. Morimoto,T. Shimizu, Jpn. J. Appl. Phys. 29 (1990) L73.
14. I. Shigaki, K. Kitahama, K. Shibutani, S. Hayashi, R. Ogawa, Y. Kawabe, S. Kawai, Cryo. Eng. 27 (1992) 158.
15. H. Fujishiro, M. Ikebe, T. Naito, M. Matsukawa, K. Noto, I. Shigaki, K. Shibutani, S. Hayashi, R. Ogawa, Physica C 235-240 (1994) 1533.
16. J. T. Fanton, D. B. Mitzi, A. Kapitulnik, B. T. Khuri-Yakub, G. S. Kino, D. Gazit, R. S. Feigelson, Appl. Phys. Lett. 55 (1989) 598.

17. H. Yusheng, X. Jiong, W. Xin, H. Aisheng, Z. Jincang, C. Fanggao, Phys. Rev. B 40 (1989) 7384.

18. I. Bozovic, Phys. Rev. B 42 (1990) 1969.

19. H. Yabuki, H. Katakura, S. Takahashi, H. Ishii, T. Hanyu, S. Yamaguchi, Jpn. J. Appl. Phys. 33 (1994) 6530.

20. J. B. Pieper, J. Goree, R. A. Quinn, J. Vac. Sci. Technol. A14 (1996) 519.

21. J. J. Dubowski, Proceedings SPIE Int. Soc. Opt. Eng. (USA), vol 668 (1986) 97.

22. H. Helbajian, L. Wiedeman, H.-S. Kim, Adv. Mater. Opt. Electron.,vol 2 (1993) 31.

Appendix B

Temperature dependence of Andreev Reflection with High-T_c superconductors

Abstract

I fabricated $YBa_2Cu_3O_{7-\delta}$/Au junctions in order to observe temperature dependence of Andreev reflection, and obtained conductance peaks not only blow T_c but also above T_c of $YBa_2Cu_3O_{7-\delta}$. The result indicate the possibility of existence of Andreev reflection above T_c, which can be direct evidence for the formation of Cooper pair for the first time.

B-1. Introduction

It has become clear that high-T_c superconductors show many unusual properties both in the normal and superconducting states. Especially, the energy gap above the T_c, so-called pseudogap, has become one of central interests for its unusual properties. This gap was seen in NMR relaxation rate $1/T_1$ at first[1], then have been observed in other experiments. Recently, the gaplike feature above T_c was directly detected in $Bi_2Sr_2CaCu_2O_8$ by both photoemission and tunneling spectroscopy[2-4]. This has been thought to be the results of the singlet pair formation. However, mechanism of pseudogap formation is not clear and properties of pseudogap, i.e. temperature dependence and the value of gap energy, are not consistent between different experiments. Moreover, some studies have insisted that pseudogap is not related with pair formation because the properties of pseudogap are much different from those of the superconducting gap[5]. Usual tunneling and photoemission studies can determine the energy gap which reflects quasipaticle density of state. However, the energy gap of density of state does not always mean existence of the paring originated in superconductivity. Similarly, the results of NMR studies are not direct evidence for superconducting pair formation and the results only indicate the formation of spin-singlet pairs. Therefore, I consider that it is much important to investigate whether the energy gap and spin-singlet pairs above T_c can be associated with superconductivity or not.

In this study, I investigate the superconducting gap structure by the observation of Andreev Reflection of superconductor/normal metal (SN) junction. At the interface of SN junction, Andreev reflection occurs and the conductance of the junction increase as described in chapter 3. As a result, differential conductance spectra of the SN junction can be expressed as shown in fig. B-1 assuming that most of incident electrons cause Andreev reflection. Therefore, the value of superconducting gap can be determined by measuring conductance of SN junction. I have measured temperature dependence of differential conductance spectra and tried to detect Andreev reflection above T_c.

B-2 Experimental

I have prepared Au/$YBa_2Cu_3O_{7-\delta}$/Au junctions as shown in fig. B-2. $YBa_2Cu_3O_{7-\delta}$

(YBCO) thin films were prepared by using pulse laser deposition method. Probability of Andreev reflection highly depends on barrier potential between a superconductor and a metal[6]. Therefore, Au thin films were successively deposited on YBCO thin films by PLD without exposing to air in order to reduce the degradation at interface between YBCO and Au. After that, the structure of the junctions have been formed with conventional photolithograph technique.

B-3 Results and discussion

Fig. B-3 shows the temperature dependence of the resistance of the junction. The drop of resistance at about 87 K shows T_c of the YBCO thin film. The resistance below T_c as inserted in fig. B-3 consists of the interface resistance (R_i) between YBCO and Au and the resistance of Au. Since R_i is thought to be independent of temperature, I estimated R_i by the extrapolation from the resistance curve into 0 K and obtained 0.5 Ω corresponding to 2×10^{-6} Ω cm^2 as the resistivity of the junction. This value is thought to be well below conpared with that of quasiparticle tunneling junction. Fig. B-4 shows temperature dependence of differential conductance curves of the junction. The differential conductance curve at 16 K gently rises to the point at zero voltage. This behavior can be observed at 100 K which is well above T_c. Since Bias voltage was applied not only to interfaces but also Au and normal state of YBCO above T_c, these conductance curve should be revised with effective bias voltage applied only to interfaces. The revised conductance curves are shown in fig. B-5. The conductance peaks are seen within the range of ±50 mV corresponding to 4Δ of YBCO. It can be clearly seen that the conductance peak exist at 120 K. The result indicates a possibility that Andreev reflection occurs above T_c. However, it is difficult to judge whether these conductance peak are originated from Andreev reflection or not because there are several serious problems described below in the measurement. Firstly, the conductance curve were unable to be measured in the bias region higher than 50 mV due to the limitation on the capacity of the current source. Since R_i is about 0.5 Ω and very small, current more than 100 mA is needed to apply more than 50 mV to the junction. If Andreev reflection are responsible for these conductance peaks, the conductance peaks are present only within superconducting gap and

the spectra should be flat in higher bias range as shown in fig. B-1. Therefore, I cannot confirm whether these conductance peaks exist only within 4Δ or not. Secondly, non-liner effect from too much current injection may responsible for conductance peak. Especially, local heating must exists with such a high current density. However, I could not observe hysteresis in I-V curves during the measurement of spectra between forward and reverse swings of bias voltage, which indicates heating effect does not dominantly contribute to conductance peak. Therefore, I consider that existence of Andreev reflection above T_c might be observed in this study.

B-4 Conclusion

I fabricated Au/YBCO/Au junctions with very low contact resistance in order to observe Andreev reflection and conductance peaks were observed in differential conductance spectra below and above T_c of YBCO. This result may indicate existence of Cooper pairs above T_c, which is much important for elucidation for superconducting mechanism of high-T_c superconductor. However, there is serious ambiguity for interpretation of spectrum with Andreev reflection, and it is necessary to perform more precise measurement with the junctions having smaller junction areas.

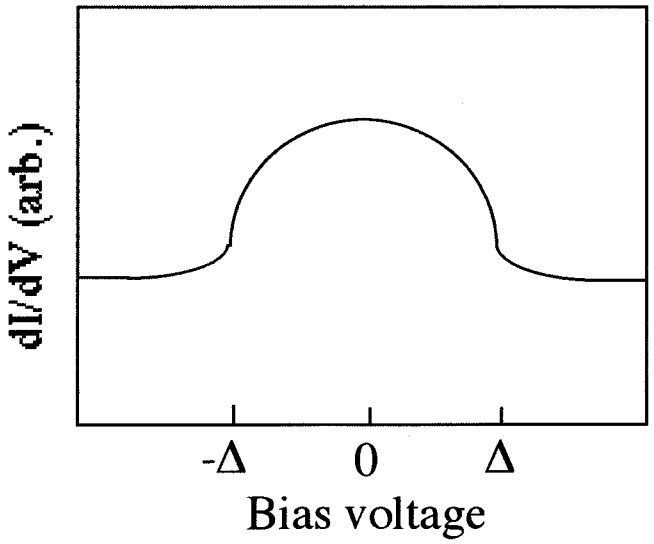

Figure B-1 Schematic illustration of bias voltage dependence of differential conductance spectrum with a superconductor/normal metal junction when Andreev reflection is dominant process at the interface between a superconductor and a normal metals.

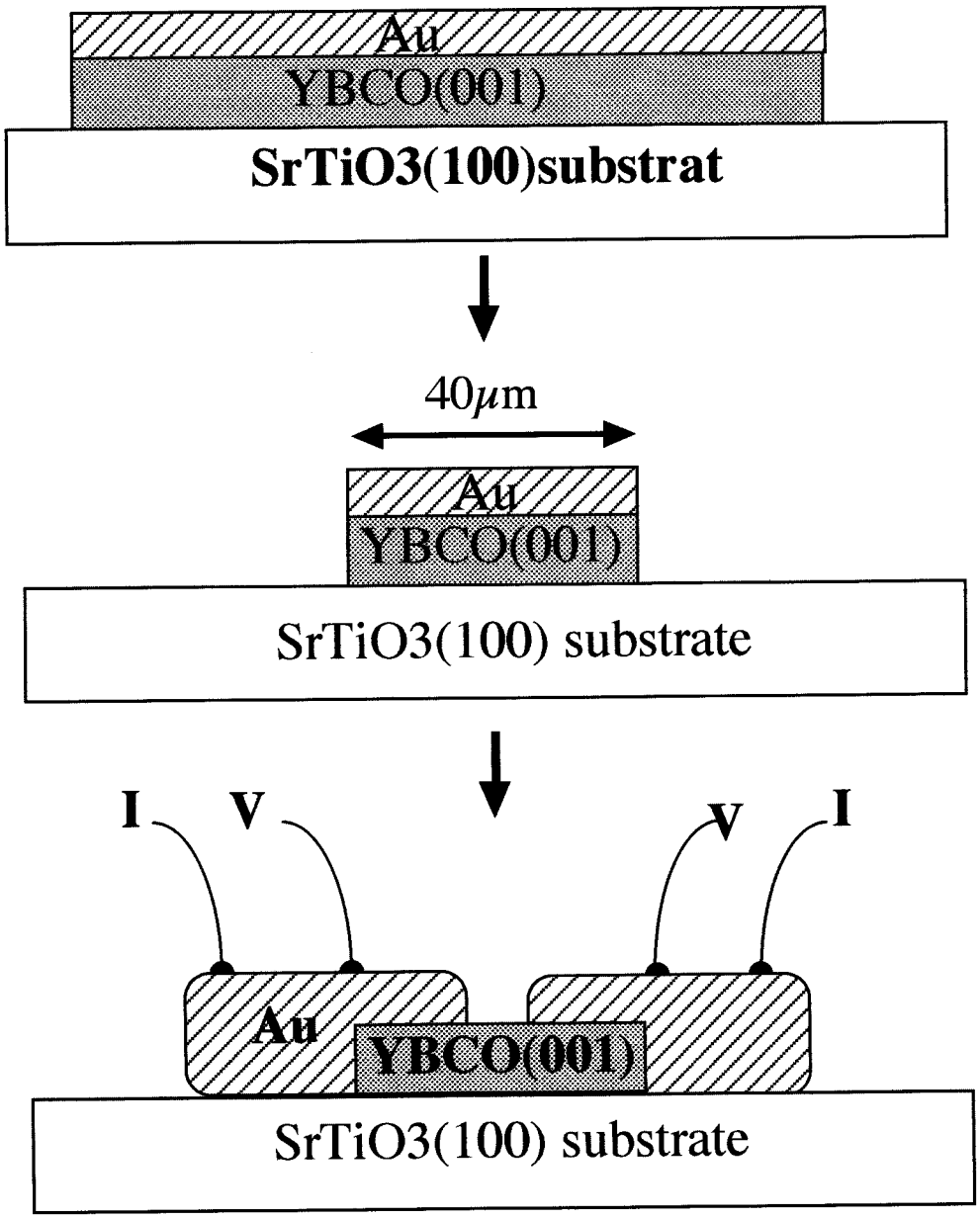

Fig B-2 Fabrication process of Au/YBCO/Au junction.

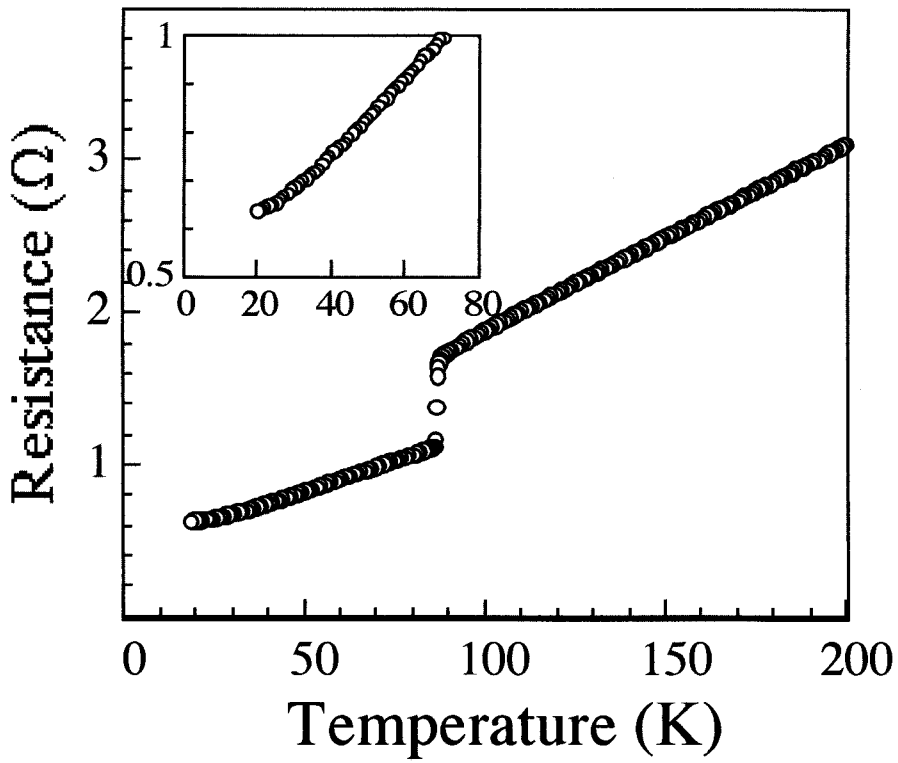

Figure B-3 Temperature dependence of the Au/YBCO/Au junction.

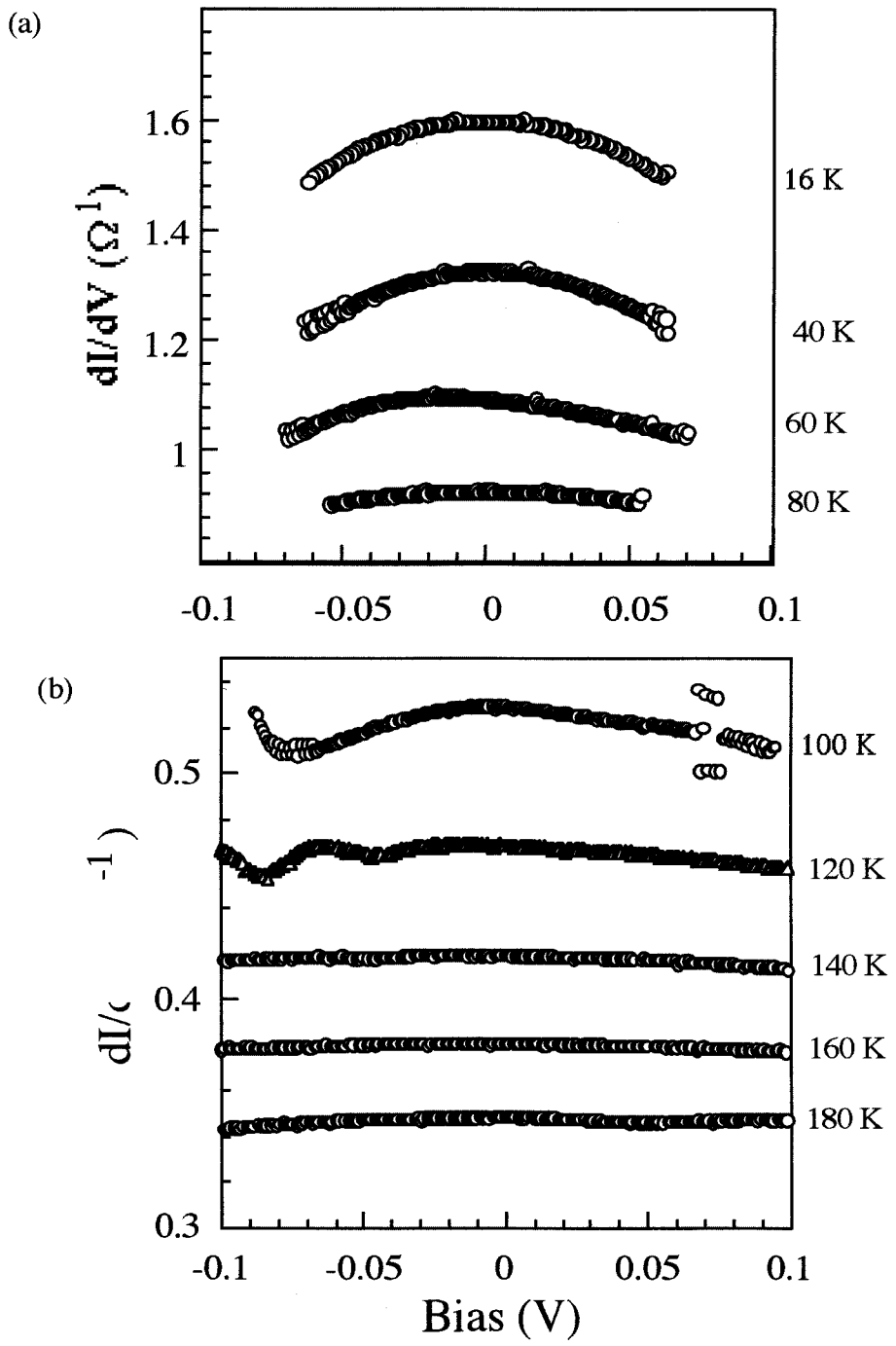

Figure B-4 Temperature dependence of differential conductance curves (a) below T_c and (b) above T_c of the Au/YBCO/Au junction.

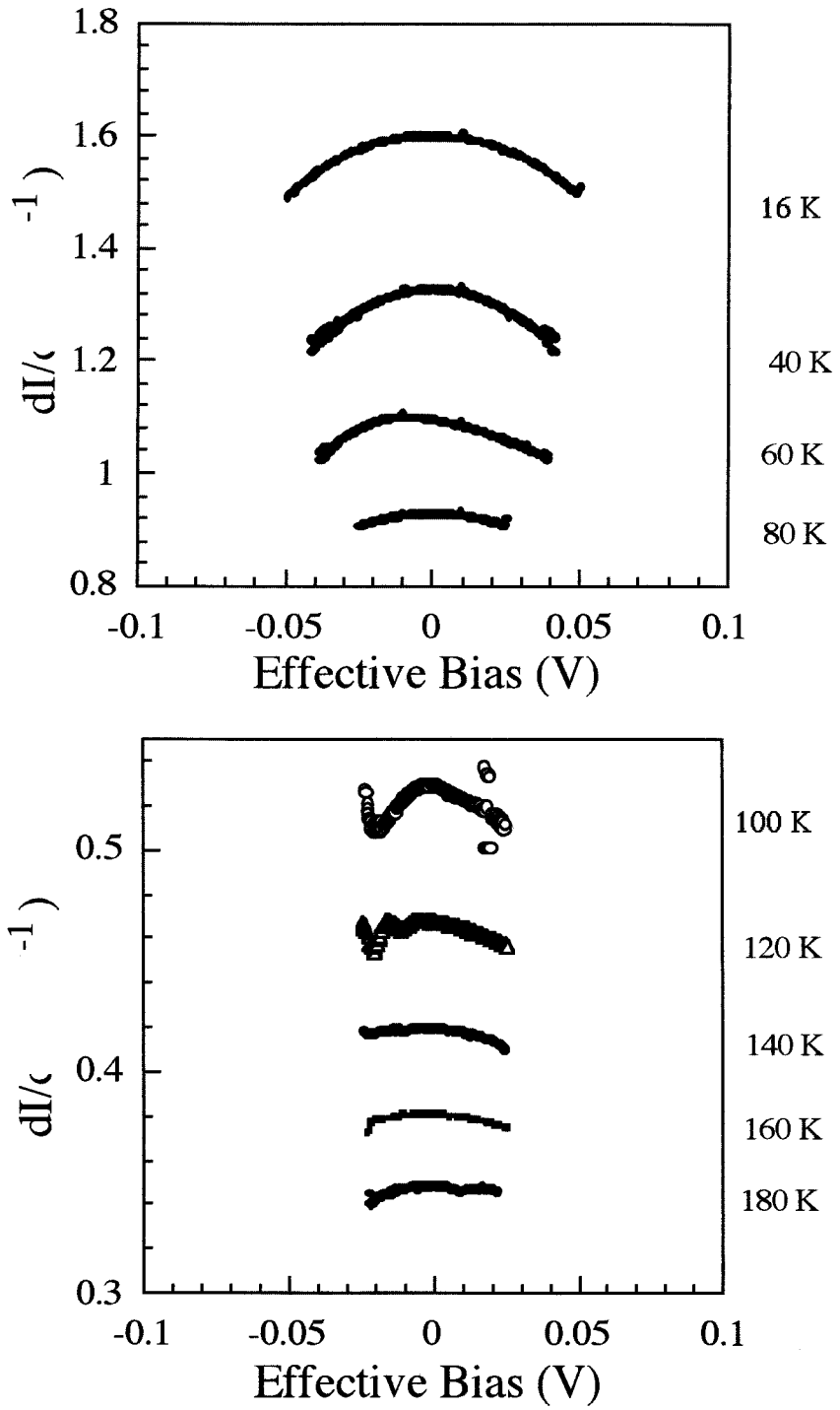

Figure B-5 Revised conductance curves (a) below T_c and (b) above Tc of Au/YBCO/Au junction by using 0.5 Ω as a contact resistance.

References

1. H. Yasuoka, T. Imai,T. Shimizu, (eds.), "Strong Correlation and Superconductivity" Springer, New York, 1989.

2. H. Ding, T. Yokota, J. C. Campuzano, T. Takahashi, M. Randeria, M. R. Norman, T. Mochiku, K. Kadowaki,J. Giapintzakis, Nature **382** (1996) 51.

3. C. Renner, B. R.-Y. Genoud, K. Kadowaki,ø. Fisher, Phys. Rev. Lett. **80** (1998) 149.

4. A. Matsuda, S. Sugita,T. Watanabe, Phys. Rev. B **60** (1999) 1377.

5. M. Suzuki, T. Watanabe,A. Matsuda, Phys. Rev. Lett. **82** (1999) 5361.

6. G. E. Blonder, M. Tinkham,T. M. Klapwijk, Phys. Rev. B **25** (1982) 4515.

List of Publications

[1] Iwao Kawayama, Masaki Kanai, and Tomoji Kawai, "Growth of $SrCuO_2$ Thin Films on Oxygen-Annealed $SrTiO_3$ (100) Substrates" Japanese Journal of Applied Physics, vol. 35, pp. L926-929, 1996.

[2] Iwao Kawayama, Masaki Kanai, and Tomoji Kawai, "Tunneling spectra of $Bi_2Sr_2CaCu_2O_8$ single crystals with well-defined artificial barriers" Physica C, vol. 298, pop. 204-207, 1997.

[3] Iwao Kawayama, Jan J. Dubowski, Hairlike , and Tomoji Kawai, "Modification of cleaved surfaces of $Bi_2Sr_2CaCu_2O_8$ single crystals Induced by ArF excimer laser irradiation" Applied Surface Science, vow. 143, pop. 313-318, 1999.

[4] Iwao Kawayama and Tomoji Kawai, " Application of laser ablation for surface engineering of oxides" J. Japan. Laser Processing So. vol. 6, pop. 104-105, 1999 [in Japanese].

[5] Iwao Kawayama, Masaki Kanai, Tomoji Kawai, Michitaka Maruyama, Akira Fujimaki, and Hisao Hayakawa, "Properties of c-axis Josephson tunneling between $Bi_2Sr_2CaCu_2O_8$ and Nb " Pysica C, vow 325, pop. 49-55, 1999

International Meeting

[1] November 27 1995 Fall Meeting of the Materials Research Society, Boston, USA
"SIS junction prepared by low temperature STM with high-T_c superconducting whisker tip"
I. Kawayama, H. Tanaka, M. Kanai, T. Kawai

[2] March 22 1999 Spring Meeting of the American Physical Society, Atlanta, USA
"Observation of Josephson Coupling in c-axis $Bi_2Sr_2CaCu_2O_8$/Au/Nb Josephson Junctions"
Iwao Kawayama, Masaki Kanai, Tomoji Kawai, Akira Fujimaki, Michitaka Maruyama, Hisao Hayakawa

Acknowledgments

The author express his appreciation and gratitude to professor T. Kawai of ISIR-Sanken, Osaka University for his encouragement and continuous guidance throughout the course of his investigation.

It is indeed a great pleasure for the author to have two supervisors for this thesis, Professor T. Nakamura and Professor T. Matsuo of Department of Chemistry, Faculty of Science, Osaka University.

The author is very grateful to Dr. M. Kanai for his valuable discussions and helpful suggestions during this study.

The author thanks Dr. J. Dubowski of Institute for Microstructual Science, National Research Council of Canada for his helpful assistance on the work in chapter 7.

The author thanks Professor H. Hayakawa, Assistant Professor A. Fujimaki and Mr. M. Maruyama for their cooperation on the measurements of Josephson effects in chapter 5.

The Author thanks Professor S. Hontsu of Department of Electronic System and Information Engineering, Faculty of Biorogy-Oriented Science and Technology, Kinki University for his helpful suggestion on my work.

The author thanks to Assistant Professor H. Tabata for his valuable comments and encouragement, and thanks to Assistant Professor T. Matsumoto for helpful discussions on the work concerning tunneling.

The author thanks Dr. K. Kitahama for his guidance on preparation of $Bi_2Sr_2CaCu_2O_8$ single crystals used in the studies, and thanks Dr. H. Tanaka for his cooperation on the measurement using scaning tunneling microscopy.

I am graatful to Dr. H. Nishikawa, Dr. Hide. Tanaka for their helpful comments and discussion through the life in Kawai laboratory.

The author wish to thank students in Kawai laboratory of ISIR-Sanken, Osaka University.

Finally, I would like to express my gratitude to my parents for their unchanged understandings on my study, and to my wife Michiru for her support to my life.